SEDIMENTOLOGY the journal of the International Association of Sedimentologists

Sedimentology (2019) **66**, 1486–1530 doi: 10.1111/sed.12541

High-frequency cycles of brachiopod shell beds on subaqueous delta-scale clinoforms (early Pliocene, south-east Spain)

DIEGO A. GARCÍA-RAMOS and MARTIN ZUSCHIN
Department of Palaeontology, University of Vienna, Althanstrasse 14, A-1090, Vienna, Austria

Associate Editor – Christopher Fielding

ABSTRACT

During the early Pliocene, subaqueous delta-scale clinoforms developed in the Águilas Basin, in a mixed temperate carbonate–siliciclastic system. The facies distribution is consistent with the infralittoral prograding wedge model. Stacking patterns and bounding surfaces indicate that the clinoforms formed during the highstand and falling sea-level stages of a high rank cycle. Twenty-two prograding clinothems were recognized over a distance of ≥1 km. Biostratigraphic data indicate a time span shorter than 700 kyr for the whole unit (MPl3 biozone of the Mediterranean Pliocene). Cyclic skeletal concentrations and occasional biostromes of suspension feeders (terebratulid brachiopods, modiolid bivalves and adeoniform bryozoan colonies), slightly evolved glauconite and occasional *Glossifungites* ichnofacies formed on the clinoforms during high-frequency pulses of relative sea-level rise. During such stages, increased accommodation space in the topsets of the clinoforms caused a strong reduction of terrigenous input into the foresets and bottomsets. This provided favourable conditions for the development of these suspension feeder palaeocommunities. During stillstand stages, however, reduced accommodation space in the topsets eventually resumed progradation in the foresets. There, the abundance of *Ditrupa* tubes indicates frequent siltation events that extirpated the terebratulid populations and other epifaunal suspension feeders in the foreset and bottomset subenvironments. The occurrence of shell beds on the clinoforms suggests that this case study represents lower progradation rates than standard examples where shell beds bound the clinobedded units at their base and top only. Importantly, the distributions of biofacies and ichnoassemblage associations contribute significantly to the understanding of the effects of relative sea-level fluctuations on the evolution of subaqueous delta-scale clinoform systems.

Keywords Brachiopods, clinoforms, high-frequency sea-level changes, mixed carbonate–siliciclastic systems, sequence stratigraphy, shell beds.

INTRODUCTION

The duration of cycles is the traditional criterion to discriminate the hierarchical order of stratigraphic sequences (Mitchum & Van Wagoner, 1991; Vail *et al.*, 1991). The assignment of sequences to orders, however, can be difficult and arbitrary because the structure of the sedimentary record conforms to a continuum rather than to distinct modes of abundance classes of cycle duration (Drummond & Wilkinson, 1996; Schlager, 2004, 2010). Many authors advocate analyzing hierarchy based on the relative scale and magnitude of sequences (Embry, 1993, 1995; Catuneanu, 2006; Neal & Abreu, 2009; Catuneanu *et al.*, 2011). Accordingly, high rank (low frequency) and low rank (high frequency) sequences are established on a case by case basis using observations from the rock record. For example, the sequence of largest magnitude in a particular

basin can be designated by the generic rank 'N', and successively lower rank sequences can be designated by ranks 'N-1', 'N-2', etc. (e.g. Massari & Chiocci, 2006). Such hierarchical systems can serve as a template for comparison with other study areas and, if good chronological control is available, these ranks can be evaluated in light of cycle duration to reconcile both approaches (Schlager, 2010). The physical expression of sequences can include the relative extension of unconformities, depth of incision of fluvial valleys, geometric relationships between the building blocks of composite sequences, magnitude of facies shifts, relative scale of clinoforms (Thorne, 1995; Helland-Hansen *et al.*, 2012; Patruno *et al.*, 2015), or the development of onlap, backlap, downlap and toplap shell beds (Kidwell, 1991; Abbott, 1997; Naish & Kamp, 1997; Kondo *et al.*, 1998; Di Celma *et al.*, 2005; Hendy *et al.*, 2006; Zecchin & Catuneanu, 2013). Except for large-scale outcrops, however, where the relationships between the rank of sequences and the distribution of shell beds can be directly traced (Beckvar & Kidwell, 1988; Massari & D'Alessandro, 2012; Zecchin & Catuneanu, 2017) (Fig. 1A), exposures with limited spatial extent hamper the observation of clinoforms. In such cases, the rank of sequences defined by the position and geometric relationship of condensed shell beds with the sequence building blocks can be difficult to elucidate (Fürsich *et al.*, 1991; Ruffell & Wach, 1998).

This study documents the distribution of cyclically arranged brachiopod shell beds in the Águilas Basin (south-east Spain) in extensive outcrops of Pliocene sediments. These pavements formed on the distal part of lower rank delta-scale (i.e. tens of metres high) clinoforms (Fig. 1B and C). Importantly, this contrasts with other examples where onlap and backlap shell beds bound lower rank delta-scale clinoforms (e.g. Massari & D'Alessandro, 2012) (Fig. 1A). Determining the scale of clinoforms in the current study area enables the identification of low rank onlap and backlap shell beds. Moreover, the development of condensed shell beds on clinoforms implies lower progradation rates than those where clinoforms of comparable scale/rank lack such hiatal concentrations.

NOMENCLATURE

Clinoforms, clinothems and scale

Clinoforms are sloping depositional surfaces commonly associated with prograding strata (Pirmez *et al.*, 1998; Patruno *et al.*, 2015, and references therein). These surfaces consist of gently dipping topset and bottomset parts bounded by a basinward steeper-dipping portion termed the foreset (Gilbert, 1885) (Fig. 2A). The sedimentary deposits (or stratal packages) bounded by two successive clinoforms of the same hierarchy/rank are termed 'clinothems' (Rich, 1951; Anell & Midtkandal, 2015; Patruno *et al.*, 2015) (Fig. 2A). In short, clinoforms are surfaces and clinothems are the deposits between them. Depending on the geometry of the clinoform, there are one or two slope break points of maximum curvature, known as 'rollovers'. An 'upper rollover' connects the topset with the foreset and a 'lower rollover' connects the foreset and the bottomset (Walsh *et al.*, 2004; Mitchell, 2012; Patruno *et al.*, 2015) (Fig. 2A). The rollover separating the topset and foreset has also been referred to as shoreline break, breakpoint, brinkpoint, offlap break or shelfbreak, depending on the scale of the clinoform and the sedimentary environment (Vail *et al.*, 1991; Hernández-Molina *et al.*, 2000; Soria *et al.*, 2003). Concerning the spatial scale, clinoforms are fractal structures that display a huge vertical range, in the order of centimetres to thousands of metres (Thorne, 1995; Pirmez *et al.*, 1998; Patruno *et al.*, 2015). Accordingly, in a proximal to distal transect, large clinoforms have been classified as subaerial delta and subaqueous delta clinoforms (both tens of metres high), shelf prisms (*ca* 100 to 500 m high) and continental margin clinoforms (thousands of metres high) (Helland-Hansen *et al.*, 2012; Patruno *et al.*, 2015) (Fig. 2B).

In rare cases, all four types are found to prograde synchronously in the same basin, forming a compound clinoform system (Patruno *et al.*, 2015) (Fig. 2B and C). In physical-accommodation dominated systems (*sensu* Pomar & Kendall, 2008), the relative progradation rates decrease from subaerial and subaqueous deltas, to shelf prisms and then to continental margin clinoforms (Patruno *et al.*, 2015) (Fig. 2B). This is important because the relative progradation rates can help to reconcile the duration of relative sea-level cycles and their physical expression in the rock record.

Delta-scale clinoforms

Both subaerial and subaqueous delta-scale clinoforms display a vertical range of tens of metres. Subaerial and subaqueous deltas should not be confused, because the former have a topset entirely or partially above sea-level (Postma,

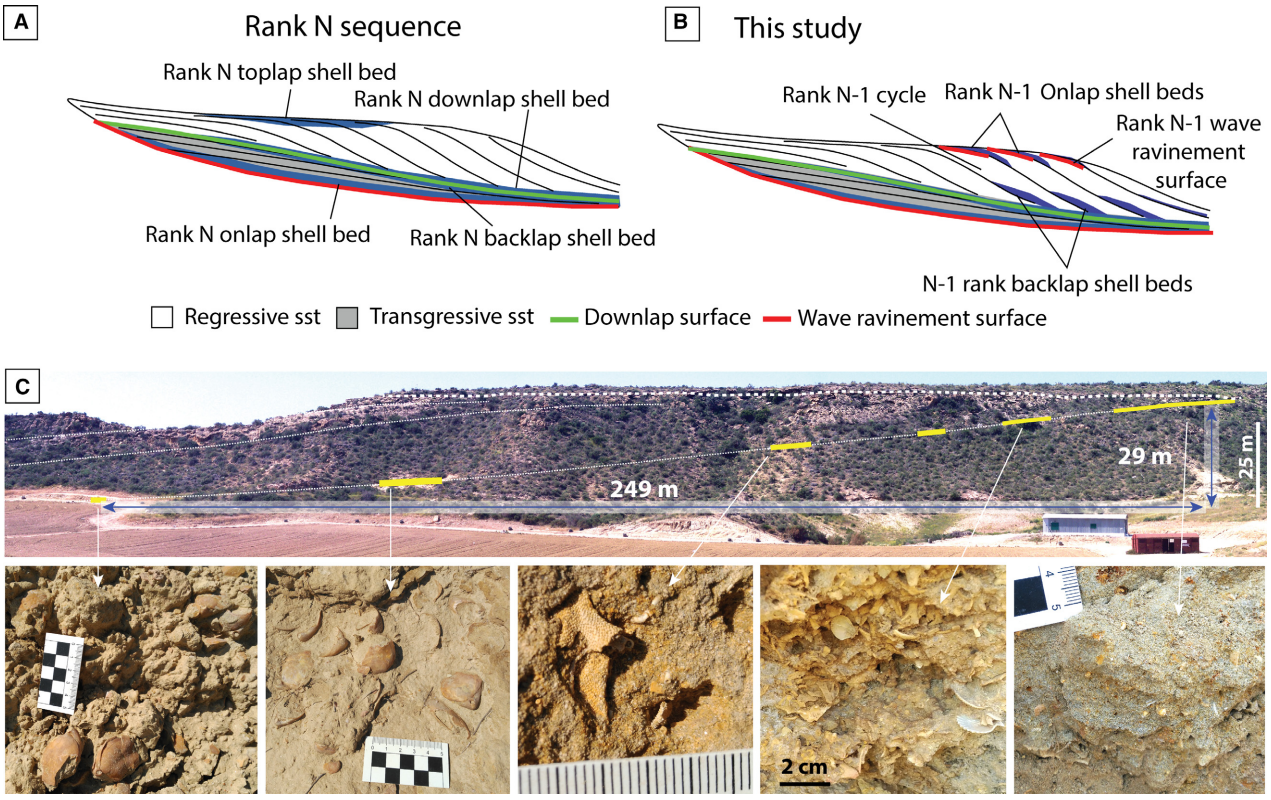

Fig. 1. Idealized sketch of the sequences with the location of condensed shell beds and the conceptual framework for a hierarchical classification of ranks based on geometry and scale. (A) Rank N sequence with indication of rank N onlap, backlap, downlap and toplap shell beds (adapted from Zecchin, 2007). (B) Rank N sequence indicating the position of both rank N and rank N-1 shell beds as described in this study. (C) Outcrop example of rank N-1 shell beds on a Pliocene subaqueous delta-scale clinoform (low rank) in the Águilas Basin (from proximal to distal: *Schizoretepora* – rhodolith debris, *Schizoretepora* and *Terebratula* facies).

1990), whereas the latter have the whole clinoform (topset, foreset and bottomset) submerged (Fig. 2C). Moreover, the rollover in subaerial deltas can be coincident with or very close to the shoreline, whereas in subaqueous deltas the rollover is on average several kilometres away from the shoreline.

In a meta-analytical study of clinoform geometry and scale, Patruno *et al.* (2015) differentiated two types of subaqueous delta-scale clinoforms: sand-prone and mud-prone. This distinction is relevant because the former display higher foreset gradients and their rollovers are closer to the shoreline than in the latter (Patruno *et al.*, 2015). The terminology of Patruno *et al.* (2015) focuses on the geometric description of clinoforms. Similar terms related to geometric aspects include 'distally steepened ramp' (Read, 1985) for carbonate environments (see also Pomar, 2001).

Other terms have been proposed following a genetic approach. For example, Hernández-Molina *et al.* (2000) introduced the term 'infralittoral prograding wedge' (IPW) for a morpho-sedimentary system characterized by narrow, shore-parallel, sigmoidal-shaped sedimentary bodies that prograde below the wave base in the offshore transitional zone of wave-dominated coasts. Geometrically, this system belongs to the category of sand-prone subaqueous delta-scale clinoforms of Patruno *et al.* (2015). Such a distinction is helpful because prograding reef platforms also produce subaqueous delta-scale clinoforms (Franseen & Mankiewicz, 1991; Pomar & Ward, 1994; Braga & Martín, 1996; Cuevas-Castell *et al.*, 2007; Kleipool *et al.*, 2017) but the genetic factors and resulting facies are quite different from those of an IPW (Pomar & Kendall, 2008).

Mixed carbonate–siliciclastic 'hybrid' deposits

For mixed carbonate–siliciclastic systems, the term 'hybrid' is often used in the literature to

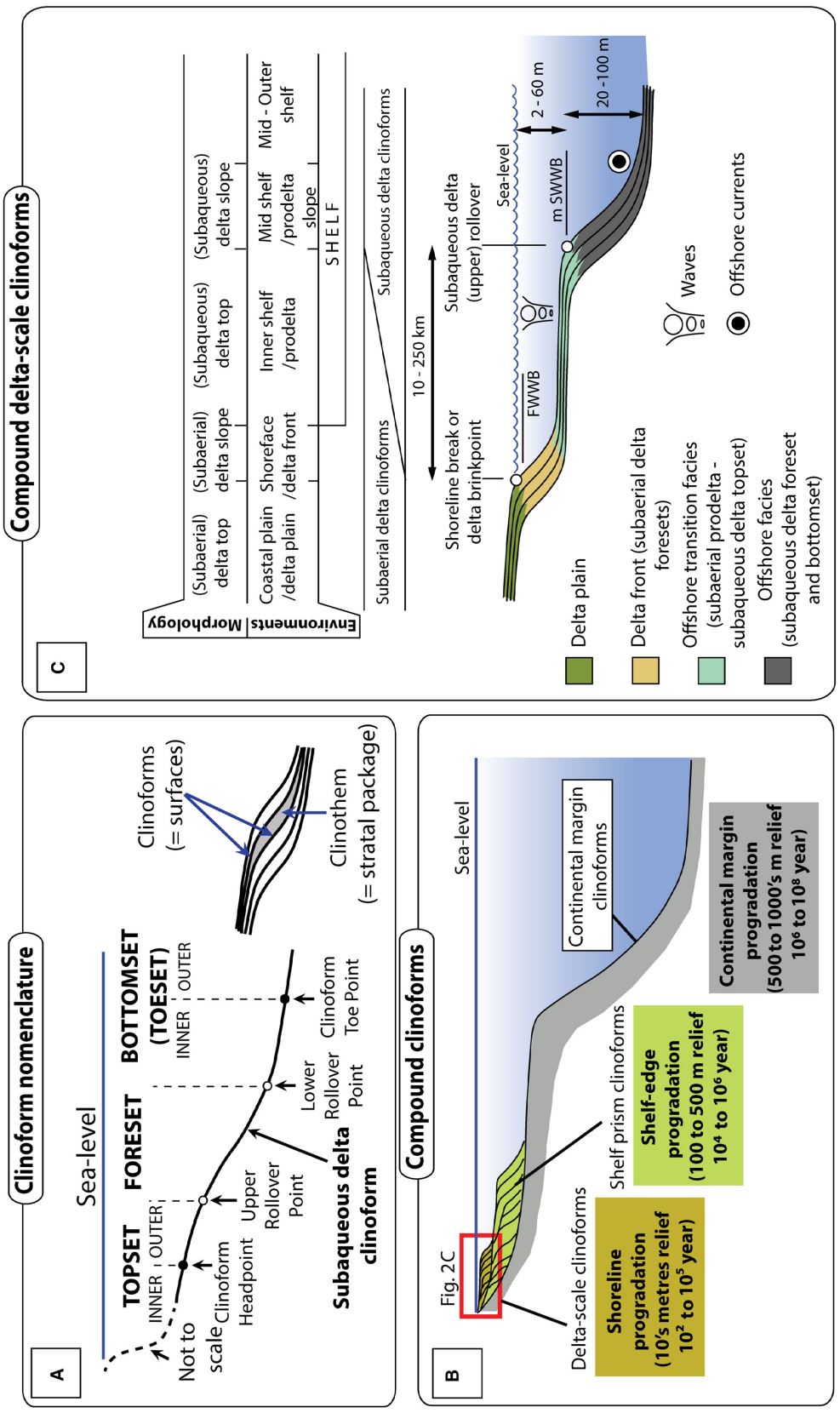

Fig. 2. (A) Terminology for the different parts of a clinoform using a subaqueous delta-scale clinoform (adapted from Patruno *et al.*, 2015). (B) A compound system with subaqueous delta-scale, shelf prism and continental margin clinoforms. The range of relief and progradation rates is indicated in insets (adapted from Patruno *et al.*, 2015). (C) Compound delta-scale clinoform system with either shoreline or subaerial delta-scale, and subaqueous delta-scale clinoforms (adapted from Patruno *et al.*, 2015): m SWWB, mean storm weather wave base; FWWB, fair weather wave base.

quickly convey the mixed character of sediments with fractions of both carbonate and siliciclastic components (Mount, 1984; Flügel, 2004; Tomassetti & Brandano, 2013; Nalin *et al.*, 2016; Zecchin & Catuneanu, 2017). Nalin *et al.* (2016) used this term for mixed deposits with a siliciclastic fraction, in particular, between 20% and 50%.

Synthem

A synthem is an unconformity-bounded unit (Ruban, 2015). In this study, the term refers to the units bounded by the local high rank unconformities.

'Pristine' preservation

This study uses the term 'pristine' as a shortcut to refer to bioclasts that barely display any signs of biostratinomic alteration. These bioclasts are articulated and complete, with well-preserved ornamental features, and have not been subject to macrobioerosion and/or encrustation by epizoan organisms.

GEOLOGICAL SETTING

The Águilas Arc (south-east Spain) (Fig. 3A), which belongs to the Inner Zones of the Betic Cordillera, is a tectonic megastructure that extends onshore over a distance of 60 km along a south-west/north-east axis. The megastructure resulted from a north–south or north-west/south-east rigid-plastic indentation of a crustal block that began in the Early Miocene due to collision of the African and Eurasian plates in the Western Mediterranean and is still active today (Coppier *et al.*, 1989; Griveaud *et al.*, 1990). This arc is delimited to the south-west and north-east by systems of left-lateral and right-lateral strike slip faults (Palomares, Cocón-Terreros and Moreras fault systems) (Coppier *et al.*, 1989; Silva *et al.*, 1993). The internal sector of this arc comprises five small basins that are open to the Mediterranean (Bardají *et al.*, 1999); their opening was probably caused by an important collapse of the southern margin of the arc, associated with transtension (Coppier *et al.*, 1989). These basins probably acted as rias (i.e. estuaries encased in high-relief fluvial valleys) and then as coastal embayments during the early Pliocene (Dabrio *et al.*, 1991; García-Ramos *et al.*, 2014). This study focuses on the south-western sector of the Águilas Basin (Fig. 3B and C), located some 5 km south-west of the town of Águilas, where the succession of Pliocene marine sediments is most complete (Montenat *et al.*, 1978).

STRATIGRAPHIC FRAMEWORK

Pliocene deposits in the current study area can be attributed to three synthems: SP0 (MPl1–MPl2 *pro parte* biozones), SP1 (MPl3 biozone) and SP2 (possibly MPl4) (Fig. 3D). The focus here is on the prograding succession of synthem SP1. The topmost part of SP1 consists of carbonates of an isolated platform abutting a volcanic ledge, that is an entirely different morpho-sedimentary system and therefore beyond the scope of this study (Fig. 3C and D). To provide a stratigraphic framework, SP0, SP1 and SP2 are briefly outlined.

The SP0 synthem is represented by glauconi-rich condensed deposits. At the 14 m thick El Barcelón section (Fig. 3C), beds are oriented N79°E/8°SE. A sharp transgression over metamorphic rocks of the Palomas Unit (Alpujárride Complex, Inner Betic Zones) (Álvarez & Aldaya, 1985) is recorded at the base. Planktonic foraminifera from SP0 indicate the MPl1 and MPl2 biozones of the Mediterranean Pliocene (Montenat *et al.*, 1978; García-Ramos *et al.*, 2012). Based on benthic and planktonic foraminifera, García-Ramos *et al.* (2014) proposed a shallowing upward trend evolving up-section to assemblages of shallow-water benthic foraminifera, devoid of planktonic foraminifera. In this section, the top of SP0 is truncated and overlain by

Fig. 3. Location of the study area in south-east Spain. (A) Tectonic Águilas Arc (modified from Bardají *et al.*, 2001). (B) Detail of the Águilas Basin with indication of outcrops of Pliocene age. (C) Cartographic sketch of the studied sector in the Cañada Brusca area, including Pliocene synthems (SP0, SP1 and SP2), the main facies associations in SP1 (FA1 to FA4), and location of the studied sections or those mentioned in the text. (D) Schematic cross-section of the studied sector to show the relationship of the identified Pliocene synthems, with indication of the studied sections (CA, Cabezo Alto; CBr W, Cañada Brusca W; CBL, Cañada Blanca). Biostratigraphically relevant planktonic foraminiferan taxa indicate the MPl3 biozone (Zanclean) for the whole synthem SP1. Vertical scale exaggerated.

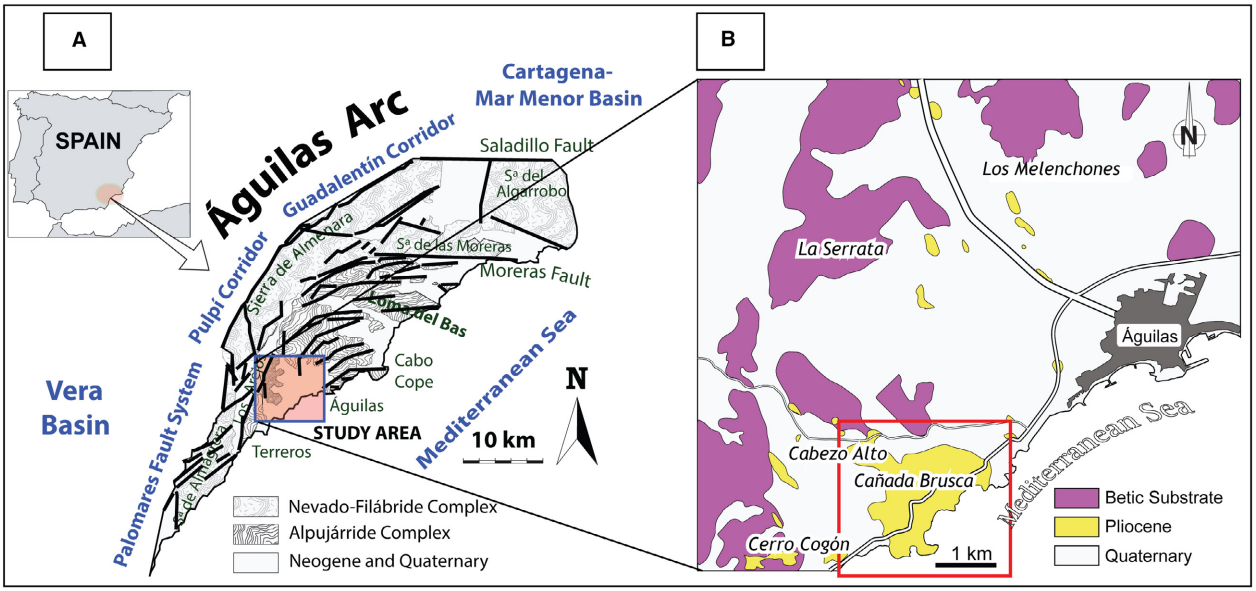

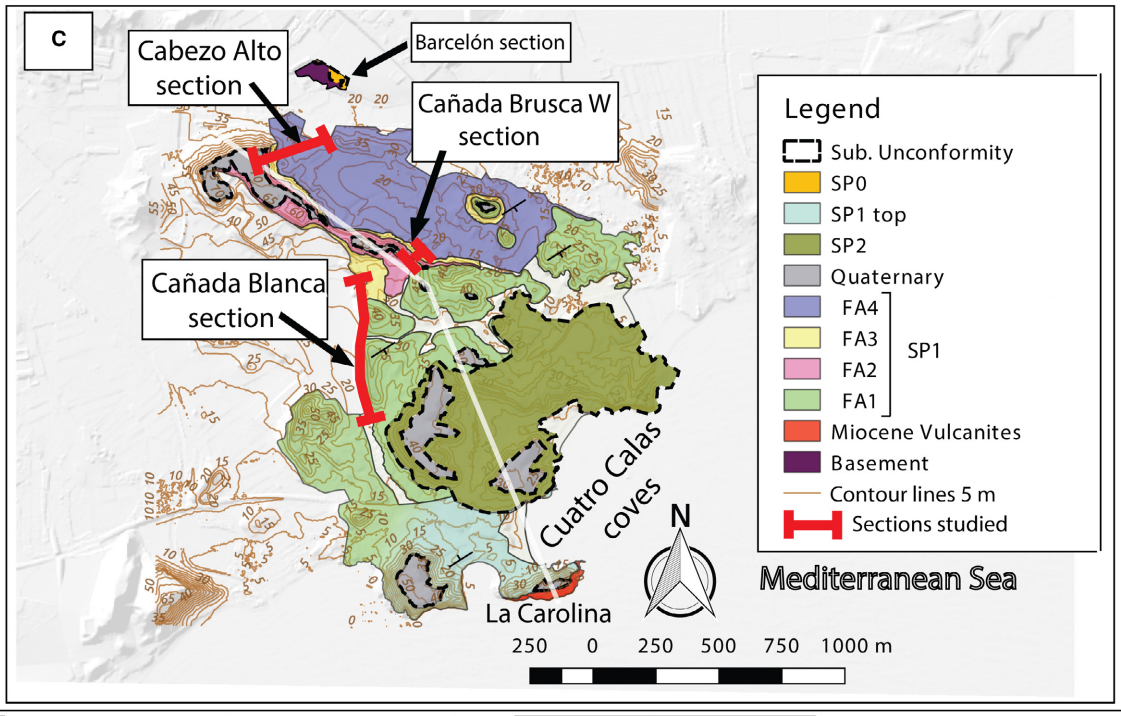

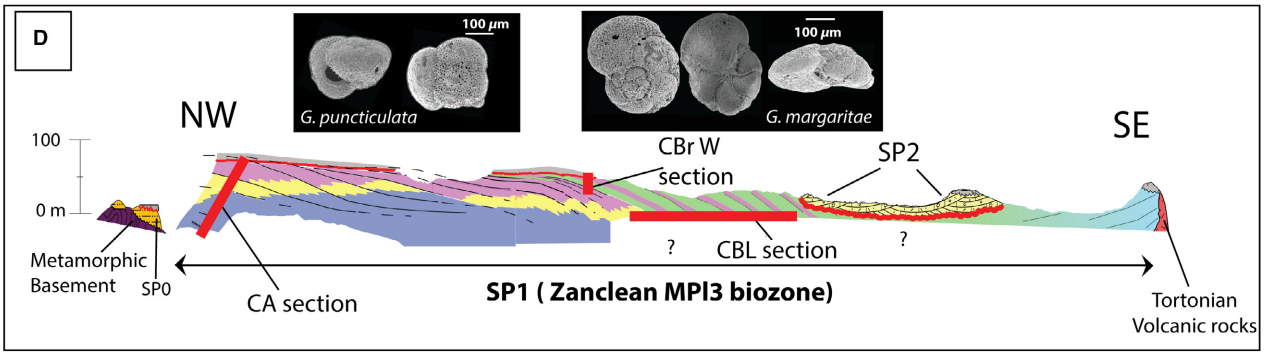

Quaternary conglomerates, and the transition from SP0 to SP1 is not exposed. An angular, erosive unconformity is inferred because of the different strike and dip of the two synthems and a conspicuous shift in benthic and planktonic foraminiferal assemblages from shallow-water to a relatively deep-water, offshore environment between the top of SP0 and the base of SP1. This unconformity crops out in a section northeast of Castillo de Terreros (Montenat *et al.*, 1978) (Fig. S1).

Synthem SP1 consists of a succession of clinobedded units that prograded over a distance of about 2 km starting from the hillock of Cabezo Alto across the area of Cañada Brusca and the Cuatro Calas coves (Fig. 3D). In SP1, clinoforms have a strike of N57°E with a variable dip (a few degrees to over 14°SE) along a northwest/south-east transect. The unconformity between SP1 and SP2 eroded part of the upper interval of SP1, which is either missing on the surface or covered by colluvial deposits. The uppermost part of SP1 crops out again, however, in the Cuatro Calas coves sector (Fig. 3C); there, the top of SP1 is also truncated and overlain by Quaternary conglomerates. The SP2 synthem was described and interpreted as a wave-dominated Gilbert-type delta system (Dabrio *et al.*, 1991): SP2 is also truncated at the top by an unconformity and covered by Quaternary marine and terrestrial units, one of which has been dated to the oxygen isotopic stage 5e based on the occurrence of the gastropod *Persististrombus latus* (Bardají *et al.*, 2001).

Biostratigraphy

The co-occurrence of *Globorotalia puncticulata* and *G. margaritae* from the base to the top of the synthem SP1 (Fig. 3D) indicates that it was deposited entirely during the MPl3 planktonic foraminiferal biozone of the Mediterranean Pliocene (4·52 to 3·81 Myr) (Iaccarino *et al.*, 2007; Violanti, 2012; Corbí & Soria, 2016). Because of truncation at the base and the top of the synthem, the exact duration of SP1 is uncertain, but must be <700 kyr.

MATERIAL AND METHODS

Fluvial incision has revealed laterally continuous outcrops oriented subparallel and subperpendicular to the depositional strike that enabled the stratal geometries and stacking patterns to be studied. Clinoforms and clinothems were mapped using outcrop panoramic photomosaics while stratigraphic contacts and facies were checked in the field. Two main sections (Figs 3C, 3D and 4), 44 m thick (Cabezo Alto) and 77 m thick (Cañada Blanca), were logged in detail, for lithology, sedimentary structures, macrofossil composition, biofabrics and ichnoassemblages to evaluate the vertical variation and stacking of facies. These sections were complemented by smaller sections to show details of stratigraphic features. The macrofauna was identified to species level whenever possible, except for most bryozoans, for which only the zooarial morphology was noted. The abundance of macrofaunal taxa was estimated in the field by distinguishing between dominant (26 to 100%), common (11 to 25%) and rare (1 to 10%) categories. This qualitative approach was conducted by visually inspecting each sampling site for 30 min (cf. time-picking of Ceregato *et al.*, 2007). Skeletal concentrations were described using qualitative criteria (Kidwell *et al.*, 1986), while biofabrics follow the semi-quantitative charts of Kidwell & Holland (1991). Macroscopic descriptions of lithofacies were complemented with representative thin sections. Some bulk samples of uncemented sediment were sieved through 500 μm, 125 μm and 63 μm meshes to explore qualitatively the content of benthic and planktonic foraminifera in the 125 μm fraction, to aid in a palaeoenvironmental interpretation and biostratigraphic characterization of the studied synthem. For 26 samples of the Cabezo Alto section, >200 benthic foraminifera were identified and counted. Taxa with >3% proportional abundance are reported.

Magnetic susceptibility, a proxy of terrigenous input (Davies *et al.*, 2013), was measured in the field, with a SM-20 magnetic susceptibility meter (Gf Instruments, Brno-Medlénky, Czechia) for the Cabezo Alto (34 sampling sites) and Cañada Blanca (68 sampling sites) sections. Five to six replicate measurements per sampling site (*ca* 1 sec measuring time) were taken on flat rock surfaces, and the mean value reported.

Carbonate content was quantified at the Institute of Geography and Regional Research (University of Vienna) with a Scheibler calcimeter for 34 samples in the Cabezo Alto section and 48 samples at the Cañada Blanca section. The procedure specified in ISO 10693:1995 has been followed (ÖNORM L 1084, 2006).

Glauconite maturity has been categorized into four stages, based on the K_2O content (Amorosi

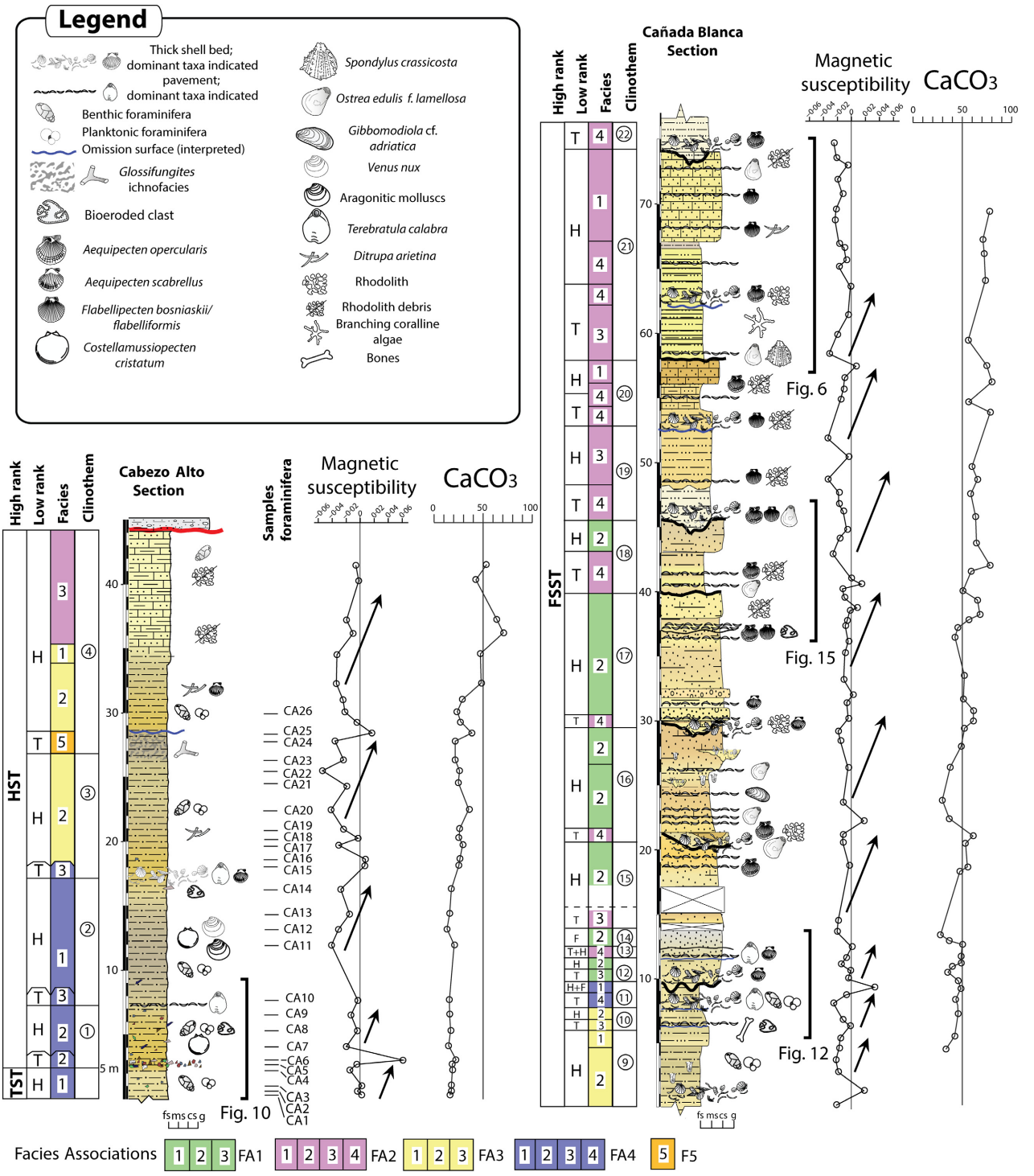

Fig. 4. Stratigraphic logs of the CA (clinothems 1 to 4) and CBL (clinothems 9 to 22) sections. The interpreted systems tracts of the high rank and low rank cycles are included, the latter with abbreviated letter codes; T (transgressive), H (highstand), F (falling stage) and L (lowstand). Numbers indicate the facies types of four facies associations (FA), the latter noted by colour code. The position of benthic foraminifera samples from the CA section is indicated. Skeletal concentrations were simplified to pavements and thick shell beds (dominant taxa indicated by the corresponding icon in the legend). Magnetic susceptibility and carbonate content trends are included. Possible cyclicity indicated by arrows. For a magnified zoom view of the interval including clinothems 9 to 14, see Fig. 12. TST or T, transgressive systems tract; FSST or F, falling stage systems tract; HST or H, highstand systems tract.

et al., 2007; Amorosi, 2012): (i) nascent (K_2O = 2 to 4%); (ii) slightly evolved (K_2O = 4 to 6%); (iii) evolved (K_2O = 6 to 8%); and (iv) highly evolved (K_2O > 8%). Glauconite K_2O content and colour are correlated: nascent to slightly evolved glauconite is light green – yellowish, mature glauconite is dark green. Glauconite composition was examined in one sample to determine its maturity. About 80 to 100 grains were picked from the 125 to 500 μm fraction, embedded in resin and polished on a slide. Glauconite analyses were performed at the Department of Lithospheric Research (University of Vienna) using a Cameca SXFive FE Electron Probe Microanalyzer (EPMA; CAMECA, Gennevilliers Cedex, France) equipped with five wavelength-dispersive and one energy-dispersive spectrometers. Well-characterized homogeneous natural and synthetic minerals were used as standards. All analyses were performed at 15 kV accelerating voltage and 20 nA beam current. Due to the K migration a defocused beam with 5 μm diameter and 10 sec counting time on peak position were used. For matrix corrections, the PAP method (Pouchou & Pichoir, 1991) was applied to all acquired data. The relative error of the laboratory internal standard is below 1%.

DESCRIPTION OF FACIES

Four main facies associations and one facies were recognized in the studied synthem. These are described in detail in Tables 1 to 4. Facies distributions are shown in stratigraphic logs and outcrop photomosaics to highlight vertical and lateral changes. In general, the facies grade into one another along a proximal-distal gradient.

Facies Association 1

The common feature of Facies Association 1 (FA1) is the occurrence of coarse-grained siliciclastics. Three facies are distinguished based on sorting, carbonate matrix and packing of macroinvertebrates.

Coarse-grained friable sandstone – F1.1
This facies was observed in only two clinothems of the Cañada Brusca W area. It consists of friable sandstone composed of well-sorted, coarse, angular grains (mainly of quartz and schists) (Fig. 5A and B). This sandstone is poorly cemented and pervasively bioturbated, therefore no physical sedimentary structures are preserved. In proximal parts it displays an intensely bioturbated ichnofabric dominated by vertically oriented *Macaronichnus* and subsidiary *Ophiomorpha* (Fig. 5A and D to H). It yields abraded and fragmented microfossils in low abundance, including ostracods (for example, *Aurila*) and benthic foraminifera, most notably *Elphidium crispum* and *Ammonia inflata* (Table 1).

Hybrid rhodolithic sandstone – F1.2
This facies mainly occurs in the Cañada Blanca section and the Cañada Brusca W sectors (Fig. 5I and J), in more distal positions than F1.1. It consists of poorly sorted coarse sandstone with a carbonate matrix. Granule-sized debris of coralline red algae is characteristic, albeit in varying proportions. The fabric in general is massive; locally, well-defined trace fossils are identifiable (Table 1).

Shell-rich hybrid sandstone – F1.3
This facies occurs in the Cañada Blanca section (clinothem 12). The matrix resembles that of F1.2 but it is distinguished by thick (>1 m), densely packed skeletal concentrations dominated by pectinids (*Aequipecten scabrellus*). It also displays a complex biofabric, with large gutter casts infilled with pectinids, and overlies an irregular erosive surface.

Interpretation of Facies Association 1
The well-sorted and winnowed texture of the coarse sands, selectively enriched in detrital quartz (Fig. 5B), suggests proximal environments affected by tidal and wave currents above the fair-weather wave base (Blomeier *et al.*, 2013). This interpretation is supported by the lateral facies change, in which beds displaying proximal facies F1.1 evolve distally into poorly-sorted and unwinnowed coarse sandstone facies F1.2 (Fig. 5I and J). The association of *Ophiomorpha* and dominant *Macaronichnus* in similar lithofacies (Fig. 5D to F) has been interpreted as either foreshore or upper shoreface environments (Frébourg *et al.*, 2012; Mayoral *et al.*, 2013; Uchman *et al.*, 2016). This is compatible with the impoverished benthic foraminiferal assemblage, with the poorly preserved shallow shelf species *Elphidium crispum* and *Ammonia inflata* (Sgarrella & Moncharmont Zei, 1993; Fiorini & Vaiani, 2001; Rasmussen, 2005). The low species richness, abundance and high taphonomic alteration of these microfossils can be

interpreted as an indication of onshore transportation (Davaud & Septfontaine, 1995). The dominance of *Flabellipecten bosniaskii* in some patches of facies F1.2 (Table 1) is consistent with proximal sandy environments (Aguirre *et al.*, 1996). The lack of physical sedimentary structures is most probably due to thorough bioturbation and/or cryptobioturbation (Pemberton *et al.*, 2008).

Facies Association 2

The main characteristic of Facies Association 2 (FA2) is the fine-grained carbonate-rich matrix ($CaCO_3$ *ca* 40 to 80%) (Fig. 4) and the frequent presence of coralline algae, either in the form of complete rhodoliths or rhodolith debris.

Calcarenite – F2.1
In contrast to other facies, this was found only in the upper two clinothems (Fig. 6A and B). The coarse-grained, well-sorted fabric is similar to F1.1 but is composed of carbonate lithoclasts. Small casts, probably of comminuted aragonitic shells, are visible. This facies is locally crudely stratified and can contain pavements of *Flabellipecten* and *Ostrea* (Table 2; Fig. 6). It has variable proportions of rhodolith debris and is pervasively bioturbated, with poorly defined trace fossils, except for intervals with well-defined *Thalassinoides* (Fig. 6B).

Hybrid rhodolithic calcirudite – F2.2
This facies only occurs locally, associated with F2.3. It consists of calcirudite mostly composed of rhodolithic debris and pectinids. It is often found infilling pods (like the ray pit trace *Pischichnus waitemata*). In clinothem 8, it forms a wedge, laterally interdigitating with facies F3.1.

Hybrid rhodolithic floatstone – F2.3
This facies is characteristic of the whole study area. The matrix consists of fine-grained siliciclastic material and micrite in variable proportions (up to 80% carbonate content). The dominant bioclastic material is rhodolith debris, which varies from coarse-grained to gravel size, but complete rhodoliths also occur and one locality exhibits pavements (Fig. 7). It is pervasively bioturbated with variable ichnoassemblages (Table 2); hence only one example of swaley cross-stratification (SCS) has been identified (Fig. 5K). In clinothem 21, however, it displays a crude stratification, forming tabular beds about 30 to 40 cm thick. The most characteristic macroinvertebrates are *Clypeaster* cf. *aegyptiacus* (often as complete tests), *Spondylus crassicosta* (often articulated), *Ostrea edulis* f. *lamellosa* and *Gigantopecten latissimus* (juveniles and adults). In some samples, coralline algae attributable to lithophylloid and melobesioid taxa were identified (Fig. 7D to F).

Shell-rich hybrid rhodolithic floatstone – F2.4
This is similar to F2.3 but contains densely packed concentrations of pectinids (*Aequipecten opercularis*) and rhodoliths and locally also *Ostrea* and *Spondylus*. This facies usually forms very thick (several metres) beds, often overlying an erosive or irregular surface. Coralline algae are sometimes present as rhodoliths or represented by small proportions of rhodolith debris.

Interpretation of Facies Association 2
The well-sorted, winnowed texture and coarse grain-size of F2.1, together with the dominance of *Flabellipecten* and *Ostrea*, points to high-energy proximal environments (Aguirre *et al.*, 1996; Blomeier *et al.*, 2013). The reduced grain-size of siliciclastics in F2.3 and F2.4 points to lower energy levels compared to FA1. The abundance of rhodoliths (Fig. 7) suggests background low-moderate energy conditions, good oxygenation, low sedimentation rates and low turbidity enabling suitable light penetration; the assemblage of melobesioids and lithophylloids (Fig. 7D to F) suggests depths in the order of several tens of metres (Aguirre *et al.*, 2012, 2017). Moreover, the characteristic macroinvertebrate species in this facies (Table 2; Fig. 5A) are common in shoreface environments (Malatesta, 1974; Ben Moussa, 1994; Mancosu & Nebelsick, 2017).

Swaley cross stratification (Fig. 5K) indicates storm deposition events (e.g. Myrow, 2005) in the offshore transitional zone (Dumas & Arnott, 2006). The occurrence of sporadic densely packed lenticular shell beds (Fig. 5), probably the product of 'cut and fill' structures, also points to major storm events (Zecchin *et al.*, 2017). The ichnoassemblage of F2.3 (*Ophiomorpha nodosa*, *Skolithos linearis* and *Planolites montanus*) (Table 2), combined with the features discussed above, is interpreted here to indicate an opportunistic response associated with storms or other high-energy disturbances (Pemberton *et al.*, 1992; Gani *et al.*, 2009; Buatois *et al.*, 2015), although individual ichnotaxa can occur under normal marine conditions. In the first scenario, *Palaeophycus* can be characteristic

Table 1. Main sedimentological and palaeontological features of Facies Association 1.

Facies	Lithology	Sedimentary structure	Ichnology	Macrofossils and taphonomy	Biofabric	Interpretation
F1.1	Coarse-grained, friable sands; moderately well-sorted; angulose grains, mainly of quartz, subordinately of schists and mica. Slightly cemented by sparite grains. Highly porous	Massive fabric	Intense bioturbation possibly responsible for the massive fabric. Only patches with preserved burrows of *Ophiomorpha* (BI = 3 to 6) associated with subvertically oriented *Macaronichnus* isp. traces. Low ichnodiversity	Strongly dominated by disarticulated, slightly fragmented valves of *Flabellipecten bosniaskii*. Subordinate articulated *Spondylus crassicosta*; fragmented *Ostrea edulis*, scarce rhodoliths, rare *Aequipecten scabrellus*	Barren to dispersed. In more distal parts there might be patches with densely packed *Flabellipecten* valves	Ichnofabrics with *Ophiomorpha* and *F. bosniaskii* indicate an upper shoreface. The *Ophiomorpha–Macaronichnus* ichnofabric, combined with the coarse-grained, well-winnowed sands, has been documented from upper-shoreface to foreshore settings. Microfossils are scarce and poorly preserved. Assemblage dominated by *Elphidium crispum* and *Ammonia inflata*. Subordinate taxa include: *Cibicidoides lobatulus*, *Neoconorbina terquemi*, *Reussella spinulosa* and *Spiroplectamina saggitula*. These taxa are typical of shallow water environments (Rasmussen, 2005)
F1.2	Hybrid grainstone and coarse-grained sand, poorly sorted (siliciclastic grains similar to those of F1.1). Small rhodolith fragments may be abundant. Poorly cemented; porous. This subfacies encompasses transitional types where the grain size of siliciclastic grains and proportion of carbonate matrix vary across a	Massive fabric	Intense bioturbation possibly responsible for the massive fabric. Burrows rarely preserved; attributable to *Ophiomorpha* and *Thalassinoides paradoxicus*. BI = 1 to 3	Occasional small aragonitic molluscs preserved as stein-kerns (shell hash). Macro-fossils scarce: disarticulated, abraded and bioeroded (*Entobia* isp.) shells of the dominant taxa *F. bosniaskii* and *A. scabrellus*. Rare *Pecten jacobaeus*. Complete rhodoliths occur rarely dis-persed in the matrix. The most distal subfacies types contain steinkerns of solitary corals (*Flabellum* sp.). Steinkerns of *Bulla* sp. are rare. Abraded small fragments of *Clypeaster* cf. *aegyptiacus* are common. Rare, nodular, massive zooaria of Celleporarian bryozoans. Tubes of *Ditrupa arietina* locally abundant. Rare *Schizechinus serialis*, *Spatangus*	Dispersed to loosely packed	This facies occurs in the top set, representing the middle shoreface. During forced regression, siliciclastic grains are transported down the foreset, mixing with reworked carbonate mud and bioclasts

Table 1. (continued)

Facies	Lithology	Sedimentary structure	Ichnology	Macrofossils and taphonomy	Biofabric	Interpretation
	proximal–distal gradient			*purpureus*, *Echinocyamus pusillus*, *Echinolampas sp. Cosmopolitodus hastalis/Isurus oxyrinchus*, *Sparus* sp., *Pinna* sp. Large acorn barnacles (*Concavus concavus*) occasionally encrusting echinoids, large bones, or large oysters in clusters of a few individuals		
F1.3	Matrix similar to F1.2 but rich in pectinids	Massive fabric	May contain poorly defined traces attributable to *Thalassinoides* isp	Dominated by diarticulated *Aequipecten scabrellus*, often complete valves. Different degrees of encrustation. Low bioerosion. Additional subsidiary taxa include *Cubitostrea frondosa* and *Spondylus crassicosta*	Densely packed, often infilling small channel-like structures, gutter casts and pods	Concentration of shoreface shells by storm-reworking and winnowing during forced regression. This facies is found only in clinothem 12 at the CBL section

of the fair-weather assemblage (Pemberton *et al.*, 1992). Finally, the rhodolith–pectinid rudstone infilling *Piscichnus* traces suggests trapping in burrows by passive filling when coarser particles are entrained during storm traction–transport (Wanless *et al.*, 1988; Zuschin & Stanton, 2002; Yesares-García & Aguirre, 2004).

The complex biofabric of thick, densely packed skeletal concentrations (facies F2.4) overlying erosive surfaces, together with the observation that they overlie FA1 (Fig. 5C to E) or F2.1 (Fig. 6), suggests that this facies formed under conditions of sediment bypass or starvation, promoting the amalgamation of event beds during transgressive phases (Kidwell, 1991; Abbott, 1997; Dattilo *et al.*, 2008; Zecchin *et al.*, 2017). They are therefore interpreted as onlap shell beds in line with conclusions drawn by Kidwell (1991) and Zecchin *et al.* (2017) elsewhere. The absence of physical sedimentary structures is interpreted here to be a result of thorough bioturbation. According to Zecchin (2007), this trait is typical of sheltered embayments.

Facies Association 3

The characteristic feature of Facies Association 3 (FA3) is the occurrence of the serpulid polychaete *Ditrupa arietina* in a fine-grained hybrid matrix. The carbonate content varies between about 30% and 50% (Fig. 4).

Hybrid packstone with Ditrupa and rhodolith debris – F3.1

Facies F3.1 is transitional between Facies Associations 2 and 3. It consists of hybrid fine-grained packstone to grainstone with small fragments of rhodolith debris. The main feature is the much smaller proportion of rhodolith debris compared to FA2. Locally it contains *Ditrupa*, pectinids or fragments of adeoniform zooaria (*Schizoretepora* sp.). Because of the high carbonate content (*ca* 50% $CaCO_3$), cementation locally defines beds varying from 30 to 40 cm to over 1 m in thickness. The fabric is massive.

Hybrid packstone with Ditrupa – F3.2

This is the most characteristic facies of FA3. *Ditrupa* is the dominant macroinvertebrate, often passively infilling pods (Fig. 8A) or forming loosely to densely packed concentrations. The grain-size of terrigenous particles is fine-grained and poorly sorted. *Macaronichnus – Teichichnus* and other traces are characteristic (Table 3). The bedding is completely disrupted by

Table 2. Main sedimentological and palaeontological features of Facies Association 2.

Facies	Lithology	Sedimentary structure	Ichnology	Macrofossils and taphonomy	Biofabric	Interpretation
F2.1	Coarse-grained calcarenite	Massive to crudely stratified in decimetre thick beds	Dominated by indistinct mottling. Well-defined *Thalassinoides* occur patchily. BI = 4 to 5	Dominated by complete, mostly disarticulated, complete valves in paucispecific beds. Either dominated by *Flabellipecten flabelliformis* or *Ostrea edulis*. Complete, rare *Ova canalifera*, *Clypeaster* cf. *aegyptiacus*, *Hinnites crispus*, and sparse rhodolith debris and/or complete rhodoliths; *Ditrupa* tubes may also occur	Molluscs occur in thin, densely packed pavements; convex-up orientation. Echinoids occur dispersed. The biofabric is otherwise dispersed	High-energy shallow-water environment (upper shoreface). The pavements with convex-up shells are similar to wave/current-winnowed shell bed taphofacies of Hendy *et al.* (2006)
F2.2	Hybrid rhodo lithic calcarenite/ calcirudite	Massive fabric	Discrete traces (BI = 1 to 2). Passively infilled with mud, vertical burrows dominate (*Skolithos* isp., *Ophiomorpha* isp.)	Dominated by small fragments of rhodoliths (rhodolith debris) and disarticulated, complete pectinids. *A. scabrellus*, common. Rare *Gigantopecten latissimus*, *Pecten jacobaeus*, *Gibbomodiola* cf. *adriatica*, *Talochamys multistriata*. Rare steinkerns of gastropods; rare epitoniid gastropods. Locally common *D. arietina*	Loosely packed	This facies occurs in the topset, often passively infilling *Piscichnus waitemata* traces. It also occurs as lenses in the upper portion of the foreset during forced regression, resulting from reworking and differential winnowing of fines under high-energy conditions, probably storms
F2.3	Hybrid rhodolith debris floatstone. Matrix of fine-grained mixed siliciclastic sand (poorly sorted) and carbonate mud	Massive fabric. Rare SCS	Variable intensity of bioturbation. BI = 1 to 5. Normally highly bioturbated. *Piscichnus waitemata* common in the first clinothems. *Thalassinoides* dominates the ichnofabrics in some clinothems. In others, *Ophiomorpha nodosa* and *Planolites montanus* or ?*Asterosoma* isp. cf. *ludwigae* dominate, with subordinate *Palaeophycus tubularis*, *Skolithos linearis*.	Dominated by rhodolith debris to complete rhodoliths. Disarticulated but complete *A. scabrellus* is frequent to abundant. Characteristic taxa are scarce *S. crassicosta* (often articulated); disarticulated, bioeroded *Gigantopecten latissimus*; rare *Calpensia nobilis* bryoliths; large disarticulated, bioeroded *Ostrea edulis*; fragments of *C.* cf. *aegyptiacus* (seldom complete tests). Scarce *P. jacobaeus*, *F. bosniaskii*, *Eucidaris desmoulinsi* (spines and disarticulated	Dispersed to loosely-packed. Except for pods and lenses with densely packed bioclast concentrations. Shell concentrations with a complex internal structure, random orientation of valves, occasionally with a trend to being concordant with the bedding plane, either con-	This facies is typical of the outer topset (lower shoreface). Some samples contain *Elphidium* sp. (thin sections) and *Planorbulina mediterranensis* (encrusting pectinids). A qualitative sample additionally contained *Biasterigerina planorbis*, *Cibicidoides lobatulus*, *Rosalina bradyi*, typical of inner shelf vegetated, sandy detritic bottoms (Sgarrella & Moncharmont Zei, 1993; Rasmussen, 2005). SCS suggests storm events in the

Table 2. (continued)

Facies	Lithology	Sedimentary structure	Ichnology	Macrofossils and taphonomy	Biofabric	Interpretation
			Sporadic *Diplocraterion parallelum*, *Cylindrichnus concentricus*. Some intervals are exclusively dominated by *Thalassinoides* isp.	ambulacral plates), S*chizechinus serialis*, *Spatangus purpureus*, *Arbacina romana*. Large shells are heavily bioeroded (most common traces are *Entobia* isp., subordinately *Caulostrepsis taeniola* and *Maeandropolydora* isp.)	cave-up or convex-up. Frequent examples of stacking and imbrication patterns (concave-up vertical stacking), rounded floating granules and clasts, and pod concentrations. In general, valves complete, disarticulated (except for *Spondylus crassicosta*)	OTZ. The densely packed lens-like skeletal concentrations are interpreted as shelly tempestites
F2.4	Shell-rich hybrid rhodolithic floatstone. Matrix as in F2.3	Massive fabric	Indistinct mottling in massive matrix	Dominated by disarticulated, complete to fragmented molluscs: *Aequipecten*, *Flabellipecten* or *Ostrea* and *Spondylus*; complete rhodoliths occasionally abundant. Additional uncommon to rare taxa may include bone fragments, steinkerns of gastropods, large acorn barnacles, menbraniporiform zooaria encrusting shells, massive celleporarian zooaria, *Pecten jacobaeus*, *Gigantopecten latissimus*, vermitid gastropods, *Flabellum* sp., *Cubitostrea frondosa*, *Hyotissa* sp., *Eucidaris desmoulinsi* plates and spines and mostly disarticulated *Terebratula*. Large shells heavily bioeroded (mostly *Entobia* isp.)	Thick beds (up to 2 to 3 m), with densely packed skeletal concentrations with concordant to chaotic orientation	When this facies overlies F2.1 or F1.2 through an erosive surface, it is interpreted as a low rank onlap shell bed formed under low sedimentation rates, and subject to multi-episodic biotic and hydraulic reworking

Table 3. Main sedimentological and palaeontological features of Facies Association 3.

Facies	Lithology	Sedimentary structure	Ichnology	Macrofossils and taphonomy	Biofabric	Interpretation
F3.1	Hybrid packstone/grainstone and medium-sized siliciclastic sand	Massive fabric. Sometimes crudely stratified beds 30 to 50 cm thick	Poorly bioturbated (BI = 1). Indistinct mottling. Occassionally, isolated *O. nodosa* traces	Small rhodolith fragments rather less abundant than in previous facies. Macrofossils scarce to common: fragments of adeoniform bryozoan colonies (*Schizoretepora* sp. and other unidentified taxa), *D. arietina*, *A. scabrellus*, rare *P. jacobaeus*, *C. frondosa*, acorn barnacles	Dispersed to loosely packed	This facies occurs in the upper foreset close to the rollover zone during highstand. A qualitative micropalaeontological sample contained scarce foraminifera, with dominant *Biasterigerina planorbis, Elphidium crispum, Cibicides refulgens*; subordinate *Dentalina* sp., *Uvigerina bononiensis*, *Hanzawaia boueana, Cibicidoides lobatulus;* very rare planktonics: *Globorotalia puncticulata, Globigerinoides obliquus, Globigerina bulloides.* The foraminiferal assemblage is typical of shallow shelf environments. *Uvigerina* and *Hanzawaia* indicate deeper settings, and organic-rich muddy substrates (Rasmussen, 2005). This facies is transitional to F2.3 proximally and F3.2 distally
F3.2	Hybrid packstone–fine-grained sand	Massive fabric	Proximal–distal gradient with bioturbation intensity and ichnodiversity increasing distally. Poximal (BI = 1): barren or rare isolated *O. nodosa*. Middle (BI = 1 to 3) *Macaronichnus segregatis – Palaeophycus heberti*, with subordinate *O. no dosa*, *Planolites montanus*, rare	Most characteristic in the oldest clinothems: *D. arietina*, often infilling pods. In distal sites a diverse calcitic assemblage can include complete, mainly disarticulated tests/valves, sometimes encrusted by bryozoans, cirripedes or ser pulids, good preservation of ornamental details: *A. scabrellus*, *T. multistriata*, *Hinnites crispus*, *Flexopecten flexuosus*,	Loosely packed within clinothem, except for pod concentrations, often of *Ditrupa*	High sedimentation rates due to frequent siltation events and storm induced high-density gravity flows, in the foreset. Episodically organic rich substrates trigger opportunistic responses from taxa like *Ditrupa arietina*, and benthic foraminifera like *Cassidulina carinata*, *Bolivina* spp., *Bulim ina aculeata*, *Globocassidulina subglobosa*. Decreased level of siltation distally favour more densely bioturbated ichnofabrics

Table 3. (continued)

Facies	Lithology	Sedimentary structure	Ichnology	Macrofossils and taphonomy	Biofabric	Interpretation
			Cylindrichnus concentricus, *Palaeophycus tubularis*. Distal (BI = 5 to 6): complex tiering, dominated by indistinct mottling. Discrete burrows dominated by *M. segregatis*, subordinately by *Teichichnus rectus* and unidentified, meniscate, back filled traces (?*Scolicia* isp.). Occasional traces: *C. concentricus*, *Diplocraterion* isp., *Scalichnus* isp. cf. *sursumdeorsum*, and rare isolated tubes of *Schaubcylindrichnus coronus*	*Limaria tuberculata*, *Gibbomodiola* cf. *adriatica*, *Pinna* sp., *Anomia ephippium*, *Cubitostrea frondosa*, *Scalina bronni*, *Epitonium* cf. *turtoni*, *Epitonium frondiculoides*, *Epitonium clathrus*, *Cirsotrema lamellosa*, *Cirsotrema pumiceum*, *Stenorhytis retusa*, *Concavus concavus*, *Solidobalanus mylensis*, *A. opercularis*, *Costellamussiopecten cristatum*, *Neopycnodonte cochlear*, *A. romana*, *S. serialis*, *Ova canalifera*, ambulacral plates and spines of *E. desmoulinsi*. In shell beds, there are casts of infaunal bivalves: venerids, cardids, nuculanids; rare *Nototeredo* sp. (*Teredolites* isp.). Some of the above and the following probably transported from shallower settings: small, abraded fragments of *Clypeaster* sp., *P. jacobaeus*, celleporarian and vinculariiform bryozoan colonies, *Calpensia nobilis* bryoliths, *F. bosniaskii*, *G. latissimus*		

Table 3. (continued)

Facies	Lithology	Sedimentary structure	Ichnology	Macrofossils and taphonomy	Biofabric	Interpretation
F3.3	Shell-rich hybrid packstone	Massive fabric	No traces identified	Dominated by disarticulated, complete and well-preserved valves of *A. scabrellus*, fragments of adeoniform zooaria (*Schizoretepora* sp.), or disarticulated valves of *Gibbomodiola* cf. *adriatica*; other aragonitic bivalves are subsidiary	Skeletal concentrations can form (matrix-supported, densely packed *Aequipecten scabrellus*; clast-supported densely packed *Gibbomodiola* cf. *adriatica*, *Pinna* sp. and other aragonitic bivalves), and loosely to densely packed fragments of adeoniform zooaria (*Schizoretepora* sp.). Nesting and stacking patterns are frequent (concave-up vertical stacking). The *Gibbomodiola* bed thickens distally (*ca* 2 m thick) without erosive surface at the base or at the top	Typical of foreset settings. Assemblages dominated by suspension feeders interpreted to reflect a decrease in sedimentation rates. In proximal settings of this facies, densely packed biofabric and erosive surface may reflect differential winnowing and reworking by storm-induced currents

Table 4. Main sedimentological and palaeontological features of Facies Association 4 and Facies 5.

Facies	Lithology	Sedimentary structure	Ichnology	Macrofossils and taphonomy	Biofabric	Interpretation
F4.1	Hybrid packstone –fine-grained sand	Massive fabric	Variable intensity of bioturbation (BI = 1 to 5). Dominance of lined bur rows: *Cylindrichnus concentricus*, *Ophiomorpha nodosa* (burrows with a diameter about 3 cm), less frequent *Schaubcylindrichnus coronus, Skolithos linearis*, *Palaeophycus tubularis*. Also *Planolites* isp., *Trichichnus linearis* and unidentified meniscate traces (?*Scolicia* isp.) in some clinothems	Paucispecific assemblage dominated by complete, disarticulated valves of *Costellamussiopecten cristatum*. Aragonitic molluscs (*Venux nux*, *Ficus* sp.) or solitary corals are dissolved but are preserved as steinkerns. Macroscopic benthic foraminifera are frequent: *Pyramidulina raphanistrum* and keeled *Lenticulina* spp. (*L. calcar*, *L. cultrata*, *L.* cf. *iota*)	Packing is barren to dispersed	In general, lower sedimentation rates than in foreset facies. Dominance of dwelling burrows point to background stable conditions with occasional high-density gravity flows that deliver outsized floating clasts and allochthonous shells from proximal environments. These events can trigger the response of deposit feeders (*Planolites* isp., ?*Scolicia* isp.)
F4.2	Paraconglomerate of floating metamorphic and bioclasts. Hybrid packstone–fine-grained sand matrix	Massive fabric	Numerous ferriginized subvertical traces and indistinct mottling. Also a similar assemblage as in F4.1	Most macrofossils are disarticulated. Mixture of complete, pristine shells and fragmented, bioeroded and encrusted ones. Characteristic and frequent macroinvertebrate taxa are: *Costellamussiopecten cristatum*, *Venus nux*, *Aequipecten opercularis*, *Flabellipecten bosniaskii* and *Cubitostrea frondosa*. The latter three are interpreted as transported from shallower settings and bear frequent encrustation by *Planorbulina mediterranensis*, *Cibicidoides lobatulus* and bryozoans. Also often bioeroded by clionaid sponges (*Entobia* isp.). Less frequent to rare taxa include: fish vertebrae, shark teeth (*Cosmopolitodus hastalis – Isurus oxyrhinchus*), crustacean dactylopodes, epitoniid gastropods (*Cirsotrema lamellosa*, *Stenorhytis retusa*, *Epitonium pseudoscalare*), bivalves (*Flex opecten flexuosus*, *Flexopecten*	Dispersing upward packing pattern, matrix-supported densely packed at the base of the paraconglomerate, to dispersed packing at the top	High rank backlap clast bed (maximum flooding zone). Similar to model III of Kidwell (1985). The bioclasts of species that occur characteristically in FA1 and FA2 are interpreted as allochthnous. These can include highly altered or well-preserved shells, as a result of being entrained in cohesive debris flows

Table 4. (continued)

Facies	Lithology	Sedimentary structure	Ichnology	Macrofossils and taphonomy	Biofabric	Interpretation
				glaber, *Talochlamys multistriata*, *Mimachlamys angelonii*, *Pseudamussium clavatum, Pecten jacobaeus, Limaria tuberculata, Neopycnodonte cochlear*), gastropods (*Aporrhais* sp. cf. *uttingeriana*, *Antisabia* sp.), echinoids (ambulacral plates and spines of *Eucidaris desmoulinsi* and other cidarids; fragments of *Ova canalifera*). Rare solitary corals (*Flabellum* sp.)		
F4.3	*Terebratula* pavements. Hybrid packstone – fine-grained sand matrix	Massive fabric	Indistinct mottling	Brachiopods occur in discrete levels about 10 to 20 cm thick, almost monospecific (mostly *Terebratula calabra,* and sometimes rare *Aphelesia bipartita*). More than 50% of specimens are articulated, complete, with well-preserved ornamental details. Barely microbioeroded or bioeroded (*Podichnus obliquus*). Rarely encrusted (*Concavus concavus*, and *Monia patelliformis*)	The terebratulid pavements dis play variable density of individuals possibly according to a proximal distal gradient, varying from loose to densely packed in the toesets. Clusters of two to four specimens are common	Low background sedimentation rates associated with pulses of relative sea rise facilitate development of terebratulid palaeocommu nities. These pavements are interpreted as mixed depos its (within habitat time-averaged and census assem blages extirpated by siltation)
F4.4	*Terebratula* biostrome. Hybrid packstone – fine-grained sand matrix	Massive fabric	*Glossifungites* ichnofacies dominated by *Thalassinoides suevicus*, with rare *Taenidium barretti* and *Skolithos linearis.* Also lined burrows *(Skolithos* isp. or *Ophiomorpha* isp.). The '*Terebratula* biostrome' contains a diversity of bioerosion traces with high dominance of *Entobia* isp., and less frequent *Podichnus obliquus*,	The '*Terebratula* biostrome' yields additional species of brachiopods but are rare (*Megerlia truncata, Megathiris detruncata, Terebratulina retusa* and *Aphelesia bipartita*, *Maltaia moysae*) or common (*Novocrania anomala* encrusting *Terebratula* shells). Mixture of pristine and altered shells (disarticulated, fragmented, abraded, encrusted and bioeroded). *Monia* spp. are very abundant, dominating *Monia squamma*, are always	The '*Terebratula* biostrome' displays variable and complex biofabrics: Packing is loose to dense. It records pod concentrations, imbrications and concave-up vertical stacking, gutter casts, and	The '*Terebratula* biostrome' indicates more sustained conditions of low sedimentation rates in time, with *Glossifungites* ichnofacies, higher diversity of bioerosion traces and brachiopods, and amalgamation of high-density gravity flows reworking and resedimenting shells. Increased diversity of suspension feeder

Table 4. (continued)

Facies	Lithology	Sedimentary structure	Ichnology	Macrofossils and taphonomy	Biofabric	Interpretation
			Gnathichnus pentax, *Centrichnus* isp., *Renichnus arcuatus*, *Caulostrepsis taeniola*, *Anellusichnus circularis* and *Oichnus simplex*	associated with the 'Terebratula biostrome', found to live encrusting terebratulids. Occurrence of taxa interpreted as transported, most notably *Spondylus crassicosta* and worn out fragments of *Clypeaster*. Diverse and common membraniporiform zooaria	clumps of pristine specimens	epizoans due to taphonomic feedback
F5	Cemented burrowed hybrid packstone	Massive fabric	Dominated by dense networks of unlined burrows, mostly *Thalassinoides suevicus*. (BI = 6)	Except for the *Terebratula* biostrome, macrofossils are not abundant. It can include pectinids and echinoids (*Ova candlifera*). The sediment infilling the burrows is similar in composition to the encasing matrix	Barren to loosely packed	Formation of stiffgrounds due to sea-floor cementation during low sedimentation rates It develops either at the toesets–bottomsets or at the foresets

bioturbation and the fabric is massive. This facies is rich in benthic (Fig. 9) and planktonic foraminifera.

Shell-rich hybrid packstone – F3.3

The matrix, which is similar to F3.1 or F3.2, contains densely packed concentrations of macroinvertebrates, either fragments of adeoniform zooaria, pectinids (*A. scabrellus*), or the mytilid *Gibbomodiola* cf. *adriatica* (Fig. 8B). Pectinids most often occur as disarticulated, but complete valves, preserving the ornamental details. Erosive surfaces were observed only in the proximally positioned localities (*Gibbomodiola* and *Schizoretepora* beds). Well-preserved acorn barnacles (*Solidobalanus mylensis*), sometimes preserving scutal and tergal plates inside the corona, form clusters on *Aequipecten*.

Interpretation of Facies Association 3

This facies association is dominated by *D. arietina*, a short-lived, free-living suspension-feeder and opportunist that can attain high densities in fine sands and muddy substrates under high sedimentation rates, high turbidity and unstable conditions (Grémare *et al.*, 1998; Sanfilippo, 1999; Ceregato *et al.*, 2007; Scarponi *et al.*, 2014). The interpreted opportunistic behaviour agrees with its high dominance (Ceregato *et al.*, 2007), as in Pliocene outcrops in the Águilas and the neighboring Cope Basins (Martinell *et al.*, 2012). A review on its ecology by Hartley (2014) emphasizes two explanations for the high densities reported in modern environments, both associated with disturbances: (i) disruption of established benthic communities, enabling successful recruitment of high numbers of *Ditrupa* larvae; and (ii) post-settlement redistribution by storms and concentration in areas of deposition. It is therefore probable that the paucispecific fossil assemblages dominated by *Ditrupa* concentrations in FA3 are associated with the action of storms or internal waves, either by redeposition, by opportunistic responses to storm-induced siltation producing organic-rich substrates, or both (Ceregato *et al.*, 2007; Hartley, 2014). The abundance of the benthic foraminifera *Cassidulina carinata*, *Bolivina* spp., *Bulimina aculeata* and *Globocassidulina subglobosa* (Fig. 9) is consistent with the organic enrichment associated with siltation (Jorissen *et al.*, 2007; Abu-Zied *et al.*, 2008; Goineau *et al.*, 2012; Pérez-Asensio *et al.*, 2017). Ichnoassemblages support the interpretation of high sedimentation rates and nutrient contents,

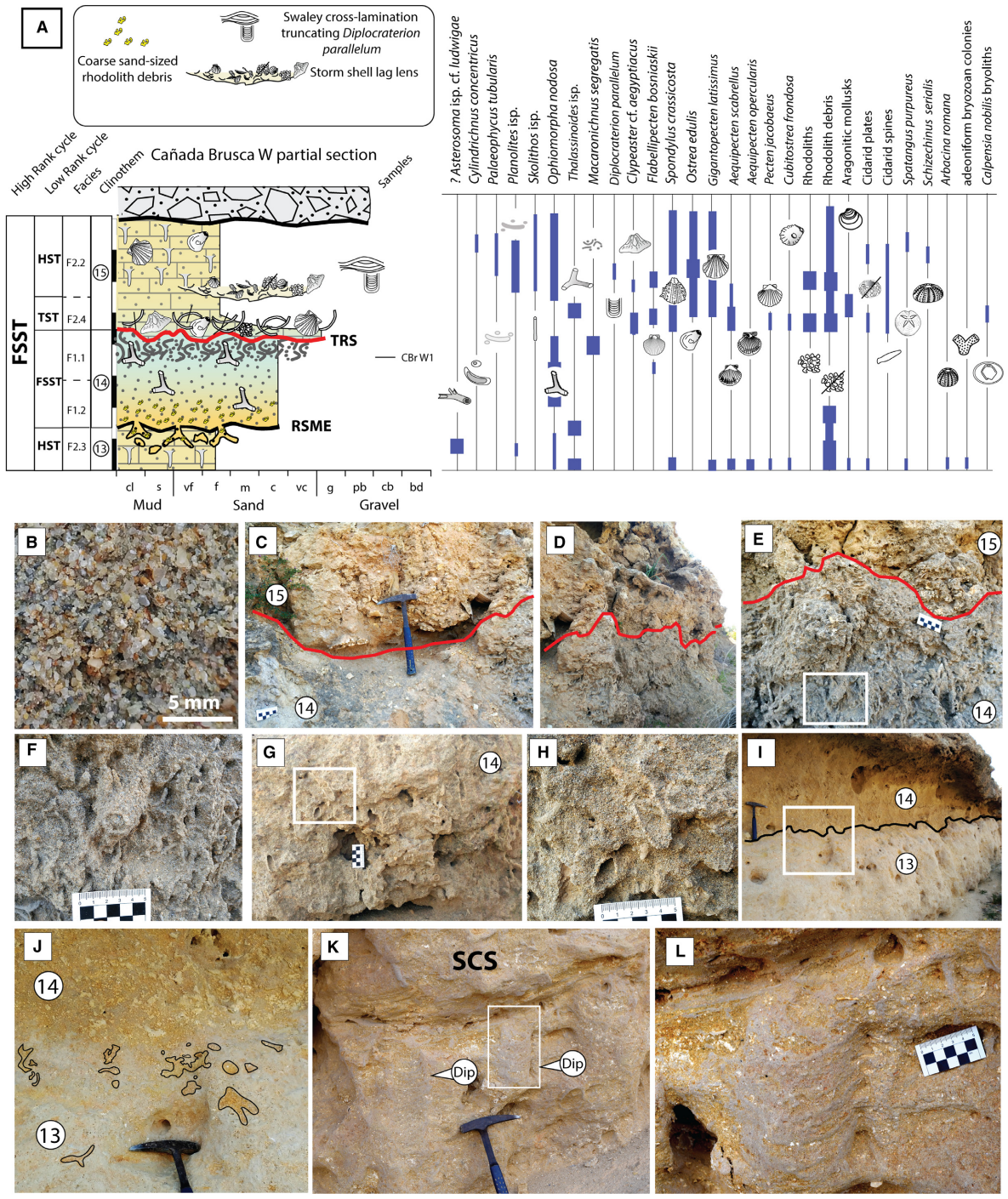

Fig. 5. Stratigraphic motif of low rank cycles from the CBr W sector. (A) Partial stratigraphic log with interpreted systems tracts (both high rank and low rank sequences), facies, clinothems and semi-quantitative abundance of traces and macrofossils. (B) Well-sorted, winnowed, coarse sandstone (F1.1) (clinothem 14). (C) to (E) Contact between clinothems 14 and 15 (red line), interpreted as a low rank transgressive ravinement surface (TRS). The shell bed overlying the TRS (facies F2.4) is interpreted as a low rank onlap shell bed (OSB). (E) Densely bioturbated *Macaronichnus* ichnofabric (clinothem 14). (F) *Ophiomorpha* burrow corresponding to the inset in (E). (G) to (H) *Ophiomorpha* ichnofabric (clinothem 14), *ca* 20 m basinward from the location shown in (C) to (F). (I) Irregular contact between clinothems 13 (facies F2.3) and 14 (black bold line), interpreted as a regressive surface of marine erosion. Hammer for scale is 33 cm long. (J) Detail from inset in (I), showing *Thalassinoides* burrows (*Glossifungites* ichnofacies) passively infilled with material from the base of clinothem 14 (facies 1.2). (K) Swaley-cross stratification (SCS) in facies F2.3, truncating two examples of *Diplocraterion parallelum*. (L) Detail of *D. parallelum* from inset in (K).

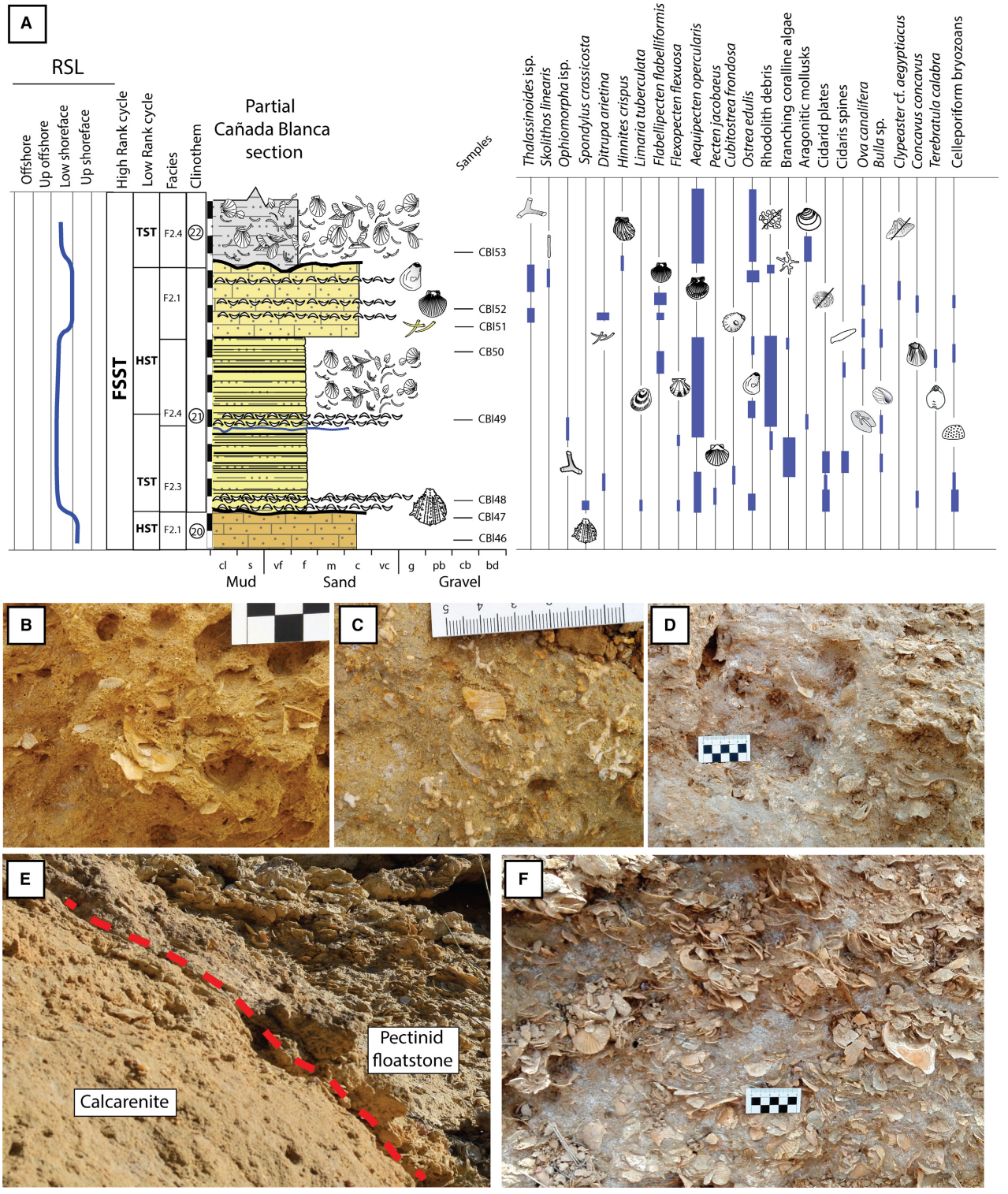

Fig. 6. Partial stratigraphic log of the Cañada Blanca section for clinothems 20 to 22. (A) Example of low rank sequence (clinothem 21). (B) Calcarenite (F2.1) with fragmented molluscs and tubes of *Ditrupa* (top of clinothem 21). (C) Hybrid coralline algal floatstone (F2.3) with branched coralline algae embedded in a fine-grained matrix (lower interval of clinothem 21). (D) Shell-rich rhodolithic floatstone (F2.4) with densely packed pectinids, rhodoliths and subsidiary oysters (middle of clinothem 21), interpreted as a low rank backlap shell bed. (E) Contact (red dashed line) between the calcarenite (top of clinothem 21) and the pectinid floatstone (F2.4) (base of clinothem 22), interpreted as a low rank onlap shell bed. (F) Detail of the pectinid floatstone of clinothem 22.

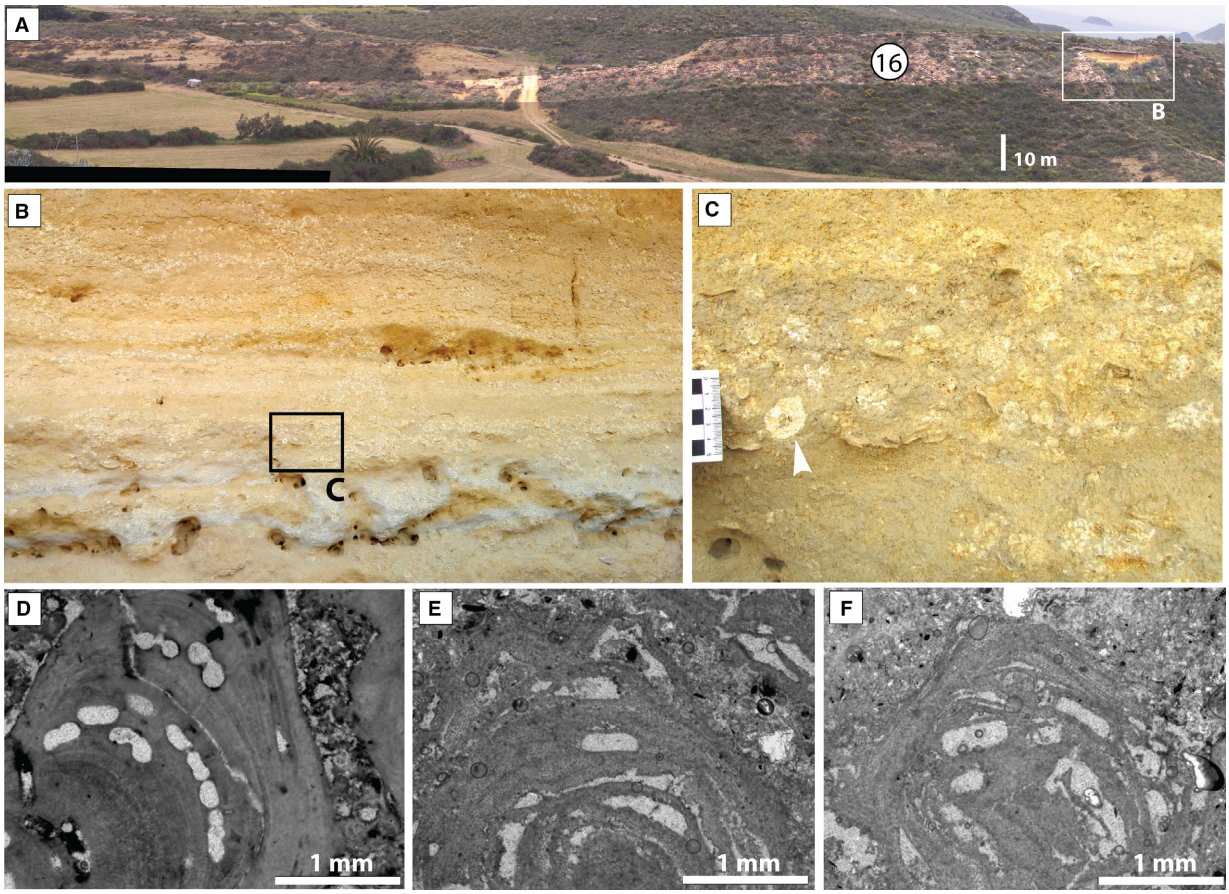

Fig. 7. Example of rhodolithic facies (FA2) in clinothem 16 (rollover zone) from the Cañada Brusca W sector. (A) Oblique view to depositional strike of clinothem 16, partially highlighted. (B) Rhodolith pavements in outer topset facies of clinothem 16. (C) Detail of a rhodolith pavement of (B), showing spheroidal growth forms (white arrowhead). Note the fine-grained hybrid carbonate matrix. (D) to (F) Thin sections of samples of FA1–FA2 facies displaying examples of coralline red algae. (D) Uniporate conceptacles of Lithophylloideae (clinothem 18). (E) and (F) Multiporate conceptacles of Melobesioideae (clinothem 17).

although there are variations in a proximal to distal gradient, with increasing ichnodiversity and density of traces towards distal positions. In general, facies F3.2 is dominated by *Macaronichnus*, which is the product of vagile, detritus-feeding worms (Bromley *et al.*, 2009; Pearson *et al.*, 2013). Such trace fossils are rarely reported from offshore settings (Aguirre *et al.*, 2010; Rodríguez-Tovar & Aguirre, 2014; Giannetti *et al.*, 2018) and their producers cope well with high sedimentation rates (Taylor *et al.*, 2003). In distal positions (the base of the Cañada Blanca section), other common ichnotaxa include *Teichichnus rectus*, attributed to a deposit-feeder in nutrient-rich sediments, which can re-equilibrate to the sediment-water interface (MacEachern *et al.*, 2012a). The intense bioturbation in distal positions (Table 3), however, suggests long colonization windows (Buatois *et al.*, 2015) under background fair-weather conditions, because the effects of siltation and/or gravity flows decrease both in intensity and frequency in these settings. The occurrence of the traces *Teichichnus*, *Diplocraterion* and *Scalichnus* in distal F3.2 (Table 3) points to re-equilibration in the aftermath of such sporadic, exceptional events (MacEachern *et al.*, 2012a).

Facies Association 4

The major characteristic of Facies Association 4 (FA4) is the presence of fine-grained hybrid packstone distally and the reduced carbonate content (*ca* 13 to 40%) (Fig. 4), characteristically dominated either by *Costellamussiopecten* or *Terebratula* (Figs 10B and 11).

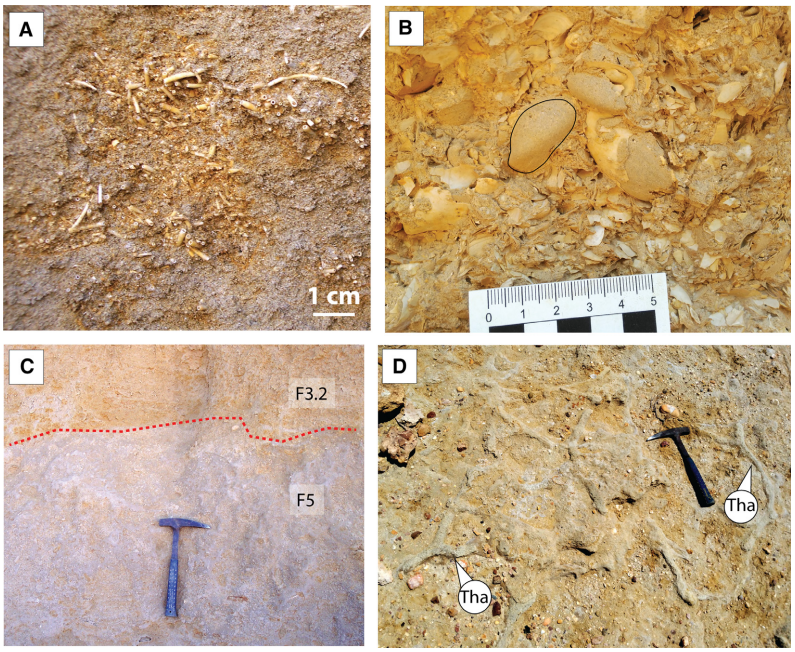

Fig. 8. Details of the main features in FA3 and F5. (A) A *Ditrupa* pod concentration in hybrid packstones. (B) Densely packed mollusc concentration (*Gibbomodiola* bed). (C) Contact (red dashed line) between F5 (*Glossifungites* ichnofacies; below red line) and the overlying *Ditrupa* rich friable hybrid packstones (F3.2) at the Cabezo Alto section. (D) *Glossifungites* ichnofacies (F5) with well-developed networks of *Thalassinoides suevicus* (marked 'Tha') in the Cañada Brusca sector.

Hybrid packstone with Costellamussiopecten – F4.1

Facies F4.1 consists of hybrid packstones with poorly sorted fine-grained sands to coarse silts (variable proportions of micrite and sparite depending on the locality). The terrigenous particles comprise angulose grains of quartz, schist and abundant mica flakes. Planktonic and benthic foraminifera (Fig. 9) are abundant, the latter including centimetre-sized tests of *Pyramidulina raphanistrum* and *Lenticulina* spp. As in the other facies, the fabric is massive and structureless. Macrofossils, most notably *Costellamussiopecten cristatum*, occur as dispersed, complete, disarticulated valves (Fig. 10B). The density of identifiable traces varies. Outsized, angular floating clasts of metamorphic material from the basement are very rare (Fig. 10C). Some of them are pebble-sized, rounded and bioeroded black dolostones (Fig. 10D).

Paraconglomerate of outsized floating clasts – F4.2

This facies occurs only at the base of the Cabezo Alto section (clinothem 1) (Fig. 10A). The matrix is similar to that of F4.1. It is characterized by a paraconglomerate of outsized, angular floating clasts and loosely packed to dispersed bioclasts (Fig. 10E). The richness of vertebrates and macroinvertebrates is the highest in the whole study area (including fish vertebrae, elasmobranch teeth, crustacean dactyla, wood remains bioeroded by *Nototeredo* sp., plant detritus and others; Fig. S2). Most shells are disarticulated, consisting of a mixture of pristine, fragmented and bioeroded/encrusted specimens of many species; some of them occur typically in FA1 and FA2 (Table 4; Fig. 10F). This facies is densely bioturbated (mostly indistinct mottling) and the richness of identifiable ichnotaxa is relatively high in comparison to other facies. The density of floating lithoclasts and bioclasts peaks at the base of clinothem 1 and decreases progressively upward (Fig. 10A and F). In the 125 to 500 μm fraction, yellowish to light-green glauconite grains (often preserved as foraminiferal casts) are frequent.

Terebratula pavements – F4.3

This facies is characteristic of the Cabezo Alto – Cañada Brusca area, where 13 outcrops were identified. They consist of *ca* 5 to 20 cm thick beds in which brachiopods appear embedded in a fine-grained matrix (Fig. 11A and B). Two outcrops showed two pavements separated by about 20 cm. These are referred to in this study as 'twin pavements' (Fig. 11C). No erosive or planar surfaces, either at the base or at the top of the skeletal concentration, were observed (Fig. 11A, B and G). No normal grading is visible in the matrix; the sediment is indistinguishable from that underlying and overlying the pavements; the shell orientation varies from random to umbo-down; bioclasts are well-preserved and only a few specimens show minor taphonomic alterations; more than 50% of the

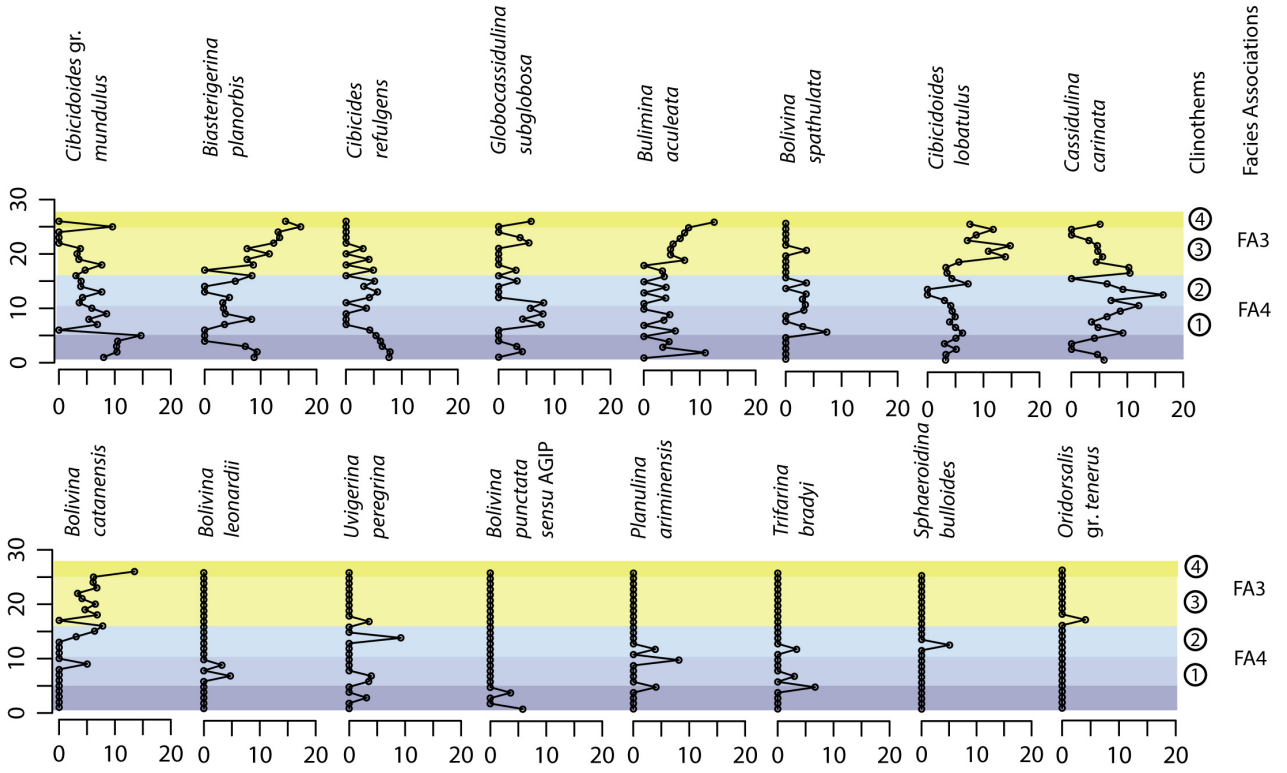

Fig. 9. Most abundant benthic foraminifera from the Cabezo Alto section in 26 samples encompassing FA4 and FA3. The position of the samples in the stratigraphic log is indicated in Fig. 4. Only peaks >3% are represented. Blue indicates FA4 (different grades for each clinothem) and yellow FA3.

specimens are articulated. Some pavements yield small juveniles. The packing of specimens is variable, from dense in the centre to loose towards distal and proximal positions of the pavement (Fig. 11G). In some cases, disrupted biological clumping occurs (Fig. 11B and F). All of the pavements studied yield yellowish to light-green glauconite grains. Chemical analysis of two glauconite grains from one sample showed a K_2O content of 4·4% and 4·3%. This facies is distributed cyclically, most often alternating with F4.1.

Terebratula biostrome – F4.4

This is one thick bed (>1 m) dominated by loosely to densely packed terebratulids (Fig. 12A). It contains a mixture of well-preserved, articulated specimens (Fig. 12B), sometimes devoid of sediment infill (Fig. 12C), and disarticulated valves (Fig. 12E and F). Many of the latter are fragmented, abraded, heavily bioeroded and encrusted by bryozoans, anomiid bivalves (Fig. 12D), serpulids and craniid brachiopods. The biofabric is variable and complex, with examples of *in situ Terebratula* clumps, pod concentrations and gutter casts (Fig. 12G). Outcrops of this single interval are recognizable for 850 m parallel to the strike, whilst at Cañada Brusca, a low abundance of additional brachiopod species (Table 4) was observed.

Interpretation of Facies Association 4

This facies association crops out in the more distal positions of the depositional profile, where the fine-grained sediment composition indicates low-energy background conditions. This is supported by the occurrence of *C. cristatum*, characteristic of F4.1, which is an extinct pectinid with delicate valves, frequently reported from offshore environments (Aguirre *et al.*, 1996; Robba, 1996; Yesares-García & Aguirre, 2004; Ceregato *et al.*, 2007). Extant species of the homeomorphic genus *Amusium* (Waller, 2011) inhabit quiet waters on fine sandy and muddy substrates of the Indo-Pacific region, at depths of 10 to 100 m (Fréneix *et al.*, 1987; Minchin, 2003). The benthic foraminiferal assemblage (Fig. 9) is also typical of offshore environments (Rasmussen, 2005). The massive

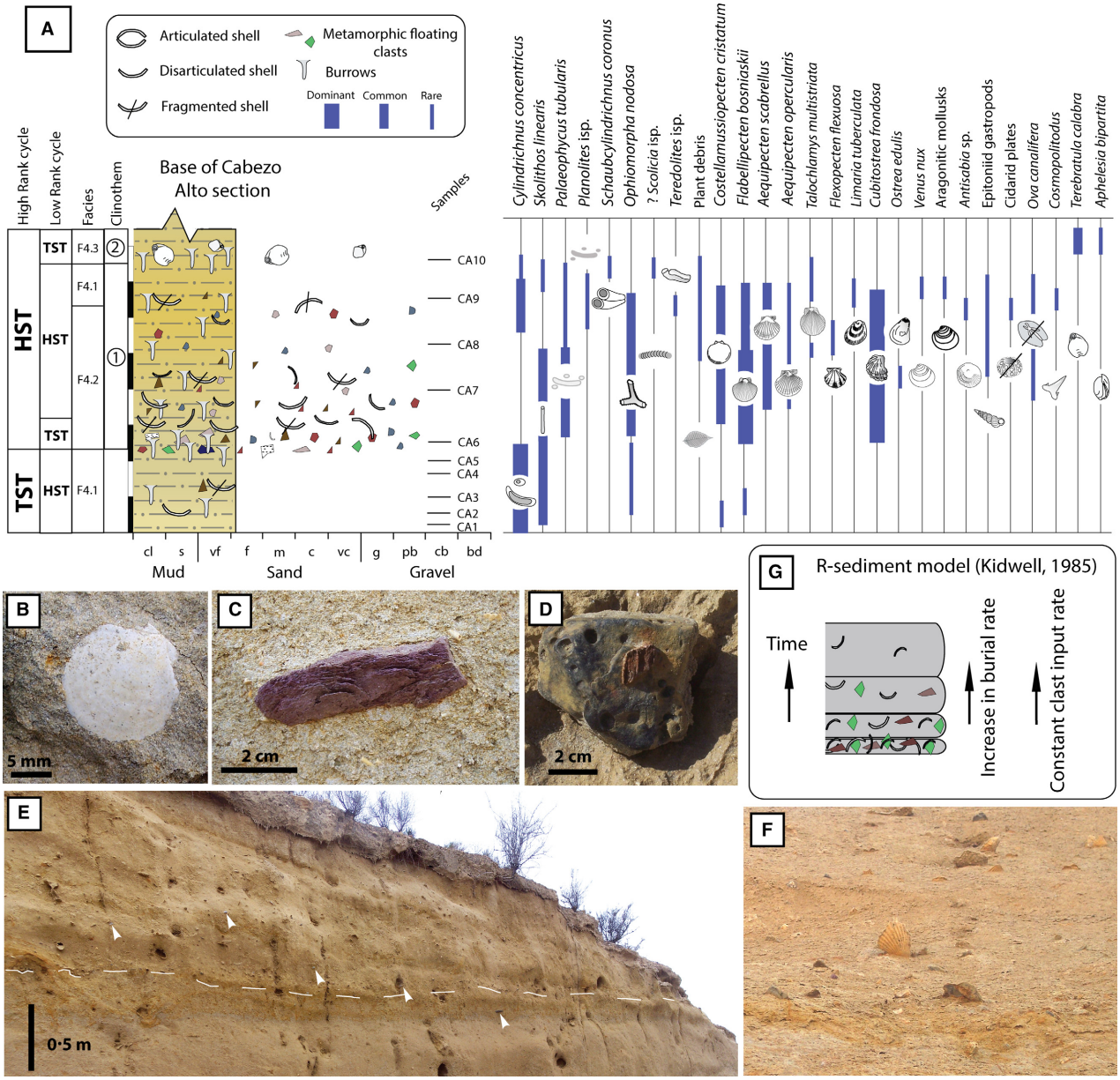

Fig. 10. Sedimentological and palaeontological features of FA4. (A) Stratigraphic log of the base of the Cabezo Alto section (clinothems 1 and 2). (B) Juvenile valve of *Costellamussiopecten cristatum*. (C) Example of cobble-sized angular, metamorphic floating clast. (D) Rounded and bioeroded dolostone clast. (E) Floating clast paraconglomerate at the base of clinothem 1 (examples with arrowheads). The dashed line highlights the base of the paraconglomerate. (F) Detail of the bioclasts in the paraconglomerate of clinothem 1 (*Flabellipecten bosniaskii* and *Cubitostrea frondosa*). (G) R-sediment model, adapted from Kidwell (1985) and Tomašových *et al.* (2006). It explains the fabric pattern with an upward decrease in density of floating clasts by a concomitant increase in burial rates.

fabric can be explained by intense bioturbation and deposition by suspension fall-out (García-García *et al.*, 2006; Longhitano, 2008). The barren to dispersed packing of F4.1 suggests high sedimentary dilution and/or low shell productivity (Tomašových *et al.*, 2006). The good taphonomic preservation of the autochthonous (and some allochthonous in F4.2) macrofossils (Table 4) fits the outer-shelf taphofacies model of Yesares-García & Aguirre (2004). The ichnofabrics also point to low–moderate background sedimentation rates probably affected episodically by high sedimentation rates, as in distal F3.2. Stable background conditions are

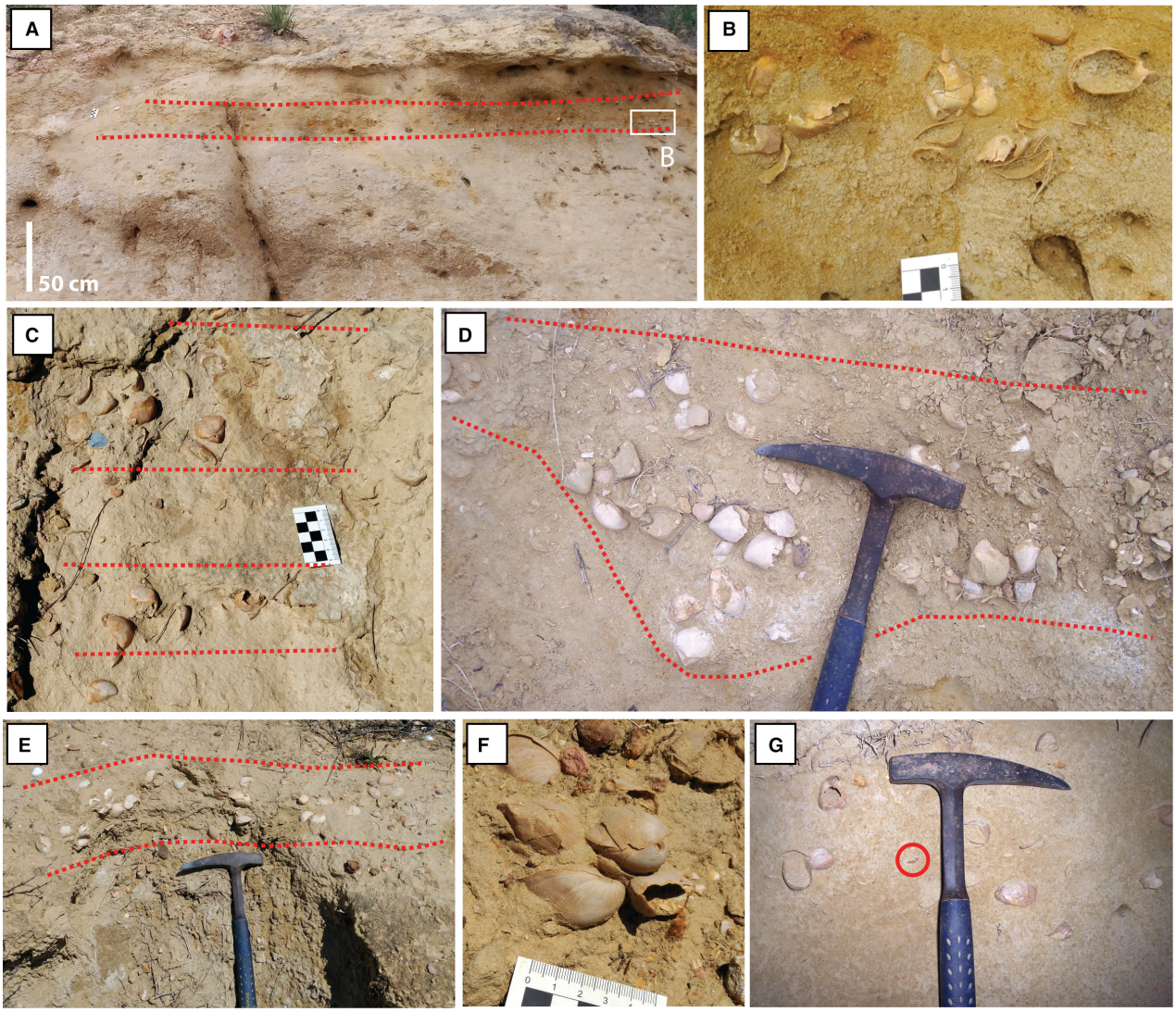

Fig. 11. Examples of facies F4.3 (*Terebratula* pavements; bounded by red dashed lines). (A) *Terebratula* pavement between clinothems 3 and 4 in the Cabezo Alto area. (B) Detail of the pavement shown in (A). Most specimens are articulated and distributed in small clusters of two to three specimens (possibly representing a disrupted biological clumping or patchiness). (C) 'Twin pavements' between clinothems 5 and 6. (D) and (E) Densely packed concentrations in the pavement between clinothems 9 and 10 in the Cañada Brusca sector. Hammer for scale is 33 cm long. (F) Possible *Terebratula* cluster. (G) Loosely packed pavement in more distal positions. The red circle pinpoints a juvenile specimen.

suggested by the dominance of lined burrows: such lining helps to stabilize burrows (constructed as permanent domiciles) in soft substrates (Bromley, 1996; Buatois & Mángano, 2011). The dominance of *Domichnia* therefore indicates well-oxygenated substrates and stable background conditions (Buatois & Mángano, 2011). The local occurrence of *Trichichnus* isp. at the CA section (clinothem 2) might be related to longer periods of stable conditions and a low food content at the sediment–water interface (Pervesler *et al.*, 2008). An event-bed suite can be interpreted based on the occurrence of some *Taenidium* and backfilled, unidentified meniscate traces (possibly *Scolicia* isp.), indicating the activity of deposit feeders. They probably reacted opportunistically to sporadic high-density gravity flows or siltation events associated with storms or other disturbances (de Gibert & Goldring, 2007).

The occurrence of outsized floating clasts (Fig. 10) across the depositional profile is interpreted as the product of storm-induced high-density gravity flows (Postma *et al.*, 1988;

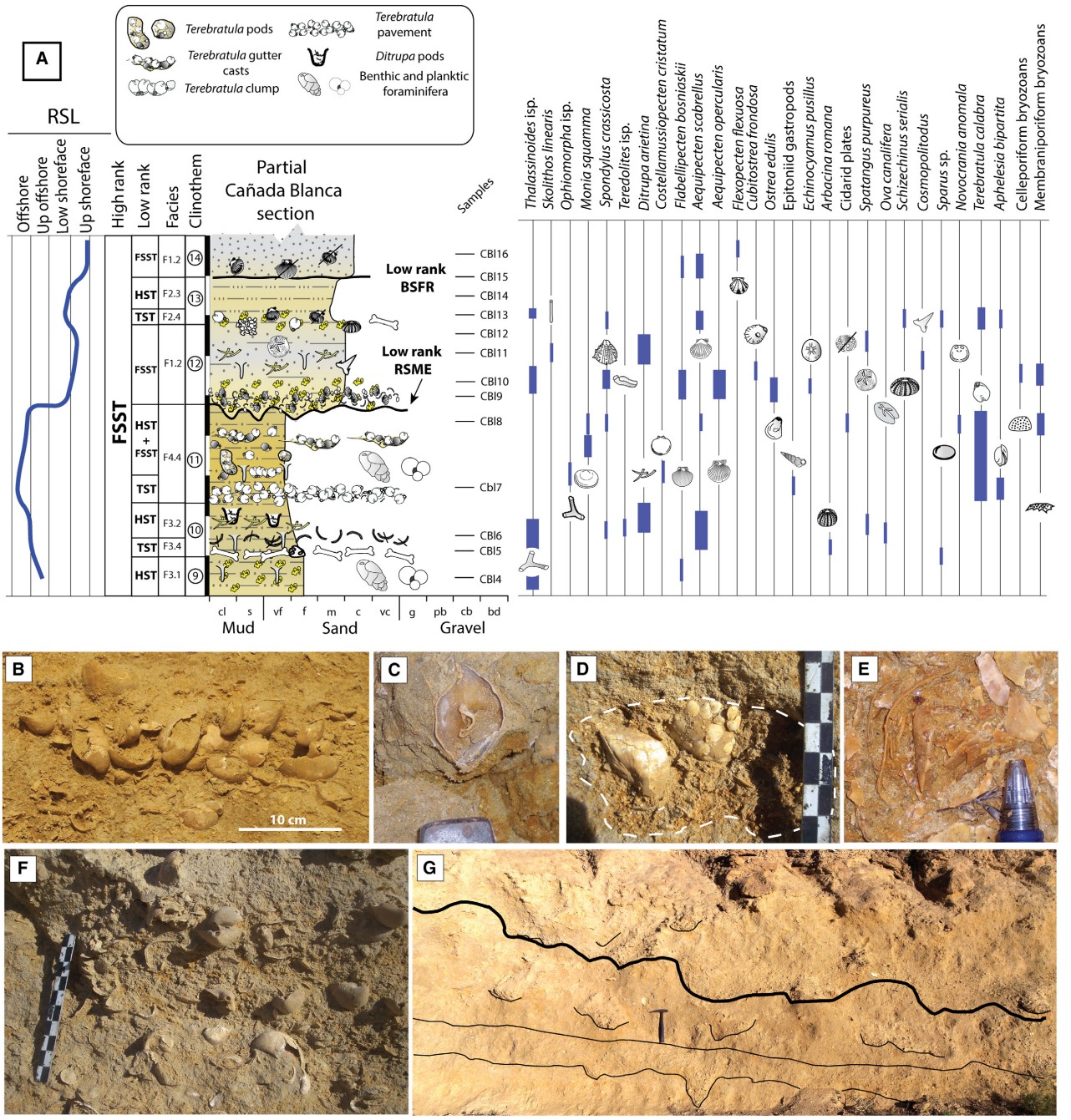

Fig. 12. Main features of FA3 and F4.4 at the Cañada Blanca section. (A) Detailed stratigraphic log for clinothems 9 to 14. (B) Clump of *in situ Terebratula* specimens. Note the articulated specimens, umbo-down orientation, presence of juveniles. (C) Void *Terebratula* displaying the brachidium (geopetal structure). Hammer tip for scale is 2 cm long. (D) Pod concentration filled with coarse siliciclastic grains, *Ditrupa* tubes and two articulated *Terebratula* specimens. Note the sharp-walled, unlined large burrow and numerous anomiid bivalves (*Monia squamma*) encrusting *Terebratula*. (E) Detail of imbricated, strongly altered *Terebratula* valves. Note the abraded foramen and right hinge-tooth in a fragmented ventral valve. Pen tip is 19 mm long. (F) Detail of gutter cast filled with disarticulated *Terebratula* shells. Concave-up, disarticulated ventral valves predominate. (G) View of the basal bed, overlain by gutter casts and the erosive surface separating clinothems 11 and 12. BSFR, basal surface of forced regression. Hammer is 33 cm long.

Mulder & Alexander, 2001; Talling *et al.*, 2012). This is consistent with source areas dominated by schists and phyllites, such as in the Águilas Basin. In particular, according to García-García (2004), the sensitivity of these lithologies to erosion favours the production of high volumes of fine fraction, which in turn enhances the formation of cohesive debris flows. The angularity of these clasts (some of which have weak lithologies) (Fig. 10C) suggests that they bypassed the depositional profile directly from the river or ephemeral stream mouth to reach the distal positions where FA4 was deposited, probably by hyperpycnal flows that transformed into cohesive debris flows. The roundness and the presence of *Gastrochaenolites* traces on the dolostone clasts suggest that the latter were stored in a delta plain, a beach or a cliff-toe (Uchman *et al.*, 2002; García-García *et al.*, 2011) and were incorporated into the flows during flash floods. The storage area would have been no further away than a few kilometres (Fig. 13), judging from the distribution and structure of the Palomas Unit (Álvarez & Aldaya, 1985). A possible alternative explanation for their occurrence is kelp or seaweed rafting as a main transportation means (Bennett *et al.*, 1994; Garden *et al.*, 2011; Frey & Dashtgard, 2012) but co-occurrence of the floating clasts with other allochthonous elements [out of habitat molluscs (Table 4), plant debris, *Teredolites* isp. and *Calpensia* bryoliths (Fig. S2)] supports the first hypothesis (MacEachern *et al.*, 2005; Ghinassi, 2007; Moissette *et al.*, 2010; Nalin *et al.*, 2010; Buatois *et al.*, 2011).

In facies F4.3, the frequent pristine preservation of terebratulids, the occurrence of juveniles and disrupted patchiness (Fig. 11A and B), together with the absence of diagnostic features for hydraulic reworking (e.g. Roetzel & Pervesler, 2004), suggest that these pavements probably represent obrution deposits of autochthonous palaeocommunities (Brett & Seilacher, 1991; Fürsich, 1995; Brett *et al.*, 2003). They can be interpreted as mixed assemblages, in part within-habitat time-averaged, and in part census death assemblages (Kidwell, 1998). The occurrence of glauconite in the terebratulid pavements points to conditions of very low terrigenous input (Odin & Fullagar, 1988; Harding *et al.*, 2014). Preservation of glauconite grains (often as well-preserved casts of foraminifera) points to their autochthonous or parautochthonous origin (Amorosi, 1997, 2012). Therefore, compared with F4.1, the *Terebratula* pavements (F4.3) indicate conditions of notably reduced sedimentation rates. The taphonomic traits and biofabric of these pavements suggest that the *Terebratula* palaeocommunities in the study area were extirpated by siltation events (Emig, 1989; Tomašových & Kidwell, 2017) because fine terrigenous particles clog the lophophore and smother these animals (He *et al.*, 2007). These siltation events probably represent the onset of the next cycle of F4.1 sedimentation. The interpretation here is, therefore, that the pattern of alternating F4.3 and F4.1 facies represents cyclical changes of decreased and increased sedimentation rates.

The '*Terebratula* biostrome' (F4.4) shares the dominance of terebratulids with F4.3 (Fig. 12). The variable taphofacies (Table 4) suggests complex taphonomic pathways of mixed biogenic–sedimentological origin (Kidwell *et al.*, 1986). The occurrence of *in situ* clumps (Fig. 12B) indicates that the terebratulids were autochthonous to the biotope where FA4 was being deposited. The dominance of *Terebratula* points to high shell productivity [high hard-part input rates *sensu* Tomašových *et al.* (2006)]. In contrast, pod concentrations, pristine void

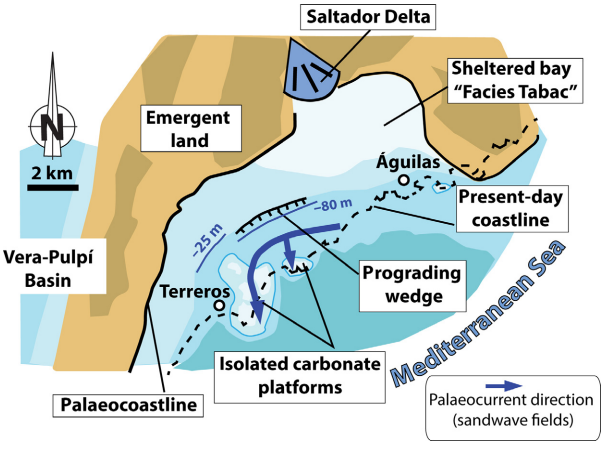

Fig. 13. Proposed palaeogeographic map of the Águilas Basin during deposition of synthem SP1 (Zanclean, MPl3 biozone). The exact position of the palaeocoastline in the western sector is tentative due to the paucity of shallow-water outcrops, and uncertainty as to their attribution to SP1. The indented black line indicates the rollover of the infralittoral prograding wedge and is shown with estimation of approximate inferred palaeobathymetry at the time of deposition of the oldest clinothems. The palaeocurrent direction is inferred from outcrops of stacked sandwave fields at the Terreros and La Carolina sectors (see Fig. 3), migrating seaward.

specimens (geopetal structures) and gutter casts infilled with highly altered and densely packed terebratulid shells, are all characteristic of episodes of rapid burial and hydraulic reworking *in situ* (Fig. 12C to F) (Baeza-Carratalá *et al.*, 2014). Hydraulic disturbances are also demonstrated by the occurrence of a few disarticulated valves of *Spondylus*, a typical element of FA2 (where it is often articulated), which suggests an allochthonous origin.

The abundant fragmented, abraded, bioeroded and encrusted shells (assemblage-level alteration) are typical for prolonged exposure at the sediment–water interface, which, together with the loose to dense packing (shelliness), points to reduced sedimentation rates (Kidwell, 1985, 1989). The rich ichnoassemblage of bioerosion traces (Table 4) is strongly uneven, dominated by *Entobia* isp. (clionaid sponges), highlighting strong hydrodynamics and background sedimentation rates between <1 g m^{-2} and *ca* 7 g m^{-2} (Carballo *et al.*, 1994). The rare occurrence of echinoid rasping traces *Gnathichnus pentax* coupled with the absence of *Radulichnus* (scratch marks by herbivorous gastropods and polyplacophorans) (de Gibert *et al.*, 2007) point to dim light or aphotic conditions (Bromley, 2005). The co-occurrence of the above taphonomically altered brachiopod bioclasts, together with abundant pristine specimens, demonstrates that the *Terebratula* palaeocommunity was able to recover from multiple episodic disturbances, where background conditions of strong hydrodynamics and low sedimentation rates were environmentally optimal for these brachiopods (Emig & García-Carrascosa, 1991; Reolid *et al.*, 2012). The co-occurrence of lined and sharp-walled, unlined burrows (Fig. 12D) suggests that the substrate within F4.4 evolved from a soft-ground to a stiffground, indicating a decrease in sedimentation rates (Taylor *et al.*, 2003; MacEachern *et al.*, 2012b).

Facies 5

Cemented burrowed hybrid packstone (Glossifungites ichnofacies)

This facies cannot be attributed to any particular facies association because in some places it adjoins FA4 but elsewhere adjoins FA3. It is treated here as a separate type. The matrix consists of a fine-grained hybrid packstone that is cemented (*ca* 40% $CaCO_3$) and completely bioturbated (Fig. 8C). In general, traces are poorly defined but some are attributable to non-compacted *Thalassinoides* burrows, except for one locality, where many well-defined, non-compacted *Thalassinoides suevicus* occur (Fig. 8D). The material infilling the burrows is similar to the surrounding matrix. In some localities, this facies displays loosely to densely packed skeletal concentrations, but *Ditrupa* is absent.

Interpretation of Facies 5

This facies, interspersed between either FA4 or FA3, is interpreted as the formation of stiffgrounds during phases of low sedimentation rates, which favoured cementation of the sea floor (Taylor *et al.*, 2003; MacEachern *et al.*, 2012b).

GEOMETRIC AND STRATIGRAPHIC STACKING PATTERNS

Geometry

The Cabezo-Alto and Cañada Brusca W sectors enable delta-scale clinoforms *sensu* Patruno *et al.* (2015) to be identified (Figs 1C, 14A and 14B). For example, the clinoform separating clinothems 5 and 6 extends for about 250 m from the toeset-point to the upper rollover (Fig. 1C). The clinoforms display a sigmoidal profile (*sensu* Adams & Schlager, 2000) where, in general, FA2 and facies 3.1 occur in the upper rollover, FA3 in the foreset and FA4 from the lower rollover basinward, in the bottomset. FA1 is best observed in the Cañada Brusca W sector where it occurs in the topset (Fig. 14D to F).

Stacking patterns

The mapping of stratigraphic surfaces on photomosaics, the outcrop study of bed surfaces and the facies distribution show that SP1 displays a south-east prograding and offlapping stacking pattern of sigmoidal clinothems. Twenty-two clinothems were identified in SP1 (numbering in Figs 4 and 14). In the Cabezo Alto (CA) sector, clinothems 1 to 6 display a forestepping pattern (progradation plus aggradation), evolving vertically from FA4 at the base to FA2 at the top; the latter is truncated and overlain by Quaternary deposits (Fig. 14A and B). The aggrading pattern is present in clinothems 5 and 6, which display facies 3.1 at the top of the sections; this contrasts with the adjacent clinothem 4, with facies 2.3 at the top (Fig. 14A and B). The contacts between these clinothems in distal positions consist of facies F4.2 (only at the base of the CA section),

F4.3 (red lines in Fig. 14A and B), or F5. Starting with clinothem 7, a downstepping pattern is visible, with strong shifts from facies F2.2 and F2.3 to F3.2 (Fig. 14A and B). The contact between these latter clinothems is erosive in the upper part of the sections (Fig. 14C). The offlapping trend is modulated by clinothem 11, which displays the more distal facies F3.1 at the Cañada Brusca W sector compared with adjacent older clinothems (Fig. 14D and E). Clinothem 11 is followed by strong shifts with facies F1.1 and F1.2 in clinothems 12 and 14, alternating with facies F2.3 in clinothems 13 and 15 through prominent erosive surfaces (Figs 5 and 14D to F). Clinothems 11 and 14 are very distinctive and make up marker beds recognized in the Cañada Brusca E, Cañada Brusca W and Cañada Blanca sectors. The Cañada Blanca section is characterized, in general, by alternating facies associations FA1 and FA2 and erosive contacts in between (Fig. 4). This pattern holds except at the base of the section which displays facies associations FA3 and FA4 up to clinothem 11, sharply overlain by facies association FA1 through an erosive surface (Figs 4 and 12).

MAGNETIC SUSCEPTIBILIY AND CARBONATE CONTENT

The overall carbonate content ranges from 13 to 80% (Fig. 4). Maximum values are attained in the rhodolith dominated facies of FA2; they decrease proximally and distally from this facies. In the CA section no cyclicity in $CaCO_3$ is recognizable, whereas in the CBL section the variation appears to roughly coincide with variation trends in magnetic susceptibility. Both the CA and CBL sections display very low magnetic susceptibility (MS) values, increasing only near the clinothem boundaries identified by sedimentological – palaeontological criteria. The maximum value in the whole studied area is recorded in the paraconglomerate interval at the base of section CA (Fig. 4).

DISCUSSION

Depositional model

Clinoforms of SP1 have the diagnostic features of sand-prone subaqueous delta-scale clinoforms (Patruno *et al.*, 2015), in particular: (i) steep foresets (≥7°, up to 14°) (Fig. 1C); (ii) a sigmoidal profile; (iii) development on a narrow shelf (an embayment about 14 km wide) (Fig. 13); and (iv) close proximity to the palaeocoast (indicated by bioeroded dolostone clasts of the Palomas Unit). Furthermore, the Pliocene Molino del Saltador delta occurs 6 km north-east from the base of the CA section. This implies that La Serrata and Los Melenchones (Fig. 3B), adjacent to where this delta developed, were already above sea-level during the early Pliocene (Fig. 13).

In general, the facies distribution in SP1 shows a proximal–distal energy gradient with decreasing grain-size distally, especially basinward, beyond the upper rollover (FA3 and FA4). This grain-size distribution matches systems dominated by physical accommodation in which facies belts reflect the hydraulic competence of the sedimentary particles (Pomar & Kendall, 2008). The geometry of the clinoforms is consistent with a prograding distally steepened ramp (Pomar, 2001; Pomar *et al.*, 2002; Martín *et al.*, 2004) or an infralittoral prograding wedge (IPW; Hernández-Molina *et al.*, 2000; Pomar *et al.*, 2015). In both cases, the rollover zone represents an energy threshold above which episodic high-energy conditions affect the topset and below which overall quiet conditions prevail offshore (seaward of the rollover). According to these genetic models, the upper rollover corresponds to the mean storm-weather wave base (SWWB), fostering sediment bypass at the topset and sediment shedding down on the foreset (Hernández-Molina *et al.*, 2000; Pomar *et al.*, 2015), the latter in the form of siltation/suspension fall-out and as sediment gravity-flows (Massari & Chiocci, 2006). Immediately offshore of the upper rollover zone, sedimentation rates peak (upper foreset) and gradually decrease distally, both in frequency and intensity (in the lower foreset and bottomset) (Walsh *et al.*, 2004; Mitchell, 2012). In the original example of an IPW from off Cabo de Gata (southern Spain) described by Hernández-Molina *et al.* (2000), the rollover lies at about 25 m water depth coincident with the mean SWWB. This bathymetry is compatible with the coralline algal assemblages in the study area (outer topset) (Fig. 7), although, during the early Pliocene, the storm intensities at this latitude were presumably stronger due to warmer sea-surface temperatures (SST) (Emanuel, 2005; Beltran *et al.*, 2011). A conservative depth of 25 to 30 m for the upper rollover zone of the Águilas subaqueous delta-scale clinoforms is, therefore, proposed. The location of the SP1 IPW in the south-western corner of the basin (Fig. 13) implies that it was probably the area most

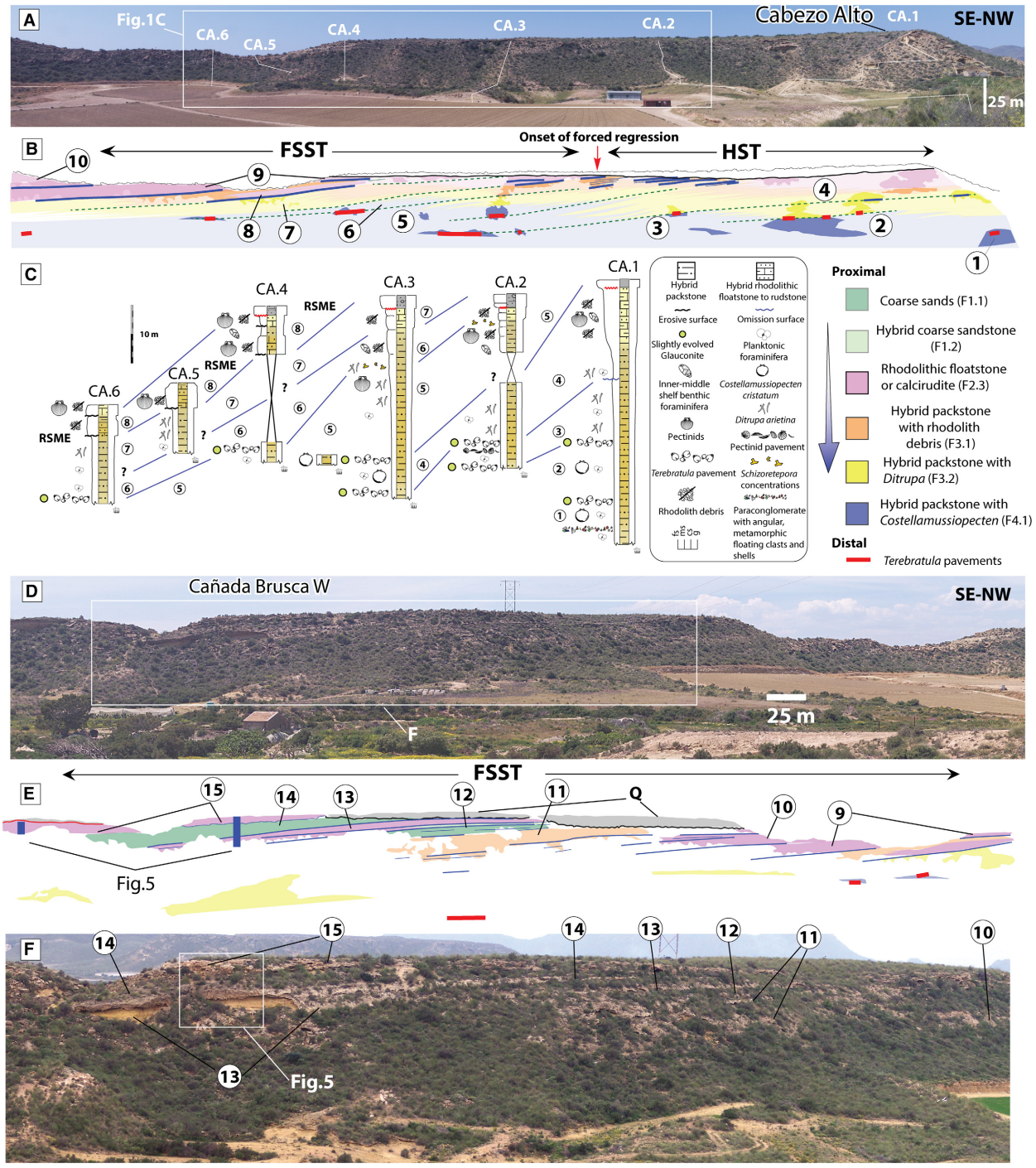

Fig. 14. Photomosaic of the early Pliocene infralittoral prograding wedge in the western sector of the Águilas Basin, synthem SP1. (A) Cabezo Alto (CA) sector (photograph parallel to depositional strike). White lines indicate the stratigraphic logs in (C). (B) Clinothems and facies indicated with colour code. Blue lines indicate beds identified in the field, red straight lines are *Terebratula* pavements, and dashed lines are the interpreted connection between beds in the topsets–foresets and terebratulid pavements at the toeset–bottomsets. Clinothems identified in the CA sector are indicated by encircled numbers. The topsets of clinothems 4 to 7 are truncated, and overlain by Quaternary conglomerates. (C) Synthetic stratigraphic logs (not composite; indicating dominant biofacies, stratigraphic contacts and correlation between adjacent sections). (D) The Cañada Brusca (CBr) sector viewed obliquely to depositional strike. Inset indicates the position of sector for details in (F). (E) Numbered clinothems and facies contacts as in (D). Colour code for facies as in (B) and (C). (F) Detail of the CBr sector from a view subparallel to depositional strike, with indication of clinothems 10 to 15.

exposed to easterly storms, as opposed to the laminated silty marls occurring in the north-eastern part of the basin, interpreted as a sheltered bay (Montenat *et al.*, 1978).

Sequence stratigraphy

Two hierarchical sequence ranks were here interpreted for the early Pliocene (late Zanclean, MPl3 biozone) SP1 synthem of the Águilas Basin. The low rank sequences (LRS) are the basic building blocks of the high rank sequence (HRS). In particular, the systems tracts of the HRS are defined both by the LRS stacking patterns and their bounding surfaces (Zecchin & Catuneanu, 2013). The LRS are represented by the identified outcropping clinothems (1 to 22); older ones were eroded, younger ones truncated or covered by colluviums.

Architecture of the high rank sequence

The interpreted HRS is bounded at the top by an extensive unconformity described by Dabrio *et al.* (1991). The basal unconformity is inferred at the Cabezo Alto sector based on changes in facies, strike, dip and micropalaeontological assemblages between the top of SP0 and base of SP1. This basal unconformity, however, crops out at the Terreros section (3·35 km to the southwest) (Fig. S1). Further work is necessary to confirm its presence throughout the study area.

The transgressive systems tract (TST) is interpreted here to crop out at the base of the CA section (only the youngest LRS) (Figs 4 and 10). Since the contact between synthems SP0 and SP1 in the Cabezo Alto does not crop out, the high rank transgressive ravinement surface has not been observed. The highstand systems tract (HST) is interpreted from the forestepping stacked clinothems 1 to 6 (Fig. 14A and B). These clinothems overlie the paraconglomerate at the base of the CA section (facies 4.2, clinothem 1) (Fig. 10), which is interpreted here as the maximum flooding zone (MFZ) (see below). Evidence for the falling stage systems tract (FSST) is shown by the generally downstepping facies stack of clinothems 7 to 22 (Fig. 14). The high rank lowstand systems tract (LST) has not been identified and is thought to occur in a deeper part in the basin, below the present-day sea-level. The general offlapping stacking pattern of the LRS in synthem SP1 (Fig. 14) indicates an overall regressive trend, typical for subaqueous deltas, which form during relative stillstands (highstands or lowstands) (Hernández-Molina *et al.*, 2000; Pepe *et al.*, 2014; Patruno *et al.*, 2015), or during falling stages of relative sea-level (RSL) (Hansen, 1999; Massari *et al.*, 1999).

High rank transgressive systems tract and maximum flooding zone

The high rank MFZ is interpreted to correspond to the paraconglomerate interval at the base of the CA section (facies 4.2) (Fig. 10), implying that most of the high rank TST does not crop out. According to Zecchin & Catuneanu (2013), the maximum flooding surface (MFS) may correspond to: "a 'cryptic' conceptual horizon within condensed deposits during the time of maximum transgression, without a clear physical expression". Condensation is interpreted here from the pattern of the dispersing upward packing of lithoclasts and bioclasts (Fig. 10), which can be explained by the R-sediment model of Kidwell (1985) (Fig. 10F). This model argues that clasts are increasingly dispersed upward concomitant with an increase in burial rates or higher sedimentary dilution (Dattilo *et al.*, 2012) at the onset of the HST, when sedimentation rates outpace accommodation space. This interpretation assumes a relatively constant frequency of the high-density gravity flow events that deliver allochthonous clasts to these depths (bottomset). In the rest of the synthem, floating lithoclasts in FA3–FA4 are rare and isolated, as expected from higher burial rates during the high rank HST and FSST (Neal & Abreu, 2009). Furthermore, the paraconglomerate interval is densely bioturbated (Zecchin & Catuneanu, 2013) and yields the deepest assemblage of benthic (Fig. 9) and planktonic foraminifera (Leckie & Olson, 2003). This includes frequent or common outer shelf taxa, such as *Planulina ariminensis* and *Uvigerina peregrina*. The high species richness of macrofossils also implies a longer window of time-averaging. Moreover, the position of this interval at the base of the prograding low rank clinothems reinforces its interpretation as the MFZ. Thus the paraconglomerate interval of clinothem 1 is here interpreted as a high rank backlap shell/clast bed. The paraconglomerate interval also coincides with the strongest magnetic susceptibility in the whole study area (Fig. 4).

High rank highstand and falling stage systems tracts

The forestepping stacking pattern (progradation plus aggradation) of clinothems 1 to 6, coupled with gradual facies changes, indicates a normal regression and are attributed to the high rank

HST (Catuneanu & Zecchin, 2016). In contrast, clinothems 7 to 22 display a general downstepping stacking pattern with strong shallowing-upward facies shifts and sharp erosional contacts. These traits are diagnostic for forced regression, and hence are interpreted as the FSST (Massari *et al.*, 2002; Massari & D'Alessandro, 2012). Forced regression is likewise indicated by frequent 'internal unconformity surfaces' (IUS) such as those reported by Massari & D'Alessandro (2012). The IUS in the study area are interpreted here to essentially represent low rank regressive surfaces of marine erosion (RSME) (Plint, 1988; Plint & Nummedal, 2000) (Figs 4 and 5). The contact between clinothems 13 and 14 in the outer topset and rollover zone is a good example of a surface interpretable as a RSME (Figs 5I and 14D to F). This surface records a strong facies shift from F2.3 (lower shoreface) to F1.2 (middle to upper shoreface), the latter prograding to F1.1 (upper shoreface to foreshore). The material of F1.2 passively filled truncated *Thalassinoides* burrows (*Glossifungites* ichnofacies) in clinohem 13 (Fig. 5J) (MacEachern *et al.*, 1992, 2012b). A subsequent low rank RSL rise partially eroded the upper shoreface–foreshore facies of clinothem 14 (F1.1) forming a low rank onlap shell bed (F2.4) (e.g. Zecchin, 2007). The lithofacies and biofacies F2.3 of clinothem 15 (Fig. 5) suggest an amplitude of about 15 to 20 m of sea-level rise with respect to clinothem 14.

The erosive surfaces at the CBL section (Figs 4, 6 and 15) are interpreted here to have formed by scouring associated with high-frequency variations of base level (Massari & D'Alessandro, 2012). However, the 'master RSME' or high rank RSME, which represents the onset of forced regression in the high rank sequence, is not the most prominent interpreted RSME in the study area. This can be explained by gradually stronger shoreface erosion at increasingly lower sea-levels (when the amplitude of the RSL fall of the low rank cycles is enhanced by the falling sea-level trend of the high rank cycle). In the Cabezo Alto sector, the erosive surfaces disappear distally and these distal portions are interpreted here as basal surfaces of forced regression.

Architecture of proximal low rank sequences

In the context of hierarchical sequence stratigraphy, Schlager (2004, 2010) recognized 'S-sequences and P-sequences'. The P-sequences have only TST and HST, while S-sequences also contain FSST and LST: P-sequences are equivalent to the small-scale cycles (metres to decametres in thickness) of Zecchin (2007), where R, T–R or T cycle types were recognized based on the predominant development of transgressive (T) or regressive (R) deposits. In general, the clinothems of SP1 can be interpreted as R and T–R cycles, with variations in the architecture depending on the position in the depositional profile and the systems tracts of the HRS. In the Cañada Blanca sector, the most common motif of LRS associated with the high rank FSST consists of R cycles bounded by erosive surfaces overlain by thick skeletal concentrations and a coarsening upward trend (Figs 4, 6 and 15). Some skeletal concentrations can be attributed to shelly tempestites because the texture and grain-size of the matrix is similar to or coarser than that of the material underlying the erosive surface (Figs 5A, 15A and 15B). Distinguishing low rank onlap shell beds (OSB) in shoreface environments from bedsets, which display tempestite amalgamation unrelated to shoreline shifts, is difficult (Zecchin *et al.*, 2017). This is because high-frequency, low-amplitude RSL fluctuations result in subtle facies variations in shoreface environments (Zecchin, 2007). Onlap shell beds form under low sedimentation rates when transgression creates accommodation space further onshore. Skeletal material then accumulates in the shoreface, producing loose to dense packing due to low sedimentary dilution (Fig. 15F). The resulting biofabric of the OSB thus reflects a complex history of multiple events of biotic (bulldozing organisms) and/or hydraulic reworking, along with differential winnowing by storms and tidal currents (Kidwell, 1991; Zecchin *et al.*, 2017). In the Cañada Blanca sector, erosive surfaces carved on coarse-grained F1.2 (Fig. 15C and D) and mantled by thick, shell-rich facies with fine-grained matrix (F2.4) (Fig. 15E) are interpreted to reflect RSL fluctuations (Massari *et al.*, 2002; Cattaneo & Steel, 2003). The abundance of complete rhodoliths in many of these shell beds (F2.4) (Fig. 6C) indicates low sedimentation rates (Aguirre *et al.*, 2017).

Architecture of distal low rank sequences

The interpretation here is that the internal architecture of the clinothems in FA4 consists of low rank TST formed by *Terebratula* pavements (F4.3) and the overlying hybrid packstone, with dispersed to barren packing (F4.1), represents the low rank HST. These cycles therefore conform to the structure of R cycles. In more proximal positions, the *Terebratula* pavements are

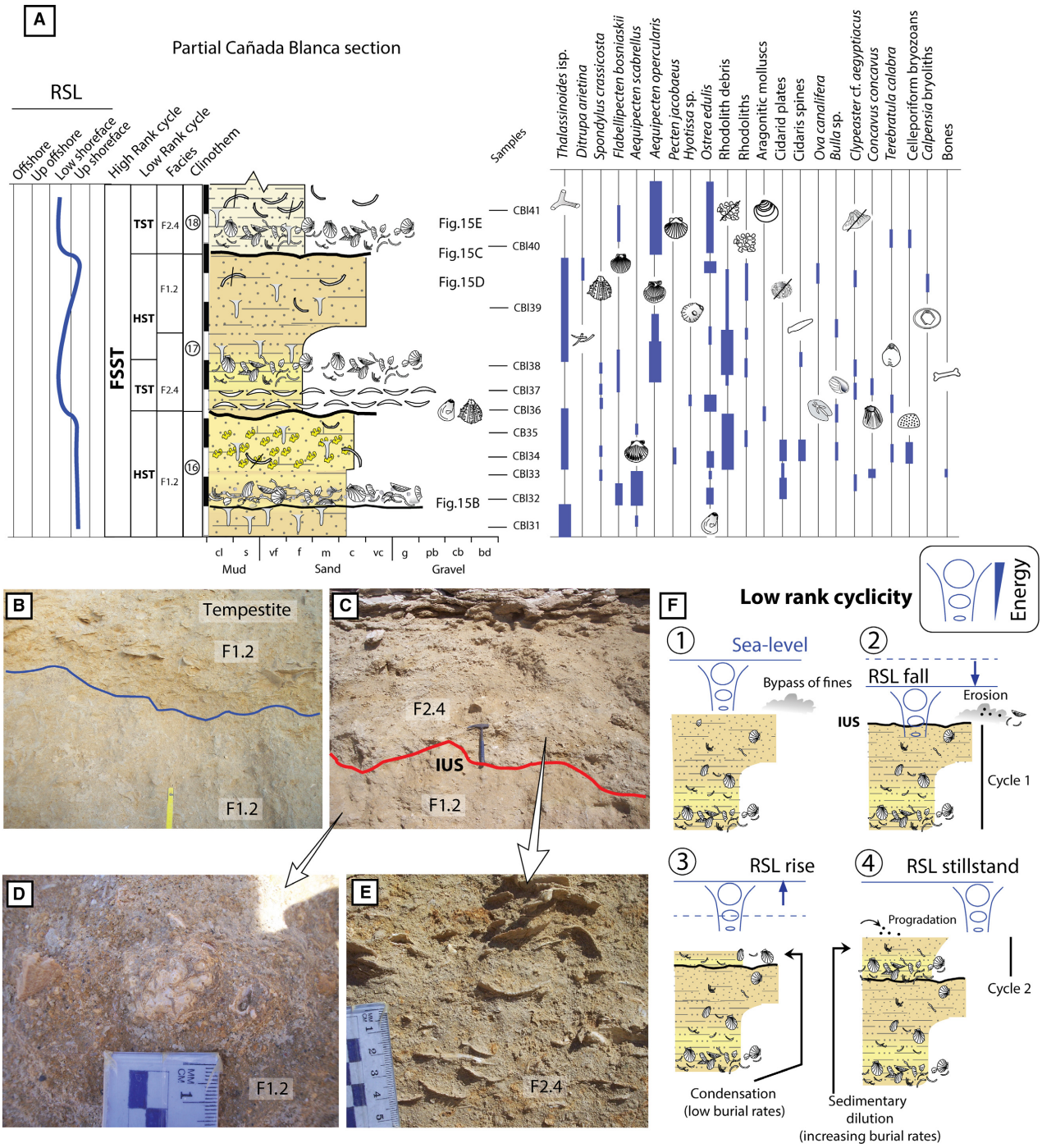

Fig. 15. Examples of low rank cycles in the Cañada Blanca section with alternating F1.2 and F2.4. (A) Detailed log for clinothem 17. (B) Example of tempestite in the upper part of clinothem 16. Yellow stick part for scale is 10 cm long. (C) Transition from clinothems 17 and 18 through an erosive surface (red line) interpreted as an 'internal unconformity surface' (IUS). Hammer is 33 cm long. (D) Rhodolith and *Clypeaster* fragment in coarse siliciclastic grains of F1.2, below the IUS. (E) Fine-grained hybrid matrix with loosely packed pectinid shells (F2.4). (F) Interpretation of the high-frequency cycle motifs at the Cañada Blanca section, bound by erosive surfaces overlain by shell-rich deposits and coarsening upward lithology.

occasionally replaced by the *Glossifungites* ichnofacies (F5) or shell beds (F3.4). A genetic model of these R cycles is presented below.

During stillstand stages of the low rank RSL, sediment aggraded in the topset until reaching the base level. Accommodation space thus

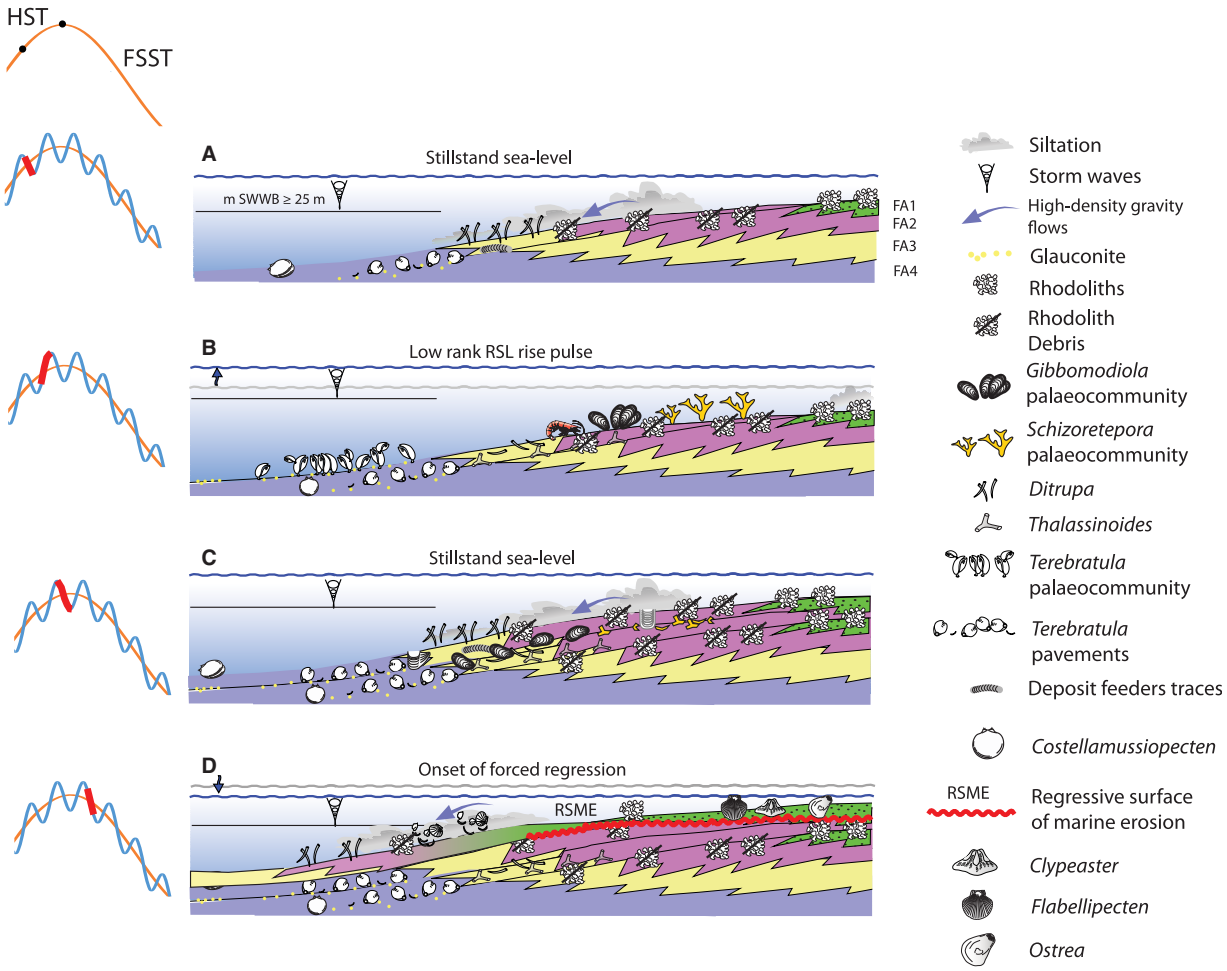

Fig. 16. Simplified depositional model for the infralittoral prograding wedge in the Águilas Basin. (A) Stillstand stage with no accommodation space at the topset. Storms sweep sediment downslope and clinothems prograde. (B) Low rank relative sea-level (RSL) rise creates accommodation space, sediments are trapped in nearshore environments. The sediment-starved distal areas are suitable for suspension feeder palaeocommunities. (C) Reduced rate of RSL rise is outpaced by sedimentation rate, filling up available space in the topset and resuming progradation in the foresets. Suspension feeder communities are extirpated or retreat offshore. *Ditrupa* and deposit feeders thrive. (D) The RSL fall produced forced regression. Base level intersects the sea floor, eroding the topset and leading to resedimentation and mixing up downslope.

became unavailable at the topset and progradation in the foreset resumed, eventually forming a new clinothem (Rich, 1951; Swift & Thorne, 1991; Pomar & Kendall, 2008; Pomar *et al.*, 2015) (Fig. 16A). Background conditions with frequent siltation events and high-density gravity flows in the foreset (F3.2) are indicated by opportunistic faunal responses, including the dominance of *Ditrupa*, infaunal benthic foraminifera and ichnoassemblages of vagile deposit feeders. During these stillstand stages, F4.1 was deposited at the lower rollover and bottomset.

During stages of low rank RSL rise (Fig. 16B), progradation in the foreset switched off and clinoforms developed as omission surfaces in the bottomsets and foresets, and often as transgressive lags or low rank OSB in the upper foresets and topsets (Massari *et al.*, 1999) (Fig. 5). This is because the base level rose concomitantly with the RSL, creating accommodation space in proximal settings of the topset. This was accompanied by reduced fluvial gradients and sediment trapping in nearshore environments, while more distal settings (mainly, foreset and bottomset) were left starved (Brett, 1998; Embry, 2009; Dattilo *et al.*, 2012). Compared with other examples of subaqueous delta-scale clinoforms (Pomar *et al.*, 2002), low rank RSL rise stages in the study area

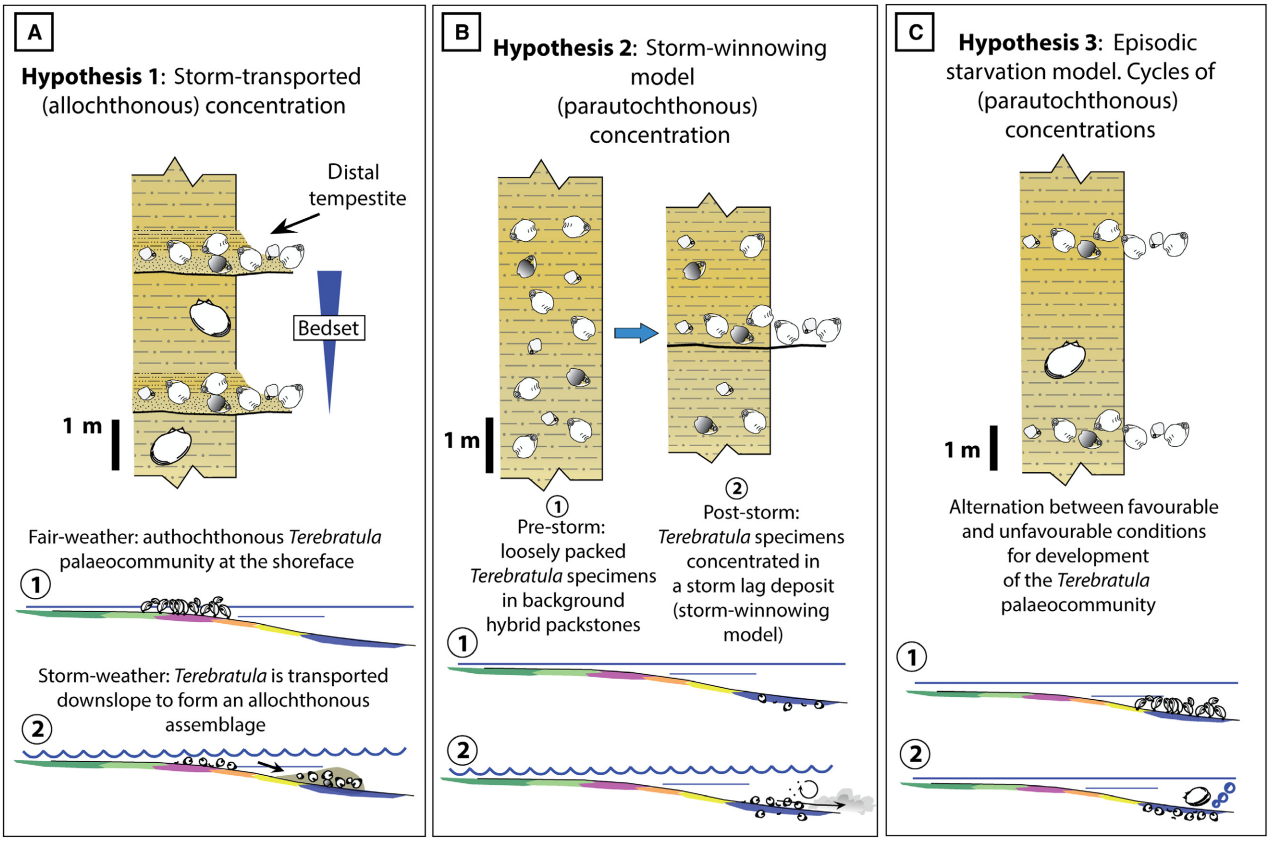

Fig. 17. Models to explain the *Terebratula* pavements in the study area. (A) The allochthonous concentration model. (B) The storm-winnowing model. (C) The episodic-starvation model.

did not result in aggrading clinothems. Rather, they were non-accretionary, forming only hiatal skeletal concentrations. This implies lower sedimentation rates of the Águilas subaqueous delta-scale clinoforms compared to those at Migjorn (Pomar *et al.*, 2002). The conditions of low-sedimentation rate fostered: (i) the colonization of the bottomsets–toesets and foresets by palaeocommunities of siltation-sensitive suspension feeders (Brett, 1998), in this case from proximal to distal: *Schizoretepora*, *Gibbomodiola* and *Terebratula* (Fig. 1C); (ii) the formation of authigenic minerals such as glauconite (Kidwell, 1991; Catuneanu, 2006; Amorosi, 2012); (iii) the development of densely packed shell beds in the middle–upper parts of the foresets (Fig. 8B) due to sediment starvation and differential winnowing (R-sediment model of Kidwell,1985); and (iv) the formation of firmgrounds associated with cementation, enabling colonization by callianassid shrimps and development of the *Glossifungites* ichnofacies (Taylor *et al.*, 2003; MacEachern *et al.*, 2012b) (Fig. 8C and D).

Hypotheses about the formation of the *Terebratula* pavements

Three main hypotheses are considered here to explain the genesis of the *Terebratula* pavements (Fig. 17):

1 The *allochthonous concentration* hypothesis (Kidwell *et al.*, 1986) envisages that the terebratulids were deposited at the lower rollover and bottomsets after being entrained in high-density gravity flows induced by storms or other disturbances (for example, internal waves). Their autochthonous habitat would be located in more proximal environments (for example, the upper rollover and outer topset) (Fig. 17A). This hypothesis is rejected because of: (i) the lack of diagnostic physical sedimentary structures for shelly tempestites (Einsele & Seilacher, 1991; Einsele, 2000; Flügel, 2004; Roetzel & Pervesler, 2004; Myrow, 2005); and (ii) the absence in nearly all pavements of other taxa that are abundant or dominant in more proximal environments of the depositional profile. An

allochthonous concentration would consist of a mixture of taxa entrained and mixed up from different habitats (Leighton & Schneider, 2004). Furthermore, to produce an allochthonous brachiopod-dominated concentration at the bottomsets, there should be high brachiopod productivity in the presumably autochthonous habitat in more proximal environments, which was not observed in the study area.

2 The *storm-winnowing model* (Dattilo *et al.*, 2008, 2012) considers that the *Terebratula* pavements are concentrated autochthonous shell lags that result from differential winnowing of the fine-grained sediment during storms (Fig. 17B). This hypothesis is rejected because, to produce such a dominance and abundance of terebratulids, high brachiopod productivity should occur throughout the stratigraphic intervals of FA4, between terebratulid pavements. These, instead, are barren or are characterized by dispersed *Costellamussiopecten*.

3 The *episodic starvation model* (Dattilo *et al.*, 2008, 2012) considers that the *Terebratula* concentrations are the result of biological processes during stages of low sedimentation rates (Fig. 17C). This hypothesis is supported by the disrupted biological patchiness, the presence of juveniles, the dominance of articulated, pristine shells and by the occurrence of glaucony, a typical proxy for condensed deposits. The occurrence of *Terebratula* clumps (*sensu* Kidwell *et al.*, 1986) in F4.4 demonstrates that *Terebratula* is autochthonous to FA4 (Hallam, 1961; Middlemiss, 1962; Fürsich, 1995).

Magnetic susceptibility and carbonate content

Quartz, calcite and organic compounds yield very weak to negative magnetic susceptibility (MS) values (diamagnetic minerals). In contrast, paramagnetic minerals such as clays (smectite, illite and chlorite); ferromagnesian minerals (biotite, tourmaline, pyroxenes and amphiboles); iron sulphides (pyrite and marcasite) and iron carbonates (siderite and ankerite), yield MS values several orders of magnitude higher than those of diamagnetic minerals, which dominate the signal when present in bulk samples (Davies *et al.*, 2013; Sullivan & Brett, 2013). Magnetic susceptibility in marine sedimentary rocks is usually considered as a proxy for the proportion of iron-rich sediments derived from terrestrial sources (Ellwood *et al.*, 2000; Sullivan & Brett, 2013). High MS values are considered to be attained during regressive stages, when increased erosion delivers proportionally higher amounts of terrestrial iron-rich sediments into the marine basin (Sullivan & Brett, 2013). This argument has been contradicted by the report of distinct MS peaks associated with surfaces of maximum starvation (Ellwood *et al.*, 2011). This can be explained by concentration of paramagnetic particles derived from aeolian sources (Reuter *et al.*, 2013). Likewise, very low to negative MS values, as in the Águilas Basin, SP1, may be explained by a very low terrigenous input and/or dilution of terrigenous particles in biogenic carbonate (Reuter *et al.*, 2013). When distinct positive MS peaks are the result of increased terrigenous input, MS trends anticorrelate with those of $CaCO_3$ (Davies *et al.*, 2013; Rothwell & Croudace, 2015). At the CA section, distinct MS peaks are coincident with a relative increase in $CaCO_3$ content (Fig. 4), suggesting that the MS values in such cases are associated with condensation. These peaks occur at the clinothem boundaries that were interpreted as omission surfaces (*Glossifungites* ichnofacies) or condensed intervals (paraconglomerate and *Terebratula* pavements) based on sedimentological and palaeontological features. The weak MS values are also potentially influenced by the slightly evolved glauconite content, which is paramagnetic (Amorosi, 1997).

Progradation rates of the lower rank cycles

Biostratigraphic data constrain the maximum possible duration of the HRS to somewhat less than 700 kyr. The yellowish to light green colour of the glauconite grains that separate the LRS in facies 4.3 suggests that, in terms of maturity, this is a slightly evolved stage. This was confirmed in one sample, where glauconite grains had a K_2O content of *ca* 4%. According to Amorosi (2012), the slightly evolved glaucony would indicate sediment-starved periods lasting about 10^4 years, implying that the LRS in the study area can be interpreted as high-frequency cycles in the Milankovitch band. The cyclicity in variation of terrigenous input is also recorded in the patterns of magnetic susceptibility and calcium carbonate content (Fig. 4). These patterns of magnetic susceptibility are similar to those reported by Davies *et al.* (2013) for the high-frequency cycles of the Llucmajor platform (Miocene, Spain), reinforcing the above interpretation. If this is true, the time-span encompassed by the HRS is considerably less than the 700 kyr suggested by biostratigraphic proxies.

CONCLUSIONS

The Águilas Basin records subaqueous delta-scale clinoforms that prograded during the early Pliocene (MPl3 biozone) in mixed temperate carbonate–siliciclastic environments. The sedimentological and palaeontological features of these clinoforms are compatible with the infralittoral prograding wedge model. The prograding units formed during the highstand and falling stages of a high rank relative sea-level cycle, and the biostratigraphic data indicate that this progradation lasted for less than 700 kyr. The basic building blocks of this sequence are clinothems whose internal architecture generally consists of skeletal concentrations overlain by a stratigraphic interval with a more disperse packing. In distal positions of the depositional profile, the skeletal concentrations consist of terebratulid brachiopod pavements. These pavements are distributed cyclically; they are interpreted here to have formed during high-frequency relative sea-level rise pulses that led to sediment starvation in these distal environments. During stillstand stages, accommodation space eventually became unavailable in the topset of the clinoforms, leading to a resumption in the progradation of the clinoform system, extirpating the brachiopod communities until the next cycle of relative sea-level rise. In other examples of subaqueous deltas, similar brachiopod assemblages bound the clinobedded unit at the base and the top, but did not occur on the clinoforms, as seen in the Águilas Basin. This implies lower progradation rates of the Águilas Basin clinoforms, allowing enough time for these benthic communities to develop. The occurrence of slightly evolved glauconite in the Águilas Basin suggests that these high-frequency cycles fall within the Milankovitch band, probably precession.

ACKNOWLEDGEMENTS

We thank Gregorio Romero Sánchez from the Paleontological Heritage Service of the Community of Murcia (Spain), for granting permits to conduct palaeontological fieldwork in the study area; Javier Souto-Derungs, Andrey Ostrovsky and Eric Wolfgring for their help with the SEM images and the identification of *Schizoretepora*. We thank Alfred Uchman for cross-checking identifications of certain trace fossils and for palaeoenvironmental suggestions about the *Macaronichnus–Ophiomorpha* ichnofabric. Thanks to Martin Maslo, Christa Hermann, Robert Peticzka and Theodoros Ntaflos for the analysis of carbonate content and glauconite. This work was inspired during fieldwork in the Águilas Arc with Jesús Soria, Hugo Corbí, Jordi Martinell, Rosa Domènech and Cristino Dabrio, all of whom are also thanked for providing literature and for discussions in the field. We thank Guillermo Díaz-Medina, Johann Hohenegger, Wolfgang Eder, Vlasta Ćosović, Adam Tomašových, Rafał Nawrot and many other colleagues for fruitful discussions and suggestions. Special thanks to Ildefonso Bajo and Enrico Borghi for their input about the taxonomy of Pliocene echinoids; to Julio Aguirre and Juan Carlos Braga for sending literature about rhodoliths and Andrés Guilabert for his help with Digital Terrain Models. We thank Michael Stachowitsch and Alexander Hugh Rice for improving the language. We thank the Editors Peir Pufahl and Christopher R. Fielding for the constructive comments during the review process. The stimulating reviews of Massimo Zecchin, Carlton Brett and an anonymous colleague significantly improved the final version of this manuscript. The authors declare that there is no conflict of interest.

REFERENCES

Abbott, S.T. (1997) Mid-cycle condensed shellbeds from mid-Pleistocene cyclothems, New Zealand: implications for sequence architecture. *Sedimentology*, **44**, 805–824.

Abu-Zied, R.H., **Rohling, E.J.**, **Jorissen, F.J.**, **Fontanier, C.**, **Casford, J.S.** and **Cooke, S.** (2008) Benthic foraminiferal response to changes in bottom-water oxygenation and organic carbon flux in the eastern Mediterranean during LGM to Recent times. *Mar. Micropaleontol.*, **67**, 46–68.

Adams, E.W. and **Schlager, W.** (2000) Basic types of submarine slope curvature. *J. Sediment. Res.*, **70**, 814–828.

Aguirre, J., **Braga, J.C.**, **Jiménez, A.P.** and **Rivas, P.** (1996) Substrate-related changes in pectinid fossil assemblages. *Palaeogeogr. Palaeoclimatol. Palaeoecol.*, **126**, 291–308.

Aguirre, J., **de Gibert, J.M.** and **Puga-Bernabéu, A.** (2010) Proximal–distal ichnofabric changes in a siliciclastic shelf, Early Pliocene, Guadalquivir Basin, southwest Spain. *Palaeogeogr. Palaeoclimatol. Palaeoecol.*, **291**, 328–337.

Aguirre, J., **Braga, J.C.**, **Martín, J.M.** and **Betzler, C.** (2012) Palaeoenvironmental and stratigraphic significance of Pliocene rhodolith beds and coralline algal bioconstructions from the Carboneras Basin (SE Spain). *Geodiversitas*, **34**, 115–136.

Aguirre, J., **Braga, J.C.** and **Bassi, D.** (2017) Rhodoliths and Rhodolith beds in the rock record. In: *Rhodolith/Mäerl Beds: A Global Perspective* (Eds R. Riosmena-Rodríguez, W. Nelson and J. Aguirre), pp. 105–138. Springer International Publishing, Basel.

Álvarez, F. and **Aldaya, F.** (1985) Las unidades de la Zona Bética en la región de Águilas-Mazarrón (Prov. de Murcia). *Estud. Geol.*, **41**, 139–148.

Amorosi, A. (1997) Detecting compositional, spatial, and temporal attributes of glaucony: a tool for provenance research. *Sed. Geol.*, **109**, 135–153.

Amorosi, A. (2012) The occurrence of glaucony in the stratigraphic record: distribution patterns and sequence-stratigraphic significance. In: *Linking Diagenesis to Sequence Stratigraphy* (Eds S. Morad, J.M. Ketzerand and L.F. De Ros), pp. 37–53. John Wiley and Sons, West Sussex.

Amorosi, A., **Sammartino, I.** and **Tateo, F.** (2007) Evolution patterns of glaucony maturity: a mineralogical and geochemical approach. *Deep Sea Res. Part II*, **54**, 1364–1374.

Anell, I. and **Midtkandal, I.** (2015) The quantifiable clinothem–types, shapes and geometric relationships in the Plio-Pleistocene Giant Foresets Formation, Taranaki Basin, New Zealand. *Basin Res.*, **29**, 277–297.

Baeza-Carratalá, J.F., **Giannetti, A.**, **Tent-Manclús, J.E.** and **Joral, F.G.** (2014) Evaluating taphonomic bias in a storm-disturbed carbonate platform: effects of compositional and environmental factors in Lower Jurassic brachiopod accumulations (Eastern Subbetic Basin, Spain) Early Jurassic Brachiopod taphofacies. *Palaios*, **29**, 55–73.

Bardají, T., **Silva, P.**, **Goy, J.L.**, **Zazo, C.**, **Dabrio, C.** and **Civis, J.** (1999) Recent evolution of the Águilas Arc Basins (SE, Spain): Sea-level record and neotectonics. *M.B.S.S. Newletters*, **21**, 21–26.

Bardají, A.T., **Zazo, C.**, **Goy, J.L.**, **Silva, P.G.** and **Dabrio, C.J.** (2001) Registro de los cambios del nivel del mar en la Cuenca de Águilas (Murcia, SE de España). In: *V Iberian Quaternary Meeting and I Quaternary Congress of Countries of Iberian Languages* (Eds R. Taborda, J. Cascalho and L. Ortlieb), pp. 245–248. Sociedade Geológica de Portugal, Lisbon.

Beckvar, N. and **Kidwell, S.M.** (1988) Hiatal shell concentrations, sequence analysis, and sealevel history of a Pleistocene coastal alluvial fan, Punta Chueca, Sonora. *Lethaia*, **21**, 257–270.

Beltran, C., **Flores, J.A.**, **Sicre, M.A.**, **Baudin, F.**, **Renard, M.** and **De Rafélis, M.** (2011) Long chain alkenones in the Early Pliocene Sicilian sediments (Trubi Formation—Punta di Maiata section): Implications for the alkenone paleothermometry. *Palaeogeogr. Palaeoclimatol. Palaeoecol.*, **308**, 253–263.

Ben Moussa, A. (1994) Les bivalves néogènes du Maroc septentrional (façade atlantique et méditerranéenne). Biostratigraphie, Paléobiogéographie et Paléoécologie. Documents du Laboratoire de Géologie de Lyon (Fr), 132, 1–281.

Bennett, M.R., **Doyle, P.**, **Mather, A.E.** and **Woodfin, J.L.** (1994) Testing the climatic significance of dropstones: an example from southeast Spain. *Geol. Mag.*, **131**, 845–848.

Blomeier, D., **Dustira, A.M.**, **Forke, H.** and **Scheibner, C.** (2013) Facies analysis and depositional environments of a storm-dominated, temperate to cold, mixed siliceous-carbonate ramp: the Permian Kapp Starostin Formation in NE Svalbard. *Norw. J. Geol./Nor. Geol. Foren.*, **93**, 75–93.

Braga, J.C. and **Martín, J.M.** (1996) Geometries of reef advance in response to relative sea-level in a Messinian (uppermost Miocene) fringing reef (Cariatiz reef, Sorbas Basin, SE Spain). *Sed. Geol.*, **107**, 61–81.

Brett, C.E. (1998) Sequence stratigraphy, paleoecology, and evolution; biotic clues and responses to sea-level fluctuations. *Palaios*, **13**, 241–262.

Brett, C.E. and **Seilacher, A.** (1991) Fossil lagerstätten; a taphonomic consequence of event sedimentation. In: *Cycles and Events in Stratigraphy* (Eds G. Einsele, W. Ricken and A. Seilacher), pp. 283–297. Springer-Verlag, Berlin.

Brett, C.E., **Algeo, T.J.** and **McLaughlin, P.I.** (2003) The use of event beds and sedimentary cycles in high-resolution stratigraphic correlation of lithologically repetitive successions: the Upper Ordovician Kope Formation of Northern Kentucky and Southern Ohio. In: *High-Resolution Stratigraphic Approaches to Paleobiology* (Eds P. Harries and D. Geary), pp. 315–351. Kluwer Academic/Plenum Press, Boston.

Bromley, R.G. (1996) *Trace Fossils. Biology, Taphonomy and Applications*, 2nd edn, p. 361. Chapman and Hall, London.

Bromley, R.G. (2005) Preliminary study of bioerosion in the deep-water coral *Lophelia*, Pleistocene, Rhodes, Greece. In: *Cold-water Corals and Ecosystems* (Eds A. Freiwaldand and J.M. Roberts), pp. 895–914. Springer, Berlin.

Bromley, R.G., **Milan, J.**, **Uchman, A.** and **Hansen, K.S.** (2009) Rheotactic *Macaronichnus*, and human and cattle trackways in Holocene beachrock, Greece: reconstruction of paleoshoreline orientation. *Ichnos*, **16**, 103–117.

Buatois, L.A. and **Mángano, M.G.** (2011) *Ichnology. Organism-Substrate Interactions in Space and Time*, p. 358. Cambridge University Press, Cambridge.

Buatois, L.A., **Saccavino, L.L.** and **Zavala, C.** (2011) Ichnologic signatures of hyperpycnal flow deposits in Cretaceous river-dominated deltas, Austral Basin, southern Argentina, Sediment transfer from shelf to deep water—Revisiting the delivery system. *AAPG Studies in Geology*, **61**, 153–170.

Buatois, L.A., **Delgado, M.** and **Mángano, M.G.** (2015) Disappeared almost without a trace: Taphonomic pathways and the recognition of hidden bioturbation events in Eocene storm deposits (Paují Formation, Lake Maracaibo, Venezuela). *Ann. Soc. Geol. Pol.*, **85**, 473–479.

Carballo, J.L., **Sánchez-Moyano, J.E.** and **García-Gómez, J.C.** (1994) Taxonomic and ecological remarks on boring sponges (Clionidae) from the Straits of Gibraltar (southern Spain): tentative bioindicators? *Zool. J. Linn. Soc.*, **112**, 407–424.

Cattaneo, A. and **Steel, R.J.** (2003) Transgressive deposits: a review of their variability. *Earth Sci. Rev.*, **62**, 187–228.

Catuneanu, O. (2006) *Principles of Sequence Stratigraphy*, p. 386. Elsevier, Amsterdam.

Catuneanu, O. and **Zecchin, M.** (2016) Unique vs. non-unique stratal geometries: relevance to sequence stratigraphy. *Mar. Pet. Geol.*, **78**, 184–195.

Catuneanu, O., **Galloway, W.E.**, **Kendall, C.G.**, **St, C.**, **Miall, A.D.**, **Posamentier, H.W.**, **Strasser, A.** and **Tucker, M.E.** (2011) Sequence stratigraphy: methodology and nomenclature. *Newsl. Stratigr.*, **44**, 173–245.

Ceregato, A., **Raffi, S.** and **Scarponi, D.** (2007) The circalittoral/bathyal paleocommunities in the Middle Pliocene of Northern Italy: The case of the *Korobkovia oblonga–Jupiteria concava* paleocommunity type. *Geobios*, **40**, 555–572.

Coppier, G., **Griveaud, P.**, **de Larouziere, F.D.**, **Montenat, C.** and **Ott d'Estevou, P.** (1989) Example of Neogene tectonic indentation in the Eastern Betic Cordilleras: the Arc of Águilas (Southeastern Spain). *Geodin. Acta*, **3**, 37–51.

Corbí, H. and **Soria, J.M.** (2016) Late Miocene–early Pliocene planktonic foraminifer event-stratigraphy of the Bajo Segura basin: A complete record of the western Mediterranean. *Mar. Pet. Geol.*, **77**, 1010–1027.

Cuevas-Castell, J.M., **Betzler, C.**, **Roessler, J.**, **Hüssner, H.** and **Peinl, M.** (2007) Integrating outcrop data and forward computer modelling to unravel the development of a Messinian carbonate platform in SE Spain (Sorbas Basin). *Sedimentology*, **54**, 423–441.

Dabrio, C.J., **Bardají, T.**, **Zazo, C.** and **Goy, J.L.** (1991) Effects of sea-level changes on a wave-worked Gilbert-type delta (Late Pliocene, Águilas Basin, SE Spain). *Cuad. Geol. Ibérica*, **15**, 103–137.

Dattilo, B.F., **Brett, C.E.**, **Tsujita, C.J.** and **Fairhurst, R.** (2008) Sediment supply versus storm winnowing in the development of muddy and shelly interbeds from the Upper Ordovician of the Cincinnati region, USA. *Can. J. Earth Sci.*, **45**, 243–265.

Dattilo, B.F., **Brett, C.E.** and **Schramm, T.J.** (2012) Tempestites in a teapot? Condensation-generated shell beds in the Upper Ordovician, Cincinnati Arch, USA. *Palaeogeogr. Palaeoclimatol. Palaeoecol.*, **367**, 44–62.

Davaud, E. and **Septfontaine, M.** (1995) Post-mortem onshore transportation of epiphytic foraminifera: recent example from the Tunisian coastline. *J. Sediment. Res.*, **65**, 136–142.

Davies, E.J., **Ratcliffe, K.T.**, **Montgomery, P.**, **Pomar, L.**, **Ellwood, B.B.** and **Wray, D.S.** (2013) Magnetic susceptibility (χ) stratigraphy and chemostratigraphy applied to an isolated carbonate platform reef complex; Llucmajor Platform, Mallorca. In: *Deposits, Architecture, and Controls of Carbonate Margin, Slope and Basinal Settings* (Eds K. Verwer, T.E. Playton and P.M. Harris), SEPM Spec. Publ., **105**, 142–156.

Di Celma, C., **Ragaini, L.**, **Cantalamessa, G.** and **Landini, W.** (2005) Basin physiography and tectonic influence on the sequence architecture and stacking pattern: Pleistocene succession of the Canoa Basin (central Ecuador). *Geol. Soc. Am. Bull.*, **117**, 1226–1241.

Drummond, C.N. and **Wilkinson, B.H.** (1996) Stratal thickness frequencies and the prevalence of orderedness in stratigraphic sequences. *J. Geol.*, **104**, 1–18.

Dumas, S. and **Arnott, R.W.C.** (2006) Origin of hummocky and swaley cross-stratification—The controlling influence of unidirectional current strength and aggradation rate. *Geology*, **34**, 1073–1076.

Einsele, G. (2000) *Sedimentary Basins: Evolution, Facies, and Sediment Budget*, p. 792. Springer-Verlag, Berlin.

Einsele, G. and **Seilacher, A.** (1991) Distinction of tempestites and Turbidites. In: *Cycles and Events in Stratigraphy* (Eds G. Einsele, W. Rickenand and A. Seilacher), pp. 377–382. Springer-Verlag, Berlin.

Ellwood, B.B., **Crick, R.E.**, **Hassani, A.E.**, **Benoist, S.L.** and **Young, R.H.** (2000) Magnetosusceptibility event and cyclostratigraphy method applied to marine rocks: detrital input versus carbonate productivity. *Geology*, **28**, 1135–1138.

Ellwood, B.B., **Algeo, T.J.**, **El Hassani, A.**, **Tomkin, J.H.** and **Rowe, H.D.** (2011) Defining the timing and duration of the Kačák Interval within the Eifelian/Givetian boundary GSSP, Mech Irdane, Morocco, using geochemical and magnetic susceptibility patterns. *Palaeogeogr. Palaeoclimatol. Palaeoecol.*, **304**, 74–84.

Emanuel, K. (2005) Increasing destructiveness of tropical cyclones over the past 30 years. *Nature*, **436**, 686.

Embry, A.F. (1993) Transgressive–regressive (T–R) sequence analysis of the Jurassic succession of the Sverdrup Basin, Canadian Arctic Archipelago. *Can. J. Earth Sci.*, **30**, 301–320.

Embry, A.F. (1995) Sequence boundaries and sequence hierarchies: problems and proposals. In: *Sequence Stratigraphy on the Northwest European Margin* (Eds R.J. Steel, F.L. Felt, E.P. Johannessen and C. Mathieu), NPF Spec. Publ., **5**, 1–11.

Embry, A.F. (2009) Practical sequence stratigraphy. *Can. Soc. Petrol. Geol.*, 81. Available at www.cspg.org

Emig, C.C. (1989) Observations préliminaires sur l'envasement de la biocoenose à *Gryphus vitreus* (Brachiopoda), sur la pente continentale du Nord de la Corse (Méditerranée). Origines et conséquences. *C. R. Acad. Sci. IIb. Mec.*, **309**, 337–342.

Emig, C.C. and **García-Carrascosa, M.A.** (1991) Distribution of *Gryphus vitreus* (Born, 1778) (Brachiopoda) on transect P 2 (Continental margin, French Mediterranean coast) investigated by submersible. *Sci. Mar.*, **55**, 385–388.

Fiorini, F. and **Vaiani, S.C.** (2001) Benthic foraminifers and transgressive-regressive cycles in the Late Quaternary subsurface sediments of the Po Plain near Ravenna (Northern Italy). *Bollettino della Societa Paleontologica Italiana*, **40**, 357–404.

Flügel, E. (2004) *Microfacies Analysis of Carbonate Rocks. Analysis, Interpretation and Application*, p. 976. Springer-Verlag, Berlin.

Franseen, E.K. and **Mankiewicz, C.** (1991) Depositional sequences and correlation of middle (?) to late Miocene carbonate complexes, Las Negras and Níjar areas, southeastern Spain. *Sedimentology*, **38**, 871–898.

Frébourg, G., **Hasler, C.A.** and **Davaud, E.** (2012) Uplifted marine terraces of the Akamas Peninsula (Cyprus): evidence of climatic conditions during the Late Quaternary highstands. *Sedimentology*, **59**, 1409–1425.

Frey, S.E. and **Dashtgard, S.E.** (2012) Seaweed-assisted, benthic gravel transport by tidal currents. *Sed. Geol.*, **265**, 121–125.

Fürsich, F.T. (1995) Shell concentrations. *Eclogae Geol. Helv.*, **88**, 643–655.

Fürsich, F.T., **Oschmann, W.**, **Jaitly, A.K.** and **Singh, I.B.** (1991) Faunal response to transgressive-regressive cycles: example from the Jurassic of western India. *Palaeogeogr. Palaeoclimatol. Palaeoecol.*, **85**, 149–159.

Gani, M.R., **Bhattacharya, J.P.** and **MacEachern, J.A.** (2009) Using ichnology to determine relative influence of waves, storms, tides, and rivers in deltaic deposits: examples from Cretaceous Western Interior Seaway, USA. In: *Applied Ichnology* (Eds J.A. MacEachern, K.L. Bann, M.K. Gingras and S.G. Pemberton), SEPM Short Course Notes, **52**, 209–225.

García-García, F. (2004) Sedimentary models of coarse-grained deltas in the Neogene basins of the Betic Cordillera (SE Spain): Tortonian and Pliocene examples. *Bol. Geol. Min.*, **115**, 469–494.

García-García, F., **Fernández, J.**, **Viseras, C.** and **Soria, J.M.** (2006) High frequency cyclicity in a vertical alternation of Gilbert-type deltas and carbonate bioconstructions in the late Tortonian, Tabernas Basin, Southern Spain. *Sed. Geol.*, **192**, 123–139.

García-García, F., **Corbí, H.**, **Soria, J.M.** and **Viseras, C.** (2011) Architecture analysis of a river flood-dominated delta during an overall sea-level rise (early Pliocene, SE Spain). *Sed. Geol.*, **237**, 102–113.

García-Ramos, D.A., **Corbí, H.A.**, **Pina, J.A.G.** and **Soria, J.M.M.** (2012) Bioestratigrafía de alta resolución basada en foraminíferos planctónicos para el Plioceno inferior del arco de Águilas (cordillera Bética oriental). In: *XXVIII*

Jornadas de la Sociedad Española de Paleontología y Simposios de los Proyectos n. 587 y 596 del PICG. Valencia y Sóller 1-6 de octubre de 2012. Homenaje a Guillem Colom Casasnovas (1900–1993) (Eds J.-C. Liao, J.A. Gámez Vintaned, J.J. Valenzuela-Ríos and A. García-Forner), pp. 67–39. Libro de Resúmenes. Universitat de València. Valencia; Sociedad Española de Paleontología, Madrid.

García-Ramos, D.A., **Corbí, H.** and **Soria, J.M.M.** (2014) Paleoenvironmental analysis of an Early Pliocene section in the Águilas Basin (Eastern Betic Cordillera). *Geogaceta*, **56**, 123–126.

Garden, C.J., **Craw, D.**, **Waters, J.M.** and **Smith, A.** (2011) Rafting rocks reveal marine biological dispersal: A case study using clasts from beach-cast macroalgal holdfasts. *Estuar. Coast. Shelf Sci.*, **95**, 388–394.

Ghinassi, M. (2007) The effects of differential subsidence and coastal topography on high-order transgressive–regressive cycles: Pliocene nearshore deposits of the Val d'Orcia Basin, Northern Apennines, Italy. *Sed. Geol.*, **202**, 677–701.

Giannetti, A., **Baeza-Carratalá, J.F.**, **Soria-Mingorance, J.M.**, **Dulai, A.**, **Tent-Manclús, J.E.** and **Peral-Lozano, J.** (2018) New paleobiogeographical and paleoenvironmental insight through the Tortonian brachiopod and ichnofauna assemblages from the Mediterranean-Atlantic seaway (Guadix Basin, SE Spain). *Facies*, **64**, 24.

de Gibert, J.M. and **Goldring, R.** (2007) An ichnofabric approach to the depositional interpretation of the intensely burrowed Bateig Limestone, Miocene, SE Spain. *Sed. Geol.*, **194**, 1–16.

de Gibert, J.M., **Domènech, R.** and **Martinell, J.** (2007) Bioerosion in shell beds from the Pliocene Roussillon Basin, France: Implications for the (macro) bioerosion ichnofacies model. *Acta Palaeontol. Pol.*, **52**, 783–798.

Gilbert, G.K. (1885) The topographic feature of lake shores. *U.S. Geol. Sur.*, Annual Report, **5**, 104–108.

Goineau, A., **Fontanier, C.**, **Jorissen, F.**, **Buscail, R.**, **Kerhervé, P.**, **Cathalot, C.**, **Pruski, A.M.**, **Lantoine, F.**, **Bourgeois, S.**, **Metzger, E.**, **Legrand, E.** and **Rabouille, C.** (2012) Temporal variability of live (stained) benthic foraminiferal faunas in a river-dominated shelf-faunal response to rapid changes of the river influence (Rhône prodelta, NW Mediterranean). *Biogeosciences*, **9**, 1367–1388.

Grémare, A., **Sardá, R.**, **Medernach, L.**, **Jordana, E.**, **Pinedo, S.**, **Amouroux, J.M.**, **Martin, D.**, **Nozais, C.** and **Charles, F.** (1998) On the dramatic increase of *Ditrupa arietina* O.F. Müller (Annelida: Polychaeta) along both the French and the Spanish Catalan coasts. *Estuar. Coast. Shelf Sci.*, **47**, 447–457.

Griveaud, P., **Coppier, G.**, **Montenat, C.** and **Ott d'Estevou, P.** (1990) Le Néogène des Sierras D'Águilas. In: Les Bassins Néogènes du Domaine Bétique Oriental (Espagne): Tectonique et sédimentation dans un couloir de décrochement. Première partie: Etude Régionale. Doc et Trav. Inst. Geol. Albert-de-Lapparent, Paris no. 12–13, 221–238.

Hallam, A. (1961) Brachiopod life assemblages from the marlstone rock-bed of Leicestershire. *Palaeontology*, **4**, 653–659.

Hansen, K.S. (1999) Development of a prograding carbonate wedge during sea level fall: Lower Pleistocene of Rhodes, Greece. *Sedimentology*, **46**, 559–576.

Harding, S.C., **Nash, B.P.**, **Petersen, E.U.**, **Ekdale, A.A.**, **Bradbury, C.D.** and **Dyar, M.D.** (2014) Mineralogy and geochemistry of the Main Glauconite Bed in the Middle Eocene of Texas: Paleoenvironmental implications for the Verdine Facies. *PLoS One*, **9**, 1–26.

Hartley, J.P. (2014) A review of the occurrence and ecology of dense populations of *Ditrupa arietina* (Polychaeta: Serpulidae). *Mus. Victoria Mem.*, **71**, 85–95.

He, W., **Shi, G.R.**, **Feng, Q.**, **Campi, M.J.**, **Gu, S.**, **Bu, J.**, **Peng, Y.** and **Meng, Y.** (2007) Brachiopod miniaturization and its possible causes during the Permian-Triassic crisis in deep water environments, South China. *Palaeogeogr. Palaeoclimatol. Palaeoecol.*, **252**, 145–163.

Helland-Hansen, W., **Steel, R.J.** and **Sømme, T.O.** (2012) Shelf genesis revisited. *J. Sediment. Res.*, **82**, 133–148.

Hendy, A.J., **Kamp, P.J.** and **Vonk, A.J.** (2006) Cool-water shell bed taphofacies from Miocene-Pliocene shelf sequences in New Zealand: Utility of taphofacies in sequence stratigraphic analysis. In: *Cool-Water Carbonates: Depositional Systems and Palaeoenvironmental Controls* (Eds H.M. Pedley and G. Carannante), Geological Society, London, Special Publications, **255**, 283–305.

Hernández-Molina, F.J., **Fernández-Salas, L.M.**, **Lobo, F.**, **Somoza, L.**, **Díaz-del-Río, V.** and **Dias, J.A.** (2000) The infralittoral prograding wedge: a new large-scale progradational sedimentary body in shallow marine environments. *Geo-Mar. Lett.*, **20**, 109–117.

Iaccarino, S., **Premoli-Silva, I.**, **Biolzi, M.**, **Foresi, L.M.**, **Lirer, F.**, **Turco, E.** and **Petrizzo, M.R.** (2007) *Practical Manual of Neogene Planktonic Foraminifera*. International School on Planktonic Foraminifera, 6th Course. Università degli Studi di Perugia, Perugia, 140 pp.

Jorissen, F.J., **Fontanier, C.** and **Thomas, E.** (2007) Paleoceanographical proxies based on deep-sea benthic foraminiferal assemblage characteristics. *Dev. Mar. Geol.*, **1**, 263–325.

Kidwell, S.M. (1985) Palaeobiological and sedimentological implications of fossil concentrations. *Nature*, **318**, 457–460.

Kidwell, S.M. (1989) Stratigraphic condensation of marine transgressive records: origin of major shell deposits in the Miocene of Maryland. *J. Geol.*, **97**, 1–24.

Kidwell, S.M. (1991) The stratigraphy of shell concentrations. In: *Taphonomy: Releasing the Data Locked in the Fossil Record* (Eds P.A. Allison and D.E.G. Briggs), p. 211–290. Plenum Press, New York, 560 pp.

Kidwell, S.M. (1998) Time-averaging in the marine fossil record: overview of strategies and uncertainties. *Geobios*, **30**, 977–995.

Kidwell, S.M. and **Holland, S.M.** (1991) Field description of coarse bioclastic fabrics. *Palaios*, **6**, 426–434.

Kidwell, S.M., **Fürsich, F.T.** and **Aigner, T.** (1986) Conceptual framework for the analysis and classification of fossil concentrations. *Palaios*, **1**, 228–238.

Kleipool, L.M., **Jong, K.**, **Vaal, E.L.** and **Reijmer, J.J.** (2017) Seismic characterization of switching platform geometries and dominant carbonate producers (Miocene, Las Negras, Spain). *Sedimentology*, **64**, 1676–1707.

Kondo, Y., **Abbott, S.T.**, **Kitamura, A.**, **Kamp, P.J.J.**, **Naish, T.R.**, **Kamataki, T.** and **Saul, G.S.** (1998) The relationship between shellbed type and sequence architecture: examples from Japan and New Zealand. *Sed. Geol.*, **122**, 109–127.

Leckie, R.M. and **Olson, H.C.** (2003) Foraminifera as proxies for sea-level change on siliciclastic margins. In: *Micropaleontologic Proxies for Sea-Level Change and Stratigraphic Discontinuities* (Eds H.C. Olson and R.M. Leckie), Spec. Publ. SEPM Soc. Sediment. Geol., **75**, 5–19.

Leighton, L.R. and **Schneider, C.L.** (2004) Neighbor proximity analysis, a technique for assessing spatial patterns in the fossil record. *Palaios*, **19**, 396–407.

Longhitano, S.G. (2008) Sedimentary facies and sequence stratigraphy of coarse-grained Gilbert-type deltas within the Pliocene thrust-top Potenza Basin (Southern Apennines, Italy). *Sed. Geol.*, **210**, 87–110.

MacEachern, J.A., **Raychaudhuri, I.** and **Pemberton, S.G.** (1992) Stratigraphic applications of the *Glossifungites* ichnofacies: delineating discontinuities in the rock record. In: *Applications of Ichnology to Petroleum Exploration* (Ed. S.G. Pemberton), pp. 169–198. Society of Economic Paleontologists and Mineralogists, Core Workshop Notes 17, Tulsa.

MacEachern, J.A., **Bann, K.L.**, **Bhattacharya, J.P.** and **Howell, C.D. Jr** (2005) Ichnology of deltas: organism responses to the dynamic interplay of rivers, waves, storms, and tides. In: *River Deltas: Concepts, Models and Examples* (Eds L. Giosan And J.P. Bhattacharya), SEPM Special Publication **83**, 49–85.

MacEachern, J., **Bann, K.**, **Gingras, M.**, **Zonneveld, J.**, **Dashtgard, S.** and **Pemberton, S.** (2012a) The ichnofacies paradigm. In: *Trace Fossils as Indicators of Sedimentary Environments* (Eds D. Knaust and R.G. Bromley), pp. 103–138. Elsevier, Amsterdam.

MacEachern, J.A., **Dashtgard, S.E.**, **Knaust, D.**, **Catuneanu, O.**, **Bann, K.L.** and **Pemberton, S.G.** (2012b) Sequence stratigraphy. In: *Trace Fossils as Indicators of Sedimentary Environments* (Eds D. Knaust, R.G. Bromley), pp. 157–194. Elsevier, Amsterdam.

Malatesta, A. (1974) Malacofauna pliocenica umbra. *Memorie per Servire alla Carta Geologica d'Italia*, **13**, 1–498.

Mancosu, A. and **Nebelsick, J.H.** (2017) Ecomorphological and taphonomic gradients in clypeasteroid-dominated echinoid assemblages along a mixed siliciclastic-carbonate shelf from the early Miocene of northern Sardinia, Italy. *Acta Palaeontol. Pol.*, **62**, 627–646.

Martín, J.M., **Braga, J.C.**, **Aguirre, J.** and **Betzler, C.** (2004) Contrasting models of temperate carbonate sedimentation in a small Mediterranean embayment: the Pliocene Carboneras Basin, SE Spain. *J. Geol. Soc.*, **161**, 387–399.

Martinell, J., **Kowalewski, M.** and **Domènech, R.** (2012) Drilling predation on serpulid polychaetes (*Ditrupa arietina*) from the Pliocene of the Cope Basin, Murcia region, southeastern Spain. *PLoS One*, **7**, 1–14.

Massari, F. and **Chiocci, F.** (2006) Biocalcarenite and mixed cool-water prograding bodies of the Mediterranean Pliocene and Pleistocene: architecture, depositional setting and forcing factors. In: *Cool-Water Carbonates: Depositional Systems and Palaeoenvironmental Controls* (Eds H.M. Pedley and G. Carannante), Geol. Soc. London Spec. Publ., **255**, 5–120.

Massari, F. and **D'Alessandro, A.** (2012) Facies partitioning and sequence stratigraphy of a mixed siliciclastic-carbonate ramp stack in the Gelasian of Sicily (S Italy): a potential model for Icehouse, distally-steepened Heterozoan ramps. *Rivista Italiana di Paleontologia e Stratigraphia*, **118**, 503–534.

Massari, F., **Sgavetti, M.**, **Rio, D.**, **D'Alessandro, A.** and **Prosser, G.** (1999) Composite sedimentary record of falling stages of Pleistocene glacio-eustatic cycles in a shelf setting (Crotone basin, south Italy). *Sed. Geol.*, **127**, 85–110.

Massari, F., **Rio, D.**, **Sgavetti, M.**, **Prosser, G.**, **D'Alessandro, A.**, **Asioli, A.**, **Capraro, L.**, **Fornaciari, E.** and **Tateo, F.** (2002) Interplay between tectonics and glacio-eustasy: Pleistocene succession of the Crotone basin, Calabria (southern Italy). *Geol. Soc. Am. Bull.*, **114**, 1183–1209.

Mayoral, E., **Ledesma-Vazquez, J.**, **Baarli, B.G.**, **Santos, A.**, **Ramalho, R.**, **Cachão, M.** and **Johnson, M.E.** (2013) Ichnology in oceanic islands; case studies from the Cape Verde Archipelago. *Palaeogeogr. Palaeoclimatol. Palaeoecol.*, **381**, 47–66.

Middlemiss, F.A. (1962) Brachiopod ecology and lower greensand palaeogeography. *Palaeontology*, **5**, 253–267.

Minchin, D. (2003) Introductions: some biological and ecological characteristics of scallops. *Aquat. Living Resour.*, **16**, 521–532.

Mitchell, N.C. (2012) Modeling the rollovers of sandy clinoforms from the gravity effect on wave-agitated sand. *J. Sediment. Res.*, **82**, 464–468.

Mitchum, R.M. and **Van Wagoner, J.C.** (1991) High-frequency sequences and their stacking patterns: sequence-stratigraphic evidence of high-frequency eustatic cycles. *Sed. Geol.*, **70**, 131–160.

Moissette, P., **Cornée, J.J.** and **Koskeridou, E.** (2010) Pleistocene rolling stones or large bryozoan nodules in a mixed siliciclastic-carbonate environment (Rhodes, Greece). *Palaios*, **25**, 24–39.

Montenat, C., **de Reneville, P.** and **Bizon, G.** (1978) Le Néogène des environs d'Aguilas (provinces de Murcia et d'Almeria) Cordilleres bétiques, Espagne. *Bulletin Musée National d'Histoire Naturelle, Sciences de la Terre*, **68**, 37–54.

Mount, J.F. (1984) Mixing of siliciclastic and carbonate sediments in shallow shelf environments. *Geology*, **112**, 432–435.

Mulder, T. and **Alexander, J.** (2001) The physical character of subaqueous sedimentary density flows and their deposits. *Sedimentology*, **48**, 269–299.

Myrow, P.M. (2005) Storms and storm deposits. In: *Encyclopedia of Geology* (Eds R.C. Selley, R. Cocks and I. Pilmer), pp. 580–587. Elsevier Limited, Oxford.

Naish, T.R. and **Kamp, P.J.J.** (1997) Sequence stratigraphy of sixth-order (41 k.y.) Pliocene-Pleistocene cyclothems, Wanganui basin, New Zealand: a case for the regressive systems tract. *Geol. Soc. Am. Bull.*, **109**, 978–999.

Nalin, R., **Ghinassi, M.** and **Basso, D.** (2010) Onset of temperate carbonate sedimentation during transgression in a low-energy siliciclastic embayment (Pliocene of the Val d'Orcia Basin, Tuscany, Italy). *Facies*, **56**, 353–368.

Nalin, R., **Ghinassi, M.**, **Foresi, L.M.** and **Dallanave, E.** (2016) Carbonate Deposition in Restricted Basins: A Pliocene Case Study From the Central Mediterranean (Northwestern Apennines), Italy. *J. Sed. Res.*, **86**, 236–267.

Neal, J. and **Abreu, V.** (2009) Sequence stratigraphy hierarchy and the accommodation succession method. *Geology*, **37**, 779–782.

Odin, G.S. and **Fullagar, P.D.** (1988) Geological significance of the glaucony facies. In: *Green Marine Clays* (Ed. G.S. Odin), Developments in Sedimentology, **45**, 295–332.

ÖNORM L 1084 (2006) Chemical analyses of soils—determination of carbonate. In: *Austrian Standards Institute* (Ed. ÖNORM L 1084), pp. 2–8. Austrian Standards Institute, Vienna.

Patruno, S., **Hampson, G.J.** and **Jackson, C.A.-L.** (2015) Quantitative characterisation of deltaic and subaqueous clinoforms. *Earth Sci. Rev.*, **142**, 79–119.

Pearson, N.J., **Gabriela Mángano, M.**, **Buatois, L.A.**, **Casadío, S.** and **Raising, M.R.** (2013) Environmental variability of

Macaronichnus ichnofabrics in Eocene tidal-embayment deposits of southern Patagonia, Argentina. *Lethaia*, **46**, 341–354.

Pemberton, S.G., **MacEachern, J.A.** and **Ranger, M.J.** (1992) Ichnology and event stratigraphy: the use of trace fossils in recognizing tempestites. In: *Applications of Ichnology to Petroleum Exploration: A Core Workshop* (Ed. S.G. Pemberton), Society for Sedimentary Geology Core Workshop, **17**, 85–118.

Pemberton, S.G., **MacEachern, J.A.**, **Gingras, M.K.** and **Saunders, T.D.** (2008) Biogenic chaos: Cryptobioturbation and the work of sedimentologically friendly organisms. *Palaeogeogr. Palaeoclimatol. Palaeoecol.*, **270**, 273–279.

Pepe, F., **Bertotti, G.**, **Ferranti, L.**, **Sacchi, M.**, **Collura, A.M.**, **Passaro, S.** and **Sulli, A.** (2014) Pattern and rate of post-20 ka vertical tectonic motion around the Capo Vaticano Promontory (W Calabria, Italy) based on offshore geomorphological indicators. *Quatern. Int.*, **332**, 85–98.

Pérez-Asensio, J.N., **Aguirre, J.** and **Rodríguez-Tovar, F.J.** (2017) The effect of bioturbation by polychaetes (Opheliidae) on benthic foraminiferal assemblages and test preservation. *Palaeontology*, **60**, 807–827.

Pervesler, P., **Uchman, A.** and **Hohenegger, J.** (2008) New methods for ichnofabric analysis and correlation with orbital cycles exemplified by the Baden-Sooss section (Middle Miocene, Vienna Basin). *Geol. Carpath.*, **59**, 395–409.

Pirmez, C., **Pratson, L.F.** and **Steckler, M.S.** (1998) Clinoform development by advection-diffusion of suspended sediment: Modeling and comparison to natural systems. *J. Geophys. Res.*, **103**, 24141–24157.

Plint, A.G. (1988) Sharp-based shoreface sequences and 'offshore bars' in the Cardium Formation of Alberta: their relationship to relative changes in sea level. In: *Sea-level Changes: An Integrated Approach* (Eds C.K. Wilgus, B.S. Hastings, C.G.St.C. Kendall, H.W. Posamentier, C.A. Rossand and J.C. Van Wagoner), Society of Economic Paleontologists and Mineralogists Special Publications, **42**, 357–370.

Plint, A.G. and **Nummedal, D.** (2000) The falling stage systems tract: recognition and importance in sequence stratigraphic analysis. *Geol. Soc., London, Spec. Pub.*, **172**, 1–17.

Pomar, L. (2001) Types of carbonate platforms: a genetic approach. *Basin Res.*, **13**, 313–334.

Pomar, L. and **Kendall, C.G.C.** (2008) Architecture of carbonate platforms: a response to hydrodynamics and evolving ecology. In: *Controls on Carbonate Platform and Reef Development* (Eds J. Lukasik and J. A Simo), SEPM Special Publication, **89**, 187–216.

Pomar, L. and **Ward, W.C.** (1994) Response of a late Miocene Mediterranean reef platform to high-frequency eustasy. *Geology*, **22**, 131–134.

Pomar, L., **Obrador, A.** and **Westphal, H.** (2002) Sub-wavebase cross-bedded grainstones on a distally steepened carbonate ramp, Upper Miocene, Menorca, Spain. *Sedimentology*, **49**, 139–169.

Pomar, L., **Aurell, M.**, **Bádenas, B.**, **Morsilli, M.** and **Al-Awwad, S.F.** (2015) Depositional model for a prograding oolitic wedge, Upper Jurassic, Iberian basin. *Mar. Pet. Geol.*, **67**, 556–582.

Postma, G. (1990) An analysis of the variation in delta architecture. *Terra Nova*, **2**, 124–130.

Postma, G., **Nemec, W.** and **Kleinspehn, K.L.** (1988) Large floating clasts in turbidites: a mechanism for their emplacement. *Sed. Geol.*, **58**, 47–61.

Pouchou, J.L. and **Pichoir, F.** (1991) Quantitative analysis of homogeneous or stratified microvolumes applying the model "PAP". In: *Electron Probe Quantitation* (Eds K.F.J. Heinrich and D.E. Newbury), pp. 31–75. Plenum Press, New York, NY.

Rasmussen, T.L. (2005) Systematic paleontology and ecology of benthic foraminifera from the Plio-Pleistocene Kallithea Bay section, Rhodes, Greece. *Cushman Foun. Spec. Pub.*, **39**, 53–157.

Read, J.F. (1985) Carbonate platform facies models. *Am. Assoc. Petrol. Geol. Bulletin*, **69**, 1–21.

Reolid, M., **García-García, F.**, **Tomašových, A.** and **Soria, J.M.** (2012) Thick brachiopod shell concentrations from prodelta and siliciclastic ramp in a Tortonian Atlantic-Mediterranean strait (Miocene, Guadix Basin, southern Spain). *Facies*, **58**, 549–571.

Reuter, M., **Piller, W.E.**, **Brandano, M.** and **Harzhauser, M.** (2013) Correlating Mediterranean shallow water deposits with global Oligocene-Miocene stratigraphy and oceanic events. *Global Planet. Change*, **111**, 226–236.

Rich, J.L. (1951) Three critical environments of deposition, and criteria for recognition of rocks deposited in each of them. *Geol. Soc. Am. Bull.*, **62**, 1–20.

Robba, E. (1996) Autoecology of some Pliocene thin-shelled pectinids. In: *Autecology of Selected Fossil Organisms: Achievements and Problems* (Ed. A. Cherchi), Bollettino della Società Paleontologica Italiana, Special Volume **3**, 159–174.

Rodríguez-Tovar, F.J. and **Aguirre, J.** (2014) Is *Macaronichnus* an exclusively small, horizontal and unbranched structure? *Macaronichnus segregatis degiberti* isubsp. nov. *Spanish J. Palaeontol.*, **29**, 131–142.

Roetzel, R. and **Pervesler, P.** (2004) Storm-induced event deposits in the type area of the Grund Formation (Middle Miocene, Lower Badenian) in the Molasse Zone of Lower Austria. *Geol. Carpath.*, **55**, 87–102.

Rothwell, R.G. and **Croudace, I.W.** (2015) Twenty years of XRF core scanning marine sediments: What do geochemical proxies tell us? In: *Micro-XRF Studies of Sediment Cores: Applications of a Non-Destructive Tool for the Environmental Sciences* (Eds I.W. Croudace and R.G. Rothwell), pp. 25–102. Springer, Dordrecht.

Ruban, D.A. (2015) Worldwide application of synthem stratigraphy in the 21st century: a bibliographical survey. *Proc. Geol. Assoc.*, **126**, 307–313.

Ruffell, A. and **Wach, G.** (1998) Firmgrounds–key surfaces in the recognition of parasequences in the Aptian Lower Greensand Group, Isle of Wight (southern England). *Sedimentology*, **45**, 91–107.

Sanfilippo, R. (1999) *Ditrupa brevis* n. sp., a new serpulid from the Mediterranean Neogene with comments on the ecology of the genus. *Riv. Ital. Paleontol. Stratigr.*, **105**, 455–463.

Scarponi, D., **Huntley, J.W.**, **Capraro, L.** and **Raffi, S.** (2014) Stratigraphic paleoecology of the Valle di Manche section (Crotone Basin, Italy): a candidate GSSP of the Middle Pleistocene. *Palaeogeogr. Palaeoclimatol. Palaeoecol.*, **402**, 30–43.

Schlager, W. (2004) Fractal nature of stratigraphic sequences. *Geology*, **32**, 185–188.

Schlager, W. (2010) Ordered hierarchy versus scale invariance in sequence stratigraphy. *Int. J. Earth Sci.*, **99**, 139–151.

Sgarrella, F. and **Moncharmont Zei, M.** (1993) Benthic Foraminifera of the Gulf of Naples (Italy): systematics and

autoecology. *Bollettino della Società Paleontologica Italiana*, **32**, 145–264.

Silva, P.G., **Goy, J.L.**, **Somoza, L.**, **Zazo, C.** and **Bardají, T.** (1993) Landscape response to strike-slip faulting linked to collisional settings: Quaternary tectonics and basin formation in the Eastern Betics, Southeast Spain. *Tectonophysics*, **224**, 289–303.

Soria, J.M., **Fernández, J.**, **García, F.** and **Viseras, C.** (2003) Correlative lowstand deltaic and shelf systems in the Guadix Basin (Late Miocene, Betic Cordillera, Spain): the stratigraphic record of forced and normal regressions. *J. Sediment. Res.*, **73**, 912–925.

Sullivan, N.B. and **Brett, C.E.** (2013) Integrating magnetic susceptibility data with sequence stratigraphy in the ironstone bearing successions (Lower Silurian) of eastern North America. *Stratigraphy*, **10**, 261–280.

Swift, D.J.P. and **Thorne, J.A.** (1991) Sedimentation on continental margins, I: a general model for shelf sedimentation. In: *Shelf Sand and Sandstone Bodies* (Eds D.J.P. Swift, G.F. Oertel, R.W. Tillman and J.A. Thorne), IAS Special Publication, **14**, 3–31.

Talling, P.J., **Masson, D.G.**, **Sumner, E.J.** and **Malgesini, G.** (2012) Subaqueous sediment density flows: depositional processes and deposit types. *Sedimentology*, **59**, 1937–2003.

Taylor, A., **Goldring, R.** and **Gowland, S.** (2003) Analysis and application of ichnofabrics. *Earth Sci. Rev.*, **60**, 227–259.

Thorne, J. (1995) On the scale independent shape of prograding stratigraphic units. In: *Fractals in Petroleum Geology and Earth Processes* (Eds C.C. Barton and P.R. La Pointe), pp. 97–112. Springer, Boston, MA.

Tomašových, A. and **Kidwell, S.M.** (2017) Nineteenth-century collapse of a benthic marine ecosystem on the open continental shelf. *Proc. R. Soc. B*, **284**, 20170328.

Tomašových, A., **Fürsich, F.T.** and **Olszewski, T.D.** (2006) Modeling shelliness and alteration in shell beds: variation in hardpart input and burial rates leads to opposing predictions. *Paleobiology*, **32**, 278–298.

Tomassetti, L. and **Brandano, M.** (2013) Sea level changes recorded in mixed siliciclastic–carbonate shallow-water deposits: The Cala di Labra Formation (Burdigalian, Corsica). *Sed. Geol.*, **294**, 58–67.

Uchman, A., **Demírcan, H.**, **Toker, V.**, **Derman, A.S.**, **Sevim, S.** and **Szulc, J.** (2002) Relative sea-level changes recorded in borings from a Miocene rocky shore of the Mut Basin, southern Turkey. *Ann. Soc. Geol. Pol.*, **72**, 263–270.

Uchman, A., **Johnson, M.E.**, **Rebelo, A.C.**, **Melo, C.**, **Cordeiro, R.**, **Ramalho, R.S.** and **Ávila, S.P.** (2016) Vertically-oriented trace fossil *Macaronichnus segregatis* from Neogene of Santa Maria Island (Azores; NE Atlantic) records vertical fluctuations of the coastal groundwater mixing zone on a small oceanic island. *Geobios*, **49**, 229–241.

Vail, P.R., **Audemard, F.**, **Bowman, S.A.**, **Eisner, P.N.** and **Pérez-Cruz, G.** (1991) The stratigraphic signatures of tectonics, eustasy and sedimentology – an overview. In: *Cycles and Events in Stratigraphy* (Eds G. Einsele, W. Ricken and A. Seilacher), pp. 617–659. Springer-Verlag, Berlin.

Violanti, D. (2012) Pliocene Mediterranean foraminiferal biostratigraphy: a synthesis and application to the paleoenvironmental evolution of Northwestern Italy. In: *Stratigraphic Analysis of Layered Deposits* (Ed. Ö. Elitok), pp. 123–160. InTech Open Access Publisher: Rijeka. Available at: https://www.intechopen.com/books/stratigraphic-analysis-of-layered-deposits/pliocene-mediterranean-foraminiferal-biostratigraphy-a-synthesis-and-application-to-the-paleoenviro

Waller, T.H. (2011) Neogene Paleontology of the Northern Dominican Republic. 24. *Propeamussiidae* and *Pectinidae* (Mollusca: Bivalvia: Pectinoidea) of the Cibao Valley. *Bull. Am. Paleontol.*, **381**, 1–198.

Walsh, J.P., **Nittrouer, C.A.**, **Palinkas, C.M.**, **Ogston, A.S.**, **Sternberg, R.W.** and **Brunskill, G.J.** (2004) Clinoform mechanics in the Gulf of Papua, New Guinea. *Cont. Shelf Res.*, **24**, 2487–2510.

Wanless, H.R., **Tedesco, L.P.** and **Tyrrell, K.M.** (1988) Production of subtidal and surficial tempestites by hurricane Kate, Caoicos platform, British West Indies. *J. Sediment. Petrol.*, **58**, 739–750.

Yesares-García, J. and **Aguirre, J.** (2004) Quantitative taphonomic analysis and taphofacies in lower Pliocene temperate carbonate–siliciclastic mixed platform deposits (Almería-Níjar basin, SE Spain). *Palaeogeogr. Palaeoclimatol. Palaeoecol.*, **207**, 83–103.

Zecchin, M. (2007) The architectural variability of small-scale cycles in shelf and ramp clastic systems: the controlling factors. *Earth Sci. Rev.*, **84**, 21–55.

Zecchin, M. and **Catuneanu, O.** (2013) High-resolution sequence stratigraphy of clastic shelves I: units and bounding surfaces. *Mar. Pet. Geol.*, **39**, 1–25.

Zecchin, M. and **Catuneanu, O.** (2017) High-resolution sequence stratigraphy of clastic shelves VI: Mixed siliciclastic-carbonate systems. *Mar. Pet. Geol.*, **88**, 712–723.

Zecchin, M., **Caffau, M.**, **Catuneanu, O.** and **Lenaz, D.** (2017) Discrimination between wave-ravinement surfaces and bedset boundaries in Pliocene shallow-marine deposits, Crotone Basin, southern Italy: an integrated sedimentological, micropaleontological and mineralogical approach. *Sedimentology*, **64**, 1755–1791.

Zuschin, M. and **Stanton, R.J. Jr** (2002) Paleocommunity reconstruction from shell beds: a case study from the Main Glauconite Bed, Eocene, Texas. *Palaios*, **17**, 602–614.

Manuscript received 3 November 2017; revision accepted 20 September 2018

Supporting Information

Additional information may be found in the online version of this article:

Fig. S1. Photomosaic of the base of the Terreros section, showing the cyclically bedded synthem SP0 (Zanclean, MPl1–MPl2 biozones) and the overlying calcirudites of SP1 (MPl3 biozone *fide* Montenat *et al.*, 1978) on top, resting on an erosion surface (SP0–SP1 unconformity).

Fig. S2. Some examples of allochthonous elements in FA4 and FA3.